Structural and Conformational Aspects of Gas Phase Peptides Probed by
Electron Capture Dissociation

Structural and Conformational Aspects of Gas Phase Peptides Probed by Electron Capture Dissociation

Structuur- en Conformatie Aspecten van Peptiden in de   asfase bestudeerd met Electronenvangst Dissociatie

(met een samenvatting in het Nederlands)

Proefschrift

**ter verkrijging van de graad van doctor
aan de Universiteit Utrecht
op gezag van de rector magnificus, prof. dr. W. H.   ispen
ingevolge het besluit van het college voor promoties
in het openbaar te verdedigen
op woensdag 7 maart 2007 des middags te 2.30 uur**

door

Romulus Mihalca

geboren op 12 december 1969, te Baia Mare, Roemenië

Promotores: prof. dr. A. J. R. Heck

prof. dr. R. M. A. Heeren

Co-promotor: dr. Y. E. M. van der Burgt

Pentru Raul si Daciana

Contents

Chapter 3

Electron capture dissociation at low temperatures reveals selective

dissociations   **73**

Chapter 4

Combined infrared multiphoton dissociation and electron-capture

dissociation using co-linear and overlapping beams in Fourier

transform ion cyclotron resonance mass spectrometry   **87**

Chapter 5

Disulfide bond cleavages observed in SORI-CID of three

nonapeptides complexed with divalent transition metal cations   **107**

Chapter 6

ECD behaviour of disulfide bond containing peptides

is determined by the type of divalent metal cation   **129**

Introduction

I.   eneral introduction

Living matter involves a large variety of biologically active macromolecules with specific functions [1]. Peptides and proteins are just two of the important classes of biomolecules that play indispensable roles in all living organisms. Their diversity originates from differences at molecular level in terms of elemental composition and (macro)molecular architecture. To understand the functions they perform in a biological system is imperative to structurally characterize them. The investigation of the structure-function relationship is of paramount interest in many Life Science disciplines including biochemistry, biology and medicine. Additional interest exists in the commercial sector for a wide range of applications ranging from health care to food and agriculture. Peptide and protein characterization involves the accurate determination of their molecular weight, primary structure (amino acid sequence), secondary structure (local three-dimensional form), tertiary structure (full three-dimensional shape), quaternary structure (arrangement of multiple folded proteins which forms a complete unit), identification and localization of posttranslational modifications and relative quantitation. Proteomics is the field that aims to identify, characterize and map expressed proteins in a biological system. Information about three-dimensional structure of peptides and proteins can be obtained from Nuclear Magnetic Resonance (NMR) [2] and X-ray crystallography [3]. Beside the fact that they are time-consuming, their major drawbacks include the use of large amounts of pure and concentrated samples. Therefore, they are hardly suitable for analysis of complex mixtures especially when limited amount of sample is available. To benefit from the maximum amount of information that can be obtained from small amounts of material, mass spectrometry (MS) is the method of choice [4].

Mass spectrometry (MS) is a widely applied technology which has demonstrated its ability to address different problems in proteomics research by virtue of its sensitivity, specificity and speed of analysis [4]. This analytical technique

measures the mass-to-charge ratio and the relative abundance of peptides, proteins and their fragments. As a straightforward consequence of the discovery and implementation of novel technologies to explore biomolecules in gas-phase, biomolecular mass spectrometry experienced a tremendous growth in the last 20 years. Nowadays, MS analytical platforms enable the separation of analytes from complex mixtures, their intact transfer from solution in to the gas-phase and to probe their structural features. Interfacing mass spectrometry with different chromatographic and ionization techniques allowed very small amounts (zeptomolar concentrations) [5] of different classes of very large and labile biomolecules and even complete viruses [6] to be thoroughly investigated. The development of soft ionization techniques such as matrix-assisted laser desorption ionization (MALDI) [7] and electrospray ionization (ESI) [8-10] are directly responsible for these advances.

Mass spectrometry generated impressive amounts of data that have paved the way for systematic identification of proteomes in intra-cellular dynamics. The growth of the MS arsenal provides more freedom and confidence to scientific community in its approach of complex problems in proteomics. These include the study of the identity, distribution, dynamics and interaction of proteins in biological systems.

One of the modern MS technologies that attracted a huge interest due to its remarkable analytical potential is Fourier transform ion cyclotron resonance mass spectrometry (FTICR-MS) [11]. A combination of magnetic and electric fields is used in FTICR-MS to trap ions in the ion cyclotron resonance (ICR) cell under high vacuum (10^{-9} mbar) conditions. Electromagnetic fields are used to manipulate the trapped ions and to investigate their interaction with particles or electromagnetic radiation. High mass resolution, mass accuracy, high sensitivity, long ion-observation times and non-destructive multichannel detection are just a few of the outstanding features of FTICR-MS. These distinctive capabilities are complemented by a collection of fragmentation techniques compatible with FTICR-MS that offer the possibility to perform gas-phase reactions for structural analysis of large intact (bio)molecules. Together with advances in informatics, FTICR-MS is developed to such that it is now capable to pre-select monisotopic ion species from

complex ion mixtures to be further subjected to tandem mass spectrometry (MS/MS or MS^n) procedures for structural investigations. The possibility to generate native states of large and fragile proteins and protein complexes in gas-phase enabled the introduction of the "top-down" approach This technique involve accurate mass measurement of intact proteins followed by MS/MS for structural analysis of post-translational modifications. The molecular puzzle can also be tackled using the so-called "bottom-up" approach within the protein, in a first stage, is proteolytically cleaved in small peptides. This is followed by protein identification based upon mass measurements of a set of peptide digestive products or by MS/MS fragmentation of one or more of these peptides. Mapping protein`s three-dimensional structure (conformational analysis) is another active area of research in mass spectrometry. All these strategies are compatible with FTICR-MS instrumentation. The "bottom-up" approach rarely leads to 100% sequence coverage of the intact protein and does not provide information about the protein conformation. Therefore, the "top-down" strategy is becoming more and more attractive because it offers the possibility to gain more insight in to the unaltered protein.

Detailed structural information can only be obtained from accurate mass determination of the protein fragmentation produced through tandem mass spectrometry. Currently used fragmentation techniques are based on ion interaction with neutral molecules as in collision-induced dissociation (CID), with active surfaces as in surface-induced dissociation (SID) or with infrared or ultraviolet photons (i.e.: Infrared Multiphoton Dissociation or IRMPD and Ultraviolet Photon Dissociation or UVPD). In all these fragmentation techniques, the internal energy of the precursor ion is increased until dissociation occurs. For that reason they are known as "slow-heating" techniques. Their utility for structural studies is well acknowledged by the mass spectrometry community. However, using these methods to locate labile groups such as posttranslational modifications (PTM`s) in a protein sequence is very difficult or even impossible because PTM`s are lost before the protein's backbone is cleaved. On the other hand, strong intramolecular bonds like disulfide bridges hamper sequence information to be obtained.

With the discovery of electron capture dissociation (ECD) in 1998 in the group of Prof. McLafferty, a new era started in proteomics that allowed the study of molecular species that are difficult to be investigated using traditional MS^n strategies. In ECD, multiply charged macromolecular ions trapped in the ICR cell reacts with low-energy electrons supplied by an electron beam to generate specific fragments. Since its conception, ECD has stimulated the discovery and development of other fragmentation techniques in gas-phase based on reactions between polypeptide ions and electrons: hot-electron capture dissociation (HECD), electron excitation dissociation (EED), electron detachment dissociation (EDD) and more recently electron transfer dissociation (ETD). What makes ECD so attractive compared with other fragmentation techniques employed by mass spectrometry? It was found that ECD leads to extensive and unselective cleavage of the polypeptide backbone. Scission of disulfide bonds is facile with ECD and non-covalent interactions are preserved intact while the strong bonds are preferentially cleaved with ECD. This later feature allows labile posttranslational modifications to be both identified and localized with ECD. The technique was improved in the last years and nowadays ECD is a high-throughput technique that generates complementary information to the information obtained with classical fragmentation techniques. It has been shown that the combination between ECD and IRMPD has a great advantage for proteomics as it generates rich and high quality MS spectra using experimental sequences on time scales compatible with different chromatographic techniques. Hence, ECD became an indispensable tool for proteomics. However, the dissociation rate with ECD is lower compared with other fragmentation techniques.

II.   Scope of the thesis

In spite of its utility, the mechanism, which underlies ECD, is still not well understood. Understanding the factors which plays a role in ECD helps to further develop this technique in to a "plug and play" method for protemics. The work presented in this thesis comprises a fundamental study of ECD, followed by instrumental development dedicated to ECD and application of this dissociation technique to biologically relevant biomolecules.

This thesis contributes to the understanding and developments of the electron capture dissociation as a useful fragmentation technique in Fourier transform ion cyclotron resonance mass spectrometry to study the structure of the ions in gas phase. This is of fundamental importance for proteomics because other tandem MS methods do not show features to produce extensive information about conformation and subtle structural changes in peptides and proteins.

The following two chapters are dedicated to FTICR-MS as a distinguished MS tool and to ECD as a method. The first part of **chapter 1** will supply the reader with the fundamental aspects of FTICR-MS followed by a description of the experimental setup. Instrumental presentation will continue with an introduction of the most used dissociation techniques in FTICR-MS and will end with a short presentation of the software tools used to process the recorded mass spectra. **Chapter 2** will be completely dedicated to electron capture dissociation. The technique will be briefly reviewed and its application to proteomics will be described.

Chapter 3 of this thesis is a fundamental study of ECD. We investigate whether the conformational heterogeneity of the precursor ions plays a role on the fragments produced in ECD. Therefore, the precursor ion population is thermally manipulated in order to achieve ion clouds with different conformation heterogeneity. It is shown that ECD at 86 K of the linear peptide substance P and the cyclic peptide gramicidin S results in less backbone fragments than at room

temperature. The fact that ECD at 86 K generates a smaller number of backbone fragments is consistent with reduced conformation heterogeneity of the ion population at low temperatures. This finding is important because shows how the conformation population of the ion packet influences the relative intensity of the fragments and the sequence coverage.

It is clear from the study mentioned above that heating the ion population is required to enhance the performances of ECD. Based on a novel approach we propose a new experimental configuration wherein IRMPD and ECD can be simultaneously performed in the ICR cell using co-linear and overlapping beams. Conformation heterogeneity of the ions is increased with IR irradiation whether ECD has the ability to achieve extensive sequence coverage using irradiation times compatible with chromatographic separation techniques. **Chapter 4** describes such an instrumental development in order to reduce the irradiation time and to improve the quality and the information content of the MS/MS spectra.

At first glance, **chapter 5** does not have anything in common with ECD. However, the idea of using SORI-CID for structural investigation of the peptides containing a disulfide bridge has roots in our recent ECD work on oxytocin complexed with different divalent transition metal cations[12]. We showed that ECD of [oxytocin+Cu^{2+}] results in formation of only *b* type of backbone fragments which are atypical for ECD being rather representative for CID experiments. Here, we demonstrate that SORI-CID of the peptides that contain a disulfide bridge when are complexed with divalent metal cations yields very rich tandem mass spectra including fragments that require cleavage of the disulfide bond. On the contrary, SORI-CID of the doubly protonated analogues result just in backbone fragments from the region that is not involved in the disulfide bond. The location of the metal ion is also explored in this study. The benefit of peptide/protein complexation with metal cations for SORI-CID is that leads to increased sequence coverage and more confidence in peptide- or protein assignment.

A further step to investigate the influence of the peptide structural changes on the ECD behaviour is made in **chapter 6**. The results indicate that not only amino acid composition of the peptide but also the identity of the charge carrier has an important role on the type of fragments and the fragmentation pattern produced by ECD.

Chapter 7 is a future outlook of three MS methods to study the structure of biomolecules in the gas-phase.

The results presented in this thesis bring new evidence that ECD is a useful and versatile technique for structural analysis of peptides and proteins, especially for obtaining high sequence coverage and to investigate the conformation of the ions in gas phase.

References

(1)   Creighton, T. E. **1993**.
(2)   Rehm, T.; Huber, R.; Holak, T. A. Structure **2002**, 10, 1613-1618.
(3)   Liu, H.-L.; Hsu, J.-P. Proteomics **2005**, 5, 2056-2068.
(4)   Aebersold, R.; Mann, M. Nature **2003**, 422, 198-207.
(5)   Belov, M. E.; Gorshkov, M. V.; Udseth, H. R.; Anderson, G. A.; Smith, R. D. Anal. Chem. **2000**, 72, 2271-2279.
(6)   Bothner, B.; Siuzdak, G. Chem. Bio. Chem. **2004**, 5, 258-260.
(7)   Karas, M.; Bachmann, D.; Bahr, U.; Hillenkamp, F. Int. J. Mass Spectrom. Ion Proc. **1987**, 78, 53-68.
(8)   Fenn, J. B.; Mann, M.; Meng, C. K.; Wong, S. F.; Whitehouse, C. M. Science **1989**, 246, 64-71.
(9)   Yamashita, M.; Fenn, J. B. J. Phys. Chem. **1984**, 88, 4451-4459.
(10)   Fenn, J. B. Int. J. Mass Spectrom. **2000**, 200, 459-478.
(11)   Marshall, A. G.; Hendrickson, C. L.; Jackson, G. S. Mass Spectrom. Rev. **1998**, 17, 1-35.
(12)   Kleinnijenhuis, A. J.; Mihalca, R.; Heeren, R. M. A.; Heck, A. J. R. Int. J. Mass Spectrom. **2006**, 253, 217-224.

Chapter 1

Fourier Transform Ion Cyclotron Resonance Mass Spectrometry

1.1   FTICR-MS basics. Principle of operation

Fourier Transform Ion Cyclotron Resonance Mass Spectrometry (FTICR-MS) is a technique that combines magnetic and electric fields to measure the molecular weight of the molecules in the gas phase. In the field of mass spectrometry, FTICR-MS combines different fragmentation techniques and can perform measurements with unmatched high mass resolution and high mass accuracy. FTICR-MS has its roots in the 1930`s when for the first time the ion cyclotron resonance phenomenon was used to accelerate protons at high kinetic energies for nuclear physics experiments [1]. At late 1940`s Sommerfeld *et al.* incorporate ICR technique in mass spectrometry to determine the Faraday constant by measuring the cyclotron resonance frequency of protons [2,3]. Three decades ago Marshall and Comisarow reported the first practical implementation of the Fourier transformation algorithm to the image charge detection of the cyclotron motion of the ions [4]. This development represented a novelty in mass spectrometry and the technique was termed Fourier Transform Ion Cyclotron Resonance Mass Spectrometry or shortly FTICR-MS. The next paragraphs of this chapter will introduce the basic concepts of FTICR-MS with an emphasis to the experimental procedures used for the work described in this thesis. More detailed introductions to this technique can be found elsewhere [5-8].

1.1.1 Ion motion in the cyclotron cell

The heart of the FTICR-MS is the ion cyclotron resonance (ICR) cell which is a Penning trap placed in the centre of a super-conducting magnet bore. The role of the ICR cell is threefold: to trap, manipulate and detect the ions of interest. Because the magnetic field is homogenous along the ICR cell an ion with non-zero kinetic energy in the *x* and *y* direction will be forced to follow a cyclotron motion in the *xy*-plane; the magnetic field is considered to be parallel with *z* axis. Two opposing trapping electrodes are used to create a potential well in order to confine the ion cloud and to avoid ion loss along the *z*-axis (fig.1.1).
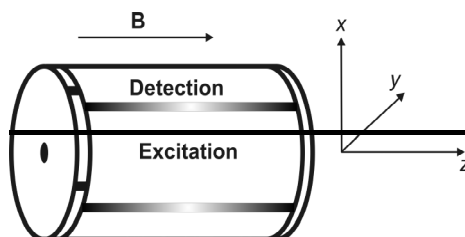
Figure 1.1: A schematic of the closed cylindrical cell. It consists of two trapping plates with a small inlet hole and two pairs of opposite electrodes, one for excitation and one for detection.

Several designs for the ICR cell have been studied and reported in literature such as rectangular [9], cubic [10,11] and cylindrical cells [12]. The undesired loss of ions along the z-axis was minimised with the introduction of the "infinity" cell [13]. A disadvantage of this ICR cell is that it has a limited access for ion introduction. When an open-ended cell [14-16] was proposed and implemented, the ion trapping became much easier because in this ICR cell design the front electrode hole has a diameter of approximately 6 cm. Other geometries for ICR traps are currently studied to minimize ion losses, to improve ion axial confinement and to produce nearly linear ion excitation/detection.

When an ion with charge q and speed v enters the ICR cell it experiences the combined force of the magnetic field B and the electrostatic trapping field E. The sum of the electric and magnetic forces that acts on the ion is given by the Lorentz force equation (eq. 1.1):

$$F_L = qE + q(v \times B) \quad (1.1)$$

If the electrostatic force is negligible, the magnitude of the Lorentz force is given by the charge, speed and the magnetic field strength. As can be seen from equation 1.1 the Lorentz force is perpendicular to the ion velocity and to the magnetic field strength B. The Lorentz force is equilibrated by the centripetal force oriented in opposite direction (fig. 1.2).
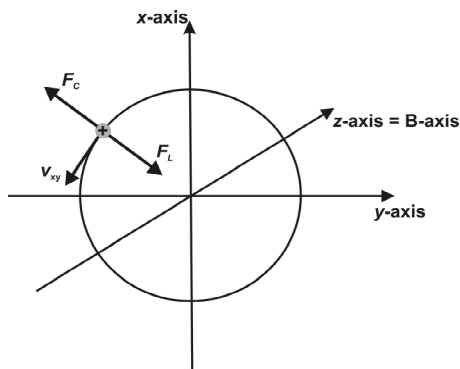
Figure 1.2: The cyclotron motion of an ion. The ion velocity perpendicular to the uniform magnetic field generates a Lorentz force (perpendicular to both) which forces the ion to move on a circular orbit.

Hence, the magnetic field bends the trajectory of the ion into a circle of radius r perpendicular to the magnetic field being mathematically expressed by equation 1.2:

$$qv_{xy}B = mv^2_{xy}/r \quad (1.2)$$

It should be mentioned that the Lorentz force changes just the direction of the velocity v_{xy} but not its magnitude. Defining the angular frequency ω_c as v_{xy}/r we obtain from equation 1.2 that for a given value of the magnetic field strength ω_c is dependent only by the mass and the charge of the ion (eq. 1.3):

$$\omega_c = qB/m \text{ or } \nu_c = qB/2\pi m \quad (1.3)$$

where $\nu_c = \omega_c/2\pi$ is the cyclotron frequency. The second observation is that ν_c is independent of the velocity of the ions and thus independent of the kinetic energy of the ions and the cyclotron radius. This is particularly important for FTICR-MS because, contrary to other mass spectrometric methods the spread in kinetic energy of the ions does not limit the mass resolution during FTICR-MS analysis.

Until now, the contribution of the trapping potential was neglected in eq. 1.3 but it can have a significant influence on the cyclotron motion and that's why it should be considered.

In a common FTICR-MS set-up, the ions are usually produced in an external ion source and transported into the ICR cell. Using ion optics, they will enter the ICR cell with some initial kinetic energy and in order to trap them, they have to be decelerated. This could be achieved either by using the retarding field produced by the trapping plates in so called gated trapping [17,18], by sidekick trapping [19] or through multiple collisions of the ions with a neutral gas (e.g. Ar), method known as gas-assisted dynamic ion trapping (GADT) [20]. Even if gated trapping is the simplest way to trap the ions, this method is not efficient enough to trap ions with wide energy and *m/z* ranges. To increase the trapping efficiency, GADT and sidekick trapping are used. However, using GADT requires introduction of a cooling gas evacuation delay which significantly extends the length of the experimental sequence. Sidekick trapping uses the deflection of the ion beam from the main axis of the instrument during introduction in to the ICR cell. In this way, the ions are trapped by the higher electrostatic potential present around the cell axis. Ions are confined inside the ICR cell and their trajectory inside the ICR trap is dependent on the amplitude of the sidekick voltage and other experimental parameters (ion energy, *m/z* ratio, introduction angle, ion coordinate). This method has the

advantages of fast trapping of ions with wide range of energy and mass-to-charge ratios. The major drawback of this trapping technique is that the ion cloud is displaced from the axis that makes ion detection to be less efficient.

Positive voltages are applied to the trapping plates to trap positive ions while for negative ions the trapping voltages are negative. The potential well keeps the ions in a trapping motion, back and forth, along the z-axis with a trapping frequency ω_T, given by equation 1.4:

$$\omega_T = \sqrt{\frac{qV_T}{md}} \qquad (1.4)$$

where V_T is the potential applied to the trapping electrodes and d is the length of the ICR cell. The radial field produced by the trapping potentials is $E=V_T r/2d^2$ and in opposite direction to the inward-directed Lorentz force. With this electric field component equation 1.1 becomes:

$$m\omega^2 r = qB\omega r - q(V_T R/2d^2) \qquad (1.5)$$

which is a quadratic equation with two distinct solutions:

$$\omega_+ = \frac{c}{2} + \sqrt{\left(\frac{c}{2}\right)^2 - \frac{z^2}{2}} \qquad (1.6)$$

$$\omega_- = \frac{c}{2} - \sqrt{\left(\frac{c}{2}\right)^2 - \frac{z^2}{2}} \qquad (1.7)$$

where ω_Z is the "trapping" oscillation frequency ($\omega_Z=\omega_T$) and ω_C is the "unperturbed" cyclotron frequency. These two solutions show that the trapping potential has two effects on the ions motion: first, it reduces the cyclotron frequency and secondly forces the ions to follow a periodic motion at low frequency, called

magnetron motion. ω_+ is the reduced cyclotron frequency and falls in the range 5 kHz – 5 MHz for a 7T magnet, which corresponds to a mass range between 100 Da and 70 kDa. ω_- is the magnetron frequency and is in the order of 1-100 Hz.

1.1.2 Ion excitation and detection in FTICR-MS

Mass determination in FTICR-MS is based on the relationship that exists between the *m/z* ratio of the ions and their cyclotron frequency (eq. 1.3 and 1.7). Even if the ions in static magnetic field move on cyclotron orbits this will not generate any signal on the ICR detection plates because the radius of the motion is very small and the ions move incoherently. In order to collect a signal it is necessary to move the ion cloud, that is situated on the ICR cell axis, close to the detection plates to induce an image current which is then recorded and digitized [6]. The ions must be excited to a coherent motion to obtain a measurable signal. Ions without a coherent motion can not be detected. Incoherency comes from random distribution of the phase and radius of the ion that enter the cell. Hence, a radio-frequency (rf) electric field, which excites the ions to a coherent motion, precedes the detection event. The form of the rf pulse has the form (eq. 1.8):

$$\mathbf{E}(t) = E_0 \cos\omega_C t \, \mathbf{j} = \frac{\alpha V_{PP}}{d} \cos\omega_C t \, \mathbf{j} \qquad (1.8)$$

where α is the geometrical constant of the ICR cell, **j** is the unit vector and V_{PP} is the peak-to-peak amplitude of the rf excitation pulse. This linearly polarised electric field could be expressed as the sum of two counter-rotating components, $\mathbf{E}_L(t)$ and $\mathbf{E}_R(t)$ (eq. 1.9 a and b):

$$\mathbf{E}_L(t) = \frac{E_0}{2} \cos\omega_C t \, \mathbf{j} - \frac{E_0}{2} \sin\omega_C t \, \mathbf{i} \qquad (1.9 \text{ a})$$

$$\mathbf{E}_R(t) = \frac{E_0}{2} \cos\omega_C t \, \mathbf{j} + \frac{E_0}{2} \sin\omega_C t \, \mathbf{i} \qquad (1.9\ b)$$

The radiofrequency component $\mathbf{E}_R(t)$ rotates the ions in the same sense and at the same frequency by pushing the ions continuously to a higher orbit. The second component, $\mathbf{E}_L(t)$, rotate the ions in an opposite sense but is 2ω off-resonance and will not have an effect on the ions orbit. During excitation time ($t_{exc.}$) the ions absorb energy and the radius of their orbit increases. If all the excitation energy is converted into kinetic energy ($A(t_{exc.}) = E_0^2 \, q^2 t_{exc.}/4m$) the final radius of the ions orbit becomes:

$$r = \frac{E_0 t_{exc.}}{2B_0} \qquad (1.10)$$

This equation (1.10) shows that the ions are excited to the same final radius independently of their mass or charge. Such a uniform excitation is achieved by applying a Stored Waveform Inverse Fourier Transform (SWIFT) [21] pulse which was introduced by Marshall in 1985 [22]. In SWIFT the amplitude and frequency range is specified and with an inverse Fourier transformation the excitation time domain pulse is calculated. The time domain excitation pulse is modulated in amplitude using a quadratic phase scrambling method. Ion excitation could also be performed with constant amplitude with so-called sweep or chirp excitation pulse. These are sinusoidal waveforms, whose frequency linearly changes in time.

For on-resonance frequencies the ions will absorb energy and will increase their orbit radius following an out warded spiral motion as long as the rf-excitation signal is applied. Thus, the cyclotron orbit radius increases until the radius is close to the dimensions of the ICR cell. The excitation signal is applied until the cyclotron radius of the ions becomes slightly smaller then the radius of the ICR cell. This coherent packet of ions induces an image charge in the detection plates. The detection plates are opposed to each other and positioned coaxially and at the same radius between the excitation plates as shown in figure 1.1. Because the ions will

periodically pass in front of the detection electrodes, an alternating potential will be induced and detected. This will produce an alternating image current. The frequency of this current is identical to the cyclotron frequency of the ions. This weak image current is amplified and converted into a voltage signal that gives the following time domain signal f(t):

$$f(t) = \sum_{i=1}^{M} N_i e^{-\frac{t}{\tau_i}} \cos(\omega_i t + \varphi_i) \quad (1.11)$$

where t is the length (in seconds) of the transient, ω_i is the cyclotron frequency of the ions, N_i is the number of ions *i* and φ_i the phase of the ions. Collisions with the background gas and charge repulsion will result in a dephasing of the coherent ion motion and a decrease of the orbit radius. As a result, the time domain signal intensity will decrease with the damping constant τ_i. The final resolution of the mass spectrum is dependent on the length of the transient. An example of the time domain signal is presented in fig. 1.3.

The time-domain signal (fig. 1.3 a) shows a clear decay and represents the sum of the individual sinusoidal signals of all ions. The time-domain signal is then Fourier transformed to obtain a frequency spectrum. By using eq. 1.3 the mass spectrum is calibrated (fig. 1.3 b). Unlike other mass spectrometric methods (with the exception of the recently introduced Orbitrap) the detection in FTICR-MS is non-destructive which allows reuse the ions after detection.

Summing N repeating spectra improves the signal-to-noise ratio with a factor of $N^{1/2}$. Another excitation pulse is needed to remove undesired ions from the ICR cell. This pulse is applied to the trapping plates to axially eject the residual ions out of the cell.
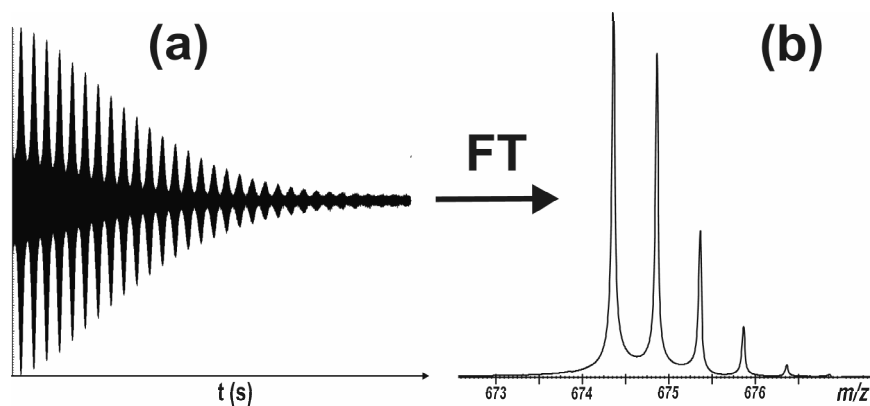
Figure 1.3 Left, (a), time domain transient measured at a magnetic field of 7T for the 2+ charge state of substance P (MW = 1347.83) and right, (b), mass spectrum of the [M+2H]$^{2+}$ isotope peaks obtained by Fourier transformation of the time domain signal.

1.2   FTICR-MS experimental set-up

1.2.1 Sequence of events

Different instrumental FTICR-MS set-ups have been reported in literature [23-25]. In principle the majority of the FTICR-MS configurations consists of three main parts: the ion source, the ion transport system and the trapping and detection region. Ions generated in the ion source are transported using electrostatic lenses or multipoles to the ICR cell where they are trapped and detected to record a MS spectrum. Alternatively, the trapped ions can be subjected to MS/MS procedures. Therefore, an FTICR-MS experiment implies a scenario with several steps separated in time. An example of such an experimental sequence that contains consecutive events is presented in figure 1.4.

First, a quench pulse is applied to the ICR cell in order to empty the cell from all residual ions followed by introduction of the ions of interest. In many cases, ion selection precedes the dissociation event. After formation of the dissociation products, the ion cloud is excited to a higher cyclotron radius and subsequently detected. The obtained signal is digitally stored and subjected to Fourier-

transformation, which finally results in a mass spectrum. For a multiple scan measurement, this succession of events is repeated several times. The total time for a MS experiment with such an experimental sequence depends on the time involved in each of these events, the type of instrument and the analysis required. When ion trapping is performed without a collision gas the duration for an FTICR-MS experiment is approximately 1s. If GADT is required, a pump delay is needed to pump away the neutral gas therefore extending the experimental sequence to several seconds.
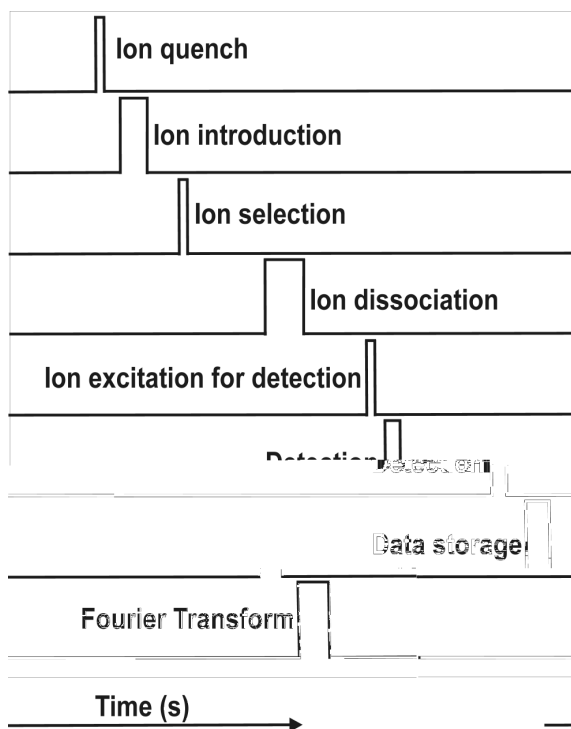
Figure 1.4 A typical experimental sequence used in FTICR mass spectrometry

1.2.2 Ionization techniques

Ion production from solid, liquid or gas-phase samples is a key factor in any MS analysis. This could be performed either in the ICR cell or in an external ion source coupled to an ion transfer system. With the external ion source, the ions are produced outside of the ICR cell, which requires introduction of a differential pumping stage between analyzing cell and the ion source for high resolution measurements. Another advantage of the external ion source is the flexibility to use different types of ion sources for ion production and different ion optical elements to store and/or select ion population prior to mass spectrometric analysis. In the early stage, molecular ionization in mass spectrometry was realized by electron impact (EI) through irradiation of a volatilized sample with 70eV electron beam. The main drawback of EI is that only volatile, low molecular weight compounds can be analysed. This makes EI unsuitable for biological samples containing biomolecules with relatively high molecular weight and containing labile modifications. Several soft ionization techniques using high electric fields [26,27], plasmas [28], laser irradiation [29,30] and particle bombardment [31,32] have been employed for this purpose in the past. Two ionization techniques, electrospray ionization (ESI) [27,33,34] and matrix-assisted laser desorption ionization (MALDI) [30] are currently applied in modern mass spectrometry to study macromolecular, non-volatile and thermally labile compounds (Figure 1.5). With MALDI, the sample is desorbed and ionized from a dry crystalline matrix through irradiation with laser pulses producing mainly singly charged ions. In MALDI ion production occurs as discrete events and if mass analysis is synchronized with ion generation small amount of sample is needed. This results in a high MALDI sensitivity that allows mass spectral data to be obtained from sub-femtomole ($< 10^{15}$ moles) sample. Moreover, quite recently MALDI was used to ionize peptides and proteins directly from a cell [35] or a tissue [36]. Compared to MALDI, ESI produces ions in continuous mode by spraying a sample solution through a capillary kept at typically 1-3 kV. The magnitude of the voltages applied to the capillary is dependent on the solvent which is used and the inner diameter of the capillary. In general, capillaries with higher inner diameter and

solvents with higher boiling points require higher voltages. Depending on the polarity of the applied voltage positive or negative ions are formed. Sometimes, the ESI process is enhanced by using a coaxial gasflow (e.g. N_2) to facilitate the nebulization process. Using ESI large molecules can be detected in low m/z region due to multiple charging and low fragmentation. The "soft" nature of ESI enabled non-covalently bound biomolecular species to be ionized intact. Moreover, ESI offers the possibility to couple liquid chromatographic techniques with different types of mass spectrometers facilitating rapid and thorough investigation of complicated biological mixtures. These advantages made ESI one of the most applied ionization techniques in proteomics. Despite of these remarkable features, two notable shortcomings are attributed to ESI: consumption of appreciable amount of sample and ion suppression caused by solutions containing high salt concentration or high-concentration analytes that can suppress ion formation from lower-concentration analytes.

The ESI source used in this thesis was designed and constructed in-house and set to work in positive ion mode (Figure 1.5). Positively charged ions were obtained by applying 1000-3000 V potential difference between the spray needle (PicoTip^{TM} Emitter, New Objective Inc., Woburn, MA, USA) and the inlet of the mass spectrometer. This potential difference creates an electric field that forces the liquid at the tip of the needle to adopt a Taylor cone where charge separation take place through an electrophoretic mechanism. A nebula of charged droplets enters the instrument through a stainlees steel capillary, which is surrounded by a ceramic heated tube maintained at ~200^0 C to enhance evaporation of the solvent.

When the repulsive coulombic forces between charges exceed the surface tension, the droplet will explode in smaller droplets. This process continues until the (macro)molecule is transferred to the gas phase and charged with one or more cations. The ions produced by ESI are focused by a tube lens through a skimmer into an octopole ion trap for accumulation and subsequently transferred to the ICR cell.
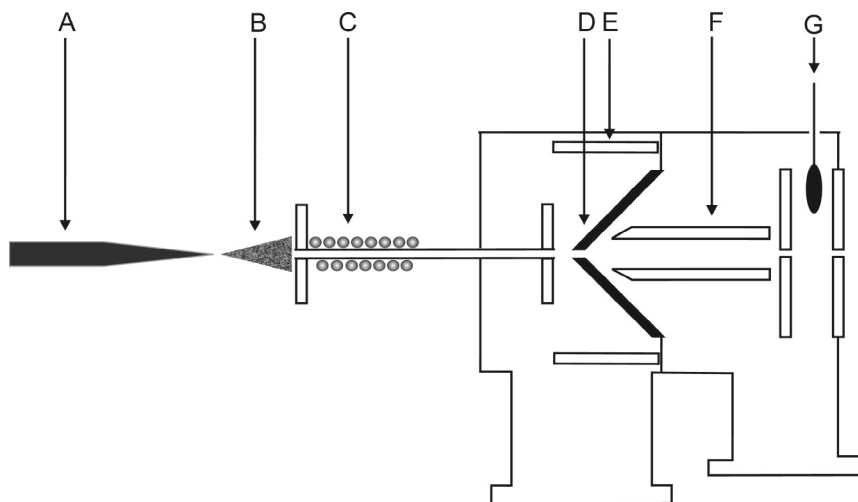
Figure 1.5 An electrospray ion source: (A) capillary needle; (B) spray cone; (C) heated capillary; (D) skimmer; (E) tube lens; (F) octopole; (G) pneumatically-actuated electrode

1.2.3 Ion transfer

External ionization sources generate ions outside of the strong-field region of the magnet and hence a guiding system is necessary to transport and introduce the ions into the ICR cell. Therefore, the guiding system must force the ions to move through the magnetic field gradient, which acts as a "magnetic mirror", towards the ICR cell. However, efficient transfer of the ions from an external ion source into the ICR cell faces serious problems [37,38]. One of these issues is that while travelling through the inhomogeneous fringe field of the magnet the ions interact with the radial component of the magnetic field. As a result, the axial velocity of the ions is converted into a radial component and eventually ions with low kinetic energy, which enter the fringe field at sufficiently large angles, will be reflected. Therefore, the ions should be injected along the fringe field lines in order to nullify the radial component of the ions velocity. Several approaches reported in literature to guide the ions from an external ion source through the magnetic field gradient include electrostatic lenses [39-41], quadrupole ion guides [42,43], octopole ion

guides [44,45] or electrostatic ion guides [46-48]. Multipole ion guides can also be used for ion accumulation and dissociation by so called multipole storage assisted dissociation (MSAD) [49] or by laser assisted or collision assisted dissociation [50].

Low pressure required by FTICR-MS is supplied in our set-up by a vacuum system including five differential pumping stages. The first vacuum pump establishes a pressure of approximately 1 mbar in the nozzle-skimmer region. The second pumping stage further decreases the pressure in the accumulation octopole to ~10^{-2} mbar. Insertion of such an accumulation octopole in the ion optics increases the sensitivity of the instrument and the transfer efficiency of ions to the ICR cell [51]. A retractable current probe is placed in front of the octopole ion trap to tune the ion source independently of the rest of the instrument. We found that this addition significantly helps ion optical tuning. From the accumulation octopole the ions are transported to the ICR cell via electrostatic lenses, gate valves and two quadrupole ion guides [52,53]. A third vacuum pump assures a pressure of 10^{-5} mbar in the region of the 1st quadrupole. Ions enter the 2nd quadrupole region (pressure is ~10^{-7} mbar) where they are guided further in to the ICR cell. The fifth pump establishes a pressure in the ICR cell of approximately 10^{-10} – 10^{-9} mbar.

1.2.4 Ion trapping and detection

Several ICR traps with different geometries were developed in the last decades ranging from trapped-ion cell (1970) [9] until the matrix-shimmed ICR trap (1999) [54]. A more detailed description of different ICR cells could be found elsewhere [55].

Among these, two types of ICR cells were used for the work described in this thesis, namely the "infinity" cell [13] and the open cell [14,15]. For the "infinity" cells the end caps consists of segmented plates in order to linearize the excitation potential. The main advantage of the infinity cell is that the trapping potentials are lower than for the open-ended cell. A Bruker Infinity^{TM} cell was used for the chapter 4, 5 and 6 of this thesis (Figure 1.6 (a)).
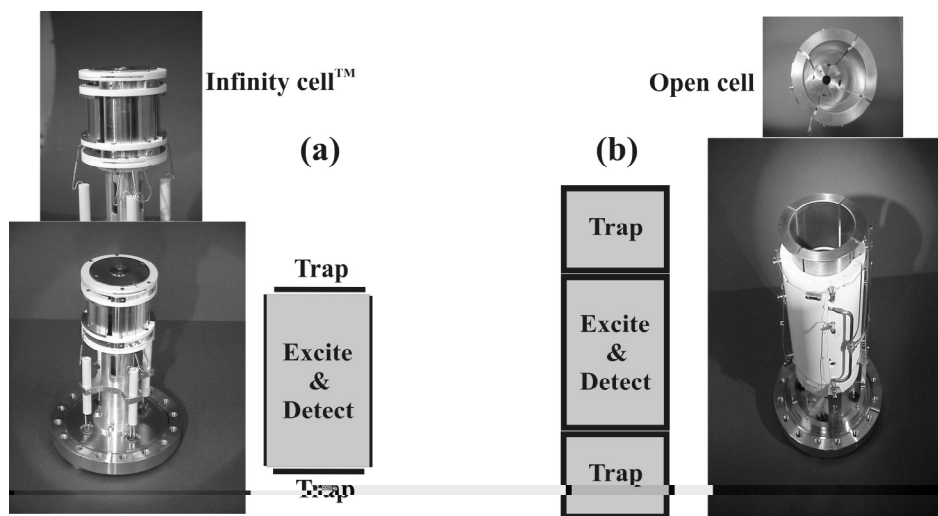
Figure 1.6 Two types of ICR cells: (a) the Infinity[TM] cell and (b) the in-house made capacitively coupled open ended cell.

The measurements for chapter 3 were performed with a home-made capacitively coupled open-ended cell (Figure 1.6 (b)) [56]. The electrodes of the cell are made from copper and are surrounded by a ceramic jacket embedded with a heating element and a cooling pipe. This jacket is electrically shielded from the ICR electrodes to prevent noise from the heater current. Liquid nitrogen was used as cooling agent to cool down the ICR cell, at low flow rates during quite long intervals (4-6 hours) to reach low temperatures (100-86 K). The role of the jacket is to assure a spatially uniform cooling/heating of the ICR cell. The temperature was measured with a Pt 100 temperature sensor inserted in the ceramic wall. During one measurement, the temperature was kept at nearly constant value (3 K variation). Such an open cell with heating and cooling facility enables the study of mechanistic aspects of ion reactions in the gas-phase. An advantage of an open-ended cell is that allows the trapping of off-axis ions thereby increasing the sensitivity for external ion sources. For both ICR cells ion trapping could be enhanced by raising the trapping voltages during ion introduction (gated trapping) or by introduction of a collision gas (e.g. Ar) at 10^{-6} mbar prior to ion introduction to kinetically cool down the ions (gas assisted trapping).

1.3 Mass spectrometry

1.3.1 Sequence of events

FTICR-MS has the ability to combine different dissociation techniques to enable ion reaction mechanistic studies or to probe the structural features of the (bio)molecules in gas-phase. This kind of studies requires a succession of different MS procedures applied at certain time intervals or simultaneously. An example of a standard experimental sequence for an MS/MS experiment is presented in figure 1.7.
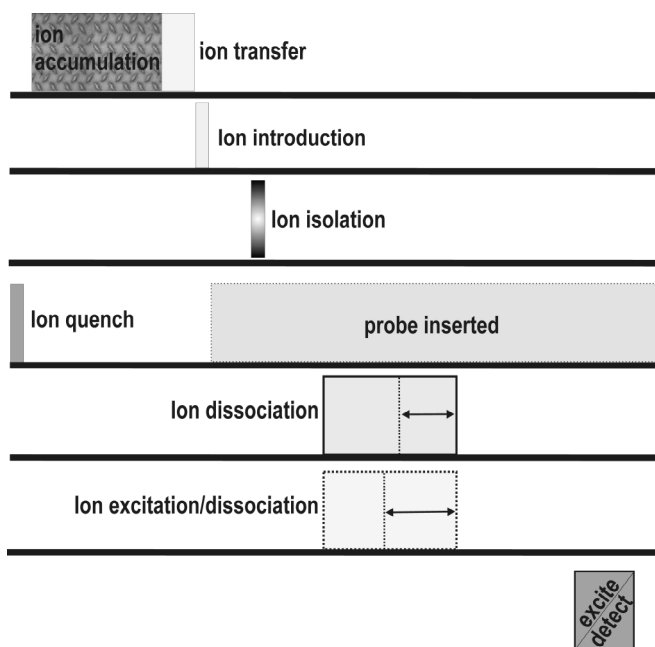
Figure 1.7 Schematic of an MS experimental sequence using a combination of two dissociation techniques (e.g. ECD and IRMPD).

After the ions are trapped using Ar as trapping gas, a delay is necessary before ion selection to reduce the pressure to 10^{-8} – 10^{-9} mbar. When the trapping event was made without gas, ion selection can be performed immediately after ion introduction thereby shortening the total length of the experimental sequence. Ion

isolation is made with a tailor made isolation pulse generated by an in-house constructed arbitrary waveform generator (AWG) [57]. All the ions are ejected from the cell except the ion(s) of interest. The ion(s) left in the cell are subsequently exposed to different fragmentation techniques or gas-phase chemical reactions and the sequence ends with detection of the reaction products.

1.3.2 Fragmentation methods (CID, SORI, IRMPD, ECD, SID)

Information on peptides and proteins can be obtained by accurately measuring their masses indicating, for instance, the amino acid composition or the presence of posttranslational modifications. A more detailed structural insight, however, requires MS/MS. As stated before, in MS/MS a precursor ion is first isolated and subsequently subjected to different dissociation techniques. The resulting MS/MS spectra contain a collection of dissociation products at different m/z values and intensities. In general, MS/MS is aimed at the structural characterization of a peptide/protein. Sequence information is obtained in MS/MS through cleavage of the peptide backbone. There are three predominant cleavages along the peptide backbone which could occur in MS/MS. If the charge is retained on the N-terminal site the fragments will be referred to *a*, *b* or *c* and if the C-terminal site carry the charge the fragments will be noted as *x*, *y* or *z*. Thus, these backbone fragments are complementary, *a/x*, *b/y* and *c/z*, and follows the nomenclature proposed by Biemann [58] and Roepstorff [59] (see Figure 1.8).
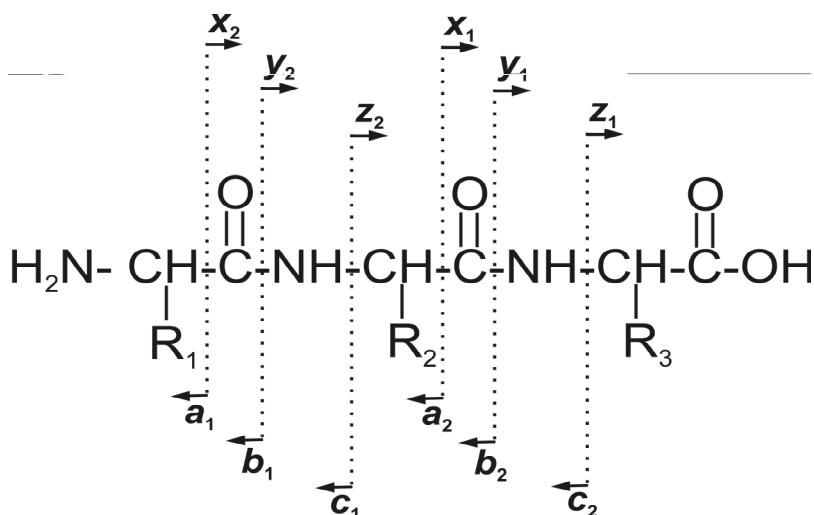
Figure 1.8. The nomenclature used for peptide backbone fragmentation. *a*, *b* and *c* are N-terminal fragments; *x*, *y* and *z* are C-terminal fragments

This nomenclature was used in this thesis for chapters 3 and 4 and a slightly adapted one for chapters 5, 6 and 7.

One of the major concerns in proteomics is to find strategies for fast and accurate determination of a peptide sequence. To achieve this goal the peptide backbone should be cleaved at many positions for unambiguous sequence assignment. Multiple cleavages can result in production of consecutive backbone fragments allowing the position and identity of the amino acids to be exactly specified. As an example, the mass difference between the b_n and $b_{(n-1)}$ ions is the mass of an amino acid at the nth position from the N-terminus.

Several tandem MS techniques have been developed to obtain high sequence coverage. The most used are Collision-Induced Dissociation (CID, also referred to as Collisionally Activated Dissociation (CAD) [60,61]), Sustained Off-resonance Induced Dissociation (SORI-CID) [61,62], InfraRed MultiPhoton Dissociation (IRMPD) [63,64], Surface Induced Dissociation (SID) [65, 66] and Electron Capture Dissociation (ECD) [67-71].

With collision-based dissociation techniques, the selected ion is kinetically excited with an rf pulse, on- or slightly off-resonance with the cyclotron frequency of

the ion. This will increase the kinetic energy of the ion. The duration and amplitude of the excitation pulse determines the kinetic energy of the ion. A part of the kinetic energy is converted in to internal energy by collisions with neutral atoms or molecules of the collision gas. Fragmentation occurs when the internal energy of the ion reaches the dissociation threshold. When on-resonance excitation is used, the ions are kinetically excited to higher orbit radius and collision with the target gas take place. Two major drawbacks derive from on-resonance CID. First, some time delay is needed for relaxation of the excited ions and for pumping out the collision gas. The second one is that fragmentation occurs far from the centre of the cell that makes the detection of the reaction products less efficient. In addition, it has been shown that on resonance excitation distorts the ion cloud thereby reducing the time domain data and lowering the mass resolving power of the instrument [61].

Off-resonance collision induced dissociation (SORI-CID) overcomes this drawback. SORI uses a low amplitude rf pulse which is 1000-1500 Hz off-resonance compared with the cyclotron frequency of the isolated ion. Compared with on-resonance excitation, the SORI pulse is alternately in- and out of phase and thus the ion is continuously (sustained) excited and de-excited. Therefore, the cyclotron orbit in SORI expands and shrinks periodically (fig. 1.9).

Modulation of the kinetic energy with SORI could be made for seconds whereas in on-resonance excitation this requires less then half a millisecond. A SORI excitation pulse is kept at low amplitude in order to produce fragmentation close to the axis of the ICR cell for efficient detection. Another advantage of SORI-CID is that the collision energy is much lower then in on-resonance CID that allows the study of the lowest fragmentation pathway.

Even if both, on-resonance CID and SORI-CID are known to produce efficient fragmentation they share some drawbacks such as introduction of a collision gas, unintentional excitation and ejection of dissociation products and distortions of isotopic distribution.
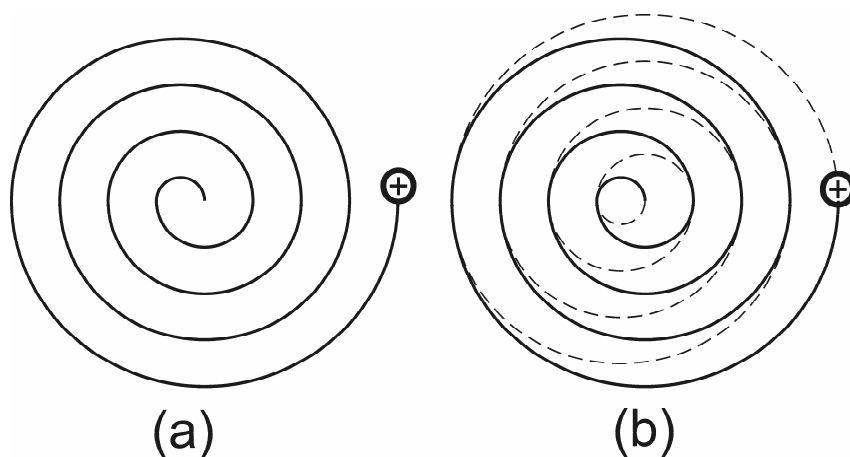
Figure 1.9: Time evolution of ion trajectory in (a) on-resonance and (b) sustained off-resonance irradiation (SORI). Note that the average SORI radius is substantially smaller compared to the on-resonance excitation.

Within the frame of collision-based dissociation techniques, surface induced dissociation (SID) is distinguished from the first two (on-resonance CID and SORI-CID) by the fact that is based on ion-surface impact thereby increasing almost instantaneously the ion's internal energy in only one single collision [72]. The SID fragmentation efficiency is dependent on the size of the precursor ion, and as no collision gas or rf excitation is used, the acquisition time for an MS/MS experiment is significantly shorter than for on-resonance CID or SORI-CID. Recent time- and energy-resolved studies made with SID on small peptides highlight the potential of this technique for detailed energetic and mechanistic studies [73,74].

Other modalities to vibrationally excite and dissociate gas-phase ions are based on photon irradiation. In IRMPD for instance, ion activation is established by irradiation of the ion cloud with a continuous or pulsed infrared laser beam. Multiple absorptions of infrared photons lead to an increase of internal energy until the dissociation limit is reached. This technique is especially suited for FTICR-MS because no excitation pulse and no collision gas are needed that considerably reduces the duty cycle. In addition, in IRMPD, all selected ions could be simultaneously excited and the dissociation fragments are produced close to the

cell axis. IRMPD could be combined with electron capture dissociation (ECD) to improve the information content of the MS/MS spectra.

1.4   Data analysis tools

The development of new mass spectrometry techniques together with the demand for protein biomarker discovery have led to a tremendous increase in the number, size and rate of mass spectrometry data. To extract useful information from such a huge data collection, a set of processing and data mining tools have been developed and implemented in proteomics in last decade. An important direction in proteomics is to develop new high-throughput technologies and computing machinery that enable rapid and accurate interpretation of the data those technologies produces. Their role is not just to enable data acquisition but also to organize, analyse and query the data base. Therefore, beside instrumental equipment and investigational techniques, a third pillar of proteomics is the data analysis software. A common requirement for these informational tools is high-throughput to permit rapid interpretation of comprehensive mass spectral data. As a consequence, the impact of informatics in proteomics resulted in formation of a distinctive field in proteomics which is known as infoproteomics with the role to develop new methods for interpreting spectral data. Beside the speed of analysis, these proteomics dedicated software should be flexible in performing trustfully qualitative and quantitative analysis, as well. In a first step, a qualitative analysis includes peptide identification using well known software modules like Mascot[TM][75], Sequest[TM][76], Pepsea[TM][77], THRASH [78] or X!Tandem[TM][79] followed by reconstruction of the protein sequence. Quite recently, based on the method called "peptide mass fingerprinting" [77], a new software, Aldente[TM][80], was proposed and made available by Swiss Institute of Bioinformatics on the ExPASy website [81]. All these programmes use a search engine approach within the acquired mass spectra should match the mass spectra from an acquired data base-derived spectra. However, in many situations, such a correlation could not be found or these spectra are mismatched. To overcome these problems, several ideas have been

advanced based on improved scoring schemes [82], filtering of bad spectra [83] and exploring peptide libraries [84]. A second step is quantification of the assigned peptides and proteins. This analysis is dependent by the analysis tools chosen to process and compare spectral data. Two approaches are currently used in quantitative proteomics: one based on isotope-tagging methods and another one which use the absolute ion intensity [85,86]. Both approaches reduce the MS experimental time and are essential for applying proteomics in drug and disease research.

References

(1)   Lawrence, E. O.; Livingston, M. S. Phys. Rev. **1932**, 40, 19-35.
(2)   Hipple, J. A.; Sommer, H.; Thomas, H. A. Phys. Rev. **1949**, 76, 1877-1878.
(3)   Sommer, H.; Thomas, H. A.; Hipple, J. A. Phys. Rev. **1951**, 82, 697-702.
(4)   Comisarow, M. B.; Marshall, A. G. Chem. Phys. Lett. **1974**, 25, 282-283.
(5)   Marshall, A. G.; Verdun, F. R. **1990**.
(6)   Marshall, A. G.; Hendrickson, C. L.; Jackson, G. S. Mass Spectrom. Rev. **1998**, 17, 1-35.
(7)   Marshall, A. G. Int. J. Mass Spectrom. **2000**, 200, 331-356.
(8)   Amster, I. J. J. Mass Spectrom. **1996**, 31, 1325-1337.
(9)   McIver Jr, R. T. Rev. Scient. Instr. **1970**, 41, 555-558.
(10)   Comisarow, M. B. Int. J. Mass Spectrom. Ion Proc. **1981**, 37, 251-257.
(11)   Comisarow, M. B. Adv. Mass Spectrom. **1980**, 8, 1698-1706.
(12)   Comisarow, M. B.; Marshall, A. G. In USA patent **1976**, 3, 937, 955.
(13)   Caravatti, P.; Allemann, M. Org. Mass Spectrom. **1991**, 26, 514-518.
(14)   Gabrielse, G.; Haarsma, L.; Rolston, S. L. Int. J. Mass Spectrom. Ion Proc. **1989**, 88, 319-332.
(15)   Beu, S. C.; Laude, D. A. J. Anal. Chem. **1992a**, 64, 177-180.
(16)   Beu, S. C.; Laude, D. A. J. Int. J. Mass Spectrom. Ion Proc. **1992b**, 112, 215-230.
(17)   Gorshkov, M. V.; Guan, S.; Marshall, A. G. Rapid Comm. Mass Spectrom. **1992**, 6, 166-172.
(18)   Gorshkov, M. V.; Masselon, C. D.; Anderson, G. A.; Udseth, H. R.; Smith, R. D. Rapid Comm. Mass Spectrom. **2001**, 15, 1558-1561.
(19)   Rakov, V. S.; Futrell, J. H.; Denisov, E. V.; Nikolaev, E. N. Eur. J. Mass Spectrom. **2000**, 6, 299-317.
(20)   Tsybin, Y. O.; Witt, M.; Baykut, G.; Hakansson, P. Rapid Comm. Mass Spectrom. **2004**, 18, 1607-1613.
(21)   Guan, S.; Marshall, A. G. Int. J. Mass Spectrom. Ion Proc. **1996**, 157/158, 5-37.
(22)   Marshall, A. G.; Wang, T. C.; Ricca, T. L. J. Am. Chem. Soc. **1985**, 107, 7893-7897.

(23)   Marshall, A. G.; Guan, S. Nuclear Instr. Meth. Phys. Res. A **1995**, *363*, 397-405.

(24)   Belov, M. E.; Gorshkov, M. V.; Udseth, H. R.; Anderson, G. A.; Tolmachev, R. D.; Prior, D. C.; Harkewicz, R.; Smith, R. D. J. Am. Soc. Mass Spectrom. **2000**, *11*, 19-23.

(25)   O`Connor, P. B.; Pittman, J. L.; Thomson, B. A.; Budnik, B. A.; Cournoyer, J. C.; Jebanathirajah, J.; Lin, C.; Moyer, S.; Zhao, C. Rapid Comm. Mass Spectrom. **2006**, *20*, 259-266.

(26)   Beckey, H. D. Pergamon Press, Oxford **1977**.

(27)   Fenn, J. B.; Mann, M.; Meng, C. K.; Wong, S. F.; Whitehouse, C. M. Science **1989**, *246*, 64-71.

(28)   Macfarlane, R. D.; Torgerson, D. F. Science **1976**, *191*, 920.

(29)   Cotter, R. J. Anal. Chim. Acta **1987**, *195*, 45-49.

(30)   Karas, M.; Bachmann, D.; Bahr, U.; Hillenkamp, F. Int. J. Mass Spectrom. Ion Proc. **1987**, *78*, 53-68.

(31)   Barber, M.; Bordoli, R. S.; Sedgwick, R. S.; Tyler, A. N. J. Chem. Soc. Chem. Commun. **1981**, 325-327.

(32)   Benninghoven, A.; Sichtermann, W. K. Anal. Chem. **1978**, *50*, 1180.

(33)   Yamashita, M.; Fenn, J. B. J. Phys. Chem. **1984**, *88*, 4451-4459.

(34)   Fenn, J. B. Int. J. Mass Spectrom. **2000**, *200*, 459-478.

(35)   Fenselau, C.; Demirev, P. A. Mass Spectrom. Rev. **2001**, *20*, 157-171.

(36)   Caprioli, R. M.; Farmer, T. B.; Gile, J. Anal. Chem. **1997**, *69*, 4751-4760.

(37)   Alford, J. M.; Williams, P. E.; Trevor, D. J.; Smalley, R. E. Int. J. Mass Spectrom. Ion Proc. **1986**, *72*, 33-51.

(38)   Kofel, P.; McMahon, T. B. Int. J. Mass Spectrom. Ion Proc. **1990**, *98*, 1-24.

(39)   Kofel, P.; Allemann, M.; Kellerhals, H.; Wanczek, K. P. Int. J. Mass Spectrom. Ion Proc. **1985**, *65*, 97-103.

(40)   Ijames, C. F.; Markey, S. P. J. Am. Soc. Mass Spectrom. **1994**, *5*, 398-406.

(41)   Kofel, P.; Allemann, M.; Kellerhals, H.; Wanczek, K. P. Int. J. Mass Spectrom. Ion Proc. **1986**, *72*, 53-61.

(42)   McIver Jr, R. T.; Hunter, R. L.; Bowers, W. D. Int. J. Mass Spectrom. Ion Proc. **1985**, *64*, 67-77.

(43)   Lebrilla, C. B.; Amster, I. J.; McIver Jr, R. T. Int. J. Mass Spectrom. Ion Proc. **1989**, *87*, R7-R13.

(44)   Huang, Y.; Guan, S.; Kim, H. S.; Marshall, A. G. Int. J. Mass Spectrom. Ion Proc. **1996**, *152*, 121-133.

(45)   Senko, M. W.; Hendrickson, C. L.; Pasa-Tolic, L.; Marto, J. A.; White, F. M.; Guan, S.; Marshall, A. G. Rapid Comm. Mass Spectrom. **1996**, *10*, 1824-1828.

(46)   Marto, J. A.; Marshall, A. G.; May, M. A.; Limbach, P. A. J. Am. Soc. Mass Spectrom. **1995**, *6*, 936-946.

(47)   Limbach, P. A.; Marshall, A. G.; Wang, M. Int. J. Mass Spectrom. Ion Proc. **1993**, *125*, 135-143.

(48)   Reents Jr., W. D.; Mandich, M. L.; DeSantolo, A. M. Int. J. Mass Spectrom. Ion Proc. **1998**, *177*, 63-81.

(49)   Sannes-Lowery, K. A.; Griffey, R. H.; Kruppa, G. H.; Speir, J. P.; Hofstadler, S. A. Rapid Comm. Mass Spectrom. **1998**, *12*, 1957-1961.

(50)   Hofstadler, S. A.; Sannes-Lowery, K. A.; Griffey, R. H. Anal. Chem. **1999**, 71, 2067-2070.

(51)   Taban, I. M.; McDonnell, L. A.; Rompp, A.; Cerjak, I.; Heeren, R. M. A. Int. J. Mass spectrom. **2005**, 244, 135-143.

(52)   Rompp, A.; Taban, I. M.; Mihalca, R.; Duursma, M. C.; Mize, T. H.; McDonnell, L. A.; Heeren, R. M. A. Eur. J. Mass Spectrom. **2005**, 11, 443-456.

(53)   Mihalca, R.; van der Burgt, Y. E. M.; McDonnell, L. A.; Duursma, M.; Cerjak, I.; Heck, A. J. R.; Heeren, R. M. A. Rapid Comm. Mass Spectrom. **2006**, 20, 1838-1844.

(54)   Jackson, G. S.; White, F. M.; Guan, S.; Marshall, A. G. J. Am. Soc. Mass Spectrom. **1999**, 10, 759-769.

(55)   Guan, S.; Marshall, A. G. Int. J. Mass Spectrom. Ion Proc. **1995**, 146, 261-296.

(56)   Guo, X.; Duursma, M.; Al-Khalili, A.; McDonnell, L. A.; Heeren, R. M. A. Int. J. Mass Spectrom. **2004**, 231, 37-45.

(57)   Mize, T. H.; Taban, I. M.; Duursma, M. C.; Seynen, M.; Konijnenburg, M.; Vijftigschild, A.; Doornik, C. v.; Rooij, G. v.; Heeren, R. M. A. Int. J. Mass spectrom. **2004**, 235, 243-253.

(58)   Biemann, K. Biomed. Environ. Mass Spectrom. **1988**, 16, 99-111.

(59)   Roepstorff, P.; Fohlman, J. Biomed. Mass Spectrom. **1984**, 11, 11.

(60)   Dienes, T.; Pastor, S. J.; Schurch, S.; Scott, J. R.; Yao, J.; Cui, S. L.; Wilkins, C. L. Mass Spectrom. Rev. **1996**, 15, 163-211.

(61)   Senko, M. W.; Speir, P. J.; McLafferty, F. W. Anal. Chem. **1994**, 66, 2801-2808.

(62)   Gauthier, J. W.; Trautman, T. R.; Jacobsen, D. B. Anal. Chim. Acta **1991**, 246, 211-225.

(63)   Little, D. P.; Spier, P. J.; Senko, M. W.; O'Connor, P. B.; McLafferty, F. W. Anal. Chem. **1994**, 66, 2809-2815.

(64)   Li, W.; Hendrickson, C. L.; Emmet, M. R.; Marshall, A. G. Anal. Chem. **1999**, 71, 4397-4402.

(65)   Ijames, C. F.; Wilkins, C. L. Anal. Chem. **1990**, 62, 1295-1299.

(66)   Chorush, R. A.; Little, D. P.; Beu, S. C.; Wood, T. D.; McLafferty, F. W. Anal. Chem. **1995**, 67, 1042-1046.

(67)   Zubarev, R. A.; Kelleher, N. L.; McLafferty, F. W. J. Am. Chem. Soc. **1998**, 120, 3265.

(68)   Zubarev, R. A.; Horn, D. M.; Fredricksson, E. K.; Kelleher, N. L.; Kruger, N. A.; Lewis, M. A.; Carpenter, B. K.; McLafferty, F. W. Anal. Chem. **2000**, 72, 563-573.

(69)   Zubarev, R. A. Mass Spectrom. Rev. **2003**, 22, 57-77.

(70)   Hakansson, K.; Cooper, H. J.; Emmet, M. R.; Costello, C. E.; Marshall, A. G.; Nilsson, C. L. Anal. Chem. **2001**, 73, 4530-4536.

(71)   Hakansson, K.; Emmett, M. R.; Hendrickson, C. L.; Marshall, A. G. Anal. Chem. **2001**, 73, 3605-3610.

(72)   WysockI, V. H.; Tsaprailis, G.; Smith, L. L.; Breci, L. A. J. Mass Spectrom. **2000**, 35, 1399-1406.

(73)   Bailey, T. H.; Laskin, J.; FutrelL, J. H. Int. J. Mass Spectrom. **2003**, 222, 313-327.

(74)   Laskin, J.; Futrell, J. H. J. Am. Soc. Mass Spectrom. **2003**, 14, 1340-1347.

(75)   Perkins, D. N.; Pappin, D. J. C.; Creasy, D. M.; Cottrell, J. S. Electrophoresis **1999**, 20, 3551-3567.

(76)   Yates, J. R.; Eng, J. K.; McCormack, A. L.; Schielts, D. Anal. Chem. **1995**, 67, 1426-1436.

(77)   Mann, M.; Hojrup, P.; Roepstorff, P. Biol. Mass Spectrom. **1993**, 22, 338-345.

(78)   Horn, D. M.; Zubarev, R. A.; McLafferty, F. W. J. Am. Soc. Mass Spectrom. **2000**, 11, 320-332.

(79)   Craig, R.; Beavis, R. C. Bioinf. **2004**, 20, 1466-1467.

(80)   Tuloup, M.; Hernandez, C.; Coro, I.; Hoogland, C.; Binz, P. A.; Appel, R. D. Swiss proteomics Society 2003 Congress [Fontis Media] **2003**, 174-176.

(81)   Gasteiger, E.; Hoogland, C.; Gattiger, A.; Duvaud, S.; Wilkins, M. R.; Appel, R. D.; Bairoch, A. In: The proteomics protocols handbook **2005**, New Jersey: Humana Press, 571-607.

(82)   Nesvizhskii, A. I.; Keller, A.; Kolker, E.; Aebersold, R. Anal. Chem. **2003**, 75, 4646-4658.

(83)   Flikka, K.; Martens, L.; Vanderkerckhoe, J.; Gevaert, K.; Eidhammer, I. Proteomics **2006**, 6, 2086-2094.

(84)   Craig, R.; Cortens, J. P.; Beavis, R. C. Rapid Comm. Mass Spectrom. **2005**, 19, 1844-1850.

(85)   Gygi, S. P.; Rist, B.; Gerber, S. A.; Turecek, F.; Gelb, M. H.; Aebersold, R. Nature Biotech. **1999**, 17, 994-999.

(86)   Silva, J. C.; Denny, R.; Dorschel, C. A.; Gorenstein, M.; Kass, I. J.; Li, G. Z.; McKenna, T.; Nold, M. J.; Richardson, K.; Young, P.; Geromanos, S. Anal. Chem. **2005**, 77, 2187-2200.

Chapter 2

Electron Capture Dissociation

2.1 Mass spectrometry techniques to study the gas-phase conformers

Mass spectrometry based proteomics requires transfer of biomolecules from liquid or solid phase into the gas phase. The advent of MALDI and ESI enables the transfer of large intact biomolecules to the gas-phase. The gentle nature of these two techniques opened new ways to investigate protein folding and their binding reactions in the absence of a solvent. The relevance of studying the conformation (three-dimensional structure) of the biological molecules in gas-phase has been debated. Clearly, the natural mode of action of a protein occurs in a solution under certain physiological conditions. It is expected that under these conditions the interaction of peptides/proteins with water, the hydrogen bonding and electrostatic interaction play a significant role in determining the conformation of a peptide or protein. This conformation is pivotal for its biological activity. To assess to which extent the solvent contributes to protein structure, it is important to characterize the molecular conformation, either in an aqueous solution or in a solvent-free environment. In addition, the study of gas-phase peptides and proteins offers the possibility to investigate the effect of the intrinsic intramolecular forces on the molecular conformation. Protein conformation has been extensively studied in the condensed phase with techniques like X-ray crystallography [1], nuclear magnetic resonance (NMR) spectroscopy [2-4], circular dichroism [5] and hydrogen exchange [6,7]. Compared with the large amount of knowledge of protein conformation in condensed phase, little is known about the conformation of proteins in gas phase. This is caused mainly by the lack of techniques to study the molecular architecture of the proteins in the gas-phase. Some mass spectrometric

techniques including hydrogen/deuterium exchange [8] and collision cross-section [9] measurement have been used to study proteins conformation in gas-phase. However, the data obtained by using these methods provide limited structural details and sometime spectral data contains ambiguous information. Bowers [10,11], Jarrold [12] and co-workers developed a new technique called ion mobility mass spectrometry to facilitate conformational studies. Here, a mass spectrometer is used to select a peptide/protein based on their *m*/*z* value, which is then transferred to an ion mobility spectrometer. Ion mobility instruments can differentiate peptide and protein structural isomers in the gas phase and provide accurate measurements of their collision cross section. Selected ion conformers can be further subjected to structural studies in a second mass spectrometer. Even if ion mobility produces valuable information, the internal energy of the ions could be increased through successive collisions with the neutral gas from the drift cell. This influences their conformation and leads to an increase of the conformational heterogeneity.

Based on differences in fragmentation pattern, Wu *et al.* showed for the first time that SORI-CID can be used to probe protein's conformation [13]. A shortcoming of this technique is that does not produce extensive fragmentation for disulfide-bridged peptides/proteins, thereby limiting the informational content to the molecular region that does not include the disulfide bond. However, as it will be shown in chapter 5 of this thesis, the disulfide bond containing peptides can be extensively sequenced with SORI-CID when they are complexed with divalent metal cations.

A method which showed a remarkable potential for sequencing peptides and proteins that contain intramolecular disulfide linkages is electron capture dissociation (ECD) [14,15]. The gentle nature of this technique made ECD an efficient tool to study proteins with labile modifications [16] and to probe secondary and tertiary structures of gaseous protein ions [17]. Therefore, ECD is a useful technique to probe conformational heterogeneity of biomolecular ions in gas-phase (see chapter 3). The following paragraphs of this chapter will give an overview of the history of ECD and will highlight its features that make this dissociation technique a powerful tool for proteomics and conformational analysis.

2.2   A brief history of electron capture dissociation
2.2.1   Dissociative recombination

Dissociation of positive gas phase molecular ions following electron capture has been observed previous to ECD. In 1931, Kaplan [18] attributed the green line (557.7 nm) observed by Campbell [19] in the night sky to the formation of the excited O (^{1}S) through the dissociation of $O_2^{+\bullet}$ molecules following one electron capture. Bates and Massey confirmed this and even nowadays, this reaction is still under observation in heavy-ion storage rings. A part of the electron recombination energy is used for dissociation. This phenomenon was termed dissociative recombination (DR) and is supposed to be responsible for a wide range of phenomena in astrophysics and plasmas, such as formation of water and organic molecules in outer space and the conversion of electrical energy in chemical energy during the ignition of gasoline in the spark engines. Even if DR shows many similarities with ECD, there are two significant differences between them. A major dissimilarity is based on the charge difference involved in these two phenomena: ECD uses multiply charged ions while DR is usually performed on singly charged cations. Another difference is that, in ECD, the intermediate species are often radical cations while in DR the electron parity of the precursor ion rarely represents a concern.

Another ECD related phenomenon was reported in 1986 by Beynon *et al.* [20] in a decomposition study of benzene $C_6H_6^{2+}$ using ion-neutral collision experiment in a magnetic sector mass spectrometer. The reaction led to unusual fragmentation pattern and was explained by electron capture from the neutral gas molecules, which actually produced the observed dissociation. The technique was called electron capture induced decomposition (ECID) and showed promising application to isomer-differentiating studies [21] but was soon abandoned due to difficulties to use in practice.

2.2.2 ECD discovery

The pioneering years of ECD started with the work of Guan *et al.* [22] in photodissociation of multiply protonated melittin and ubiquitin cations using irradiation with a 193 nm ultraviolet (UV) laser. They observed not just charge reduction of the isolated precursor but also unusual *c* and *z* fragments that provided sequence information. This was quite unexpected because CID [23-25] and IRMPD [26,27] applied to peptides and proteins produces mainly *b* and *y* fragment ions. Charge reduction of the precursor ion was an indication that electrons reacted with the parent cation. The low-energy electrons in this case were thought to be produced by the UV laser heating the walls of the ICR cell. A further step was made by Zubarev *et al.* [14] by adding two extra electrodes outside the ion cell electrodes. When these outside electrodes were kept at positive potential, the UV laser irradiation of the trapped $[M+11H]^{11+}$ ubiquitin ions produced just *b* and *y* ions not *c* and *z*. When the potential applied to these electrodes was negative (e.g. −1 V), the spectra contained *c* and *z* ions along with the $[M+11H]^{10+}$ molecular ions. Because the $[M+11H]^{10+}$ ions are 1 Da heavier then the $[M+10H]^{10+}$ this shows that the initial (11+) molecular cation captured one electron that reduced the charge from 11+ to 10+. Such an observation is consistent with the fact that secondary electrons produced by the UV laser hitting the edge of the electrode react with the ubiquitin ions causing charge reduction and/or amine bond cleavages that leads to the formation of *c/z* fragments. It was clear from this experiment that not the UV photons but the low energy electrons were the cause for the generation of the *c* and *z* fragments. When a directly heated filament, placed at the backside of the ICR cell, was used as a source of electrons, instead of the UV laser, the production of *c* and *z* ions and the number of cleavage sites (sequence coverage) significantly increased. Thus, a new dissociation technique called electron capture dissociation (ECD) was born.

Several characteristic features of ECD kept peoples attention from the beginning. One of these is that the type of the fragment ions produced in ECD is fundamentally different from those obtained using other conventional dissociation techniques. Moreover, the cleavage sites in ECD are often complementary to those

produced in IRMPD making the combination of these two techniques a powerful tool for peptides and proteins studies. Another advantage of ECD is that exhibits less backbone cleavages selectivity compared to CID generating more extensive sequence coverage.

2.3   ECD in protonated species – fundamental aspects

Extended sequence coverage from peptides/proteins that contain mono and/or disulfide–bridges is difficult to obtain due to the high activation energy necessary to cleave these bonds. With ECD it has been shown that not just disulfide-bridges but also thioether bonds are selectively cleaved [15,28]. Even though the mechanism of ECD has been investigated both theoretically and experimentally, there are still many open questions. Cumulative knowledge from different experimental approaches proposed a cleavage mechanism based on the "hot hydrogen" model [14] that postulates electron capture at the solvated proton followed by transfer of the H$^\bullet$ to the sites with high hydrogen radical affinity like carbonyl oxygens, sulfide bonds, or tryptophan residues to induce cleavage. A theoretical contribution to the study of the ECD mechanism suggests that electron capture leads to a high-n Rydberg state that could cross with dissociative states [29,30].

2.3.1 The electron capture event

The first condition to maximize the electron capture efficiency is to increase the electron capture cross section. For a given flux of electrons, the electron capture cross section is inversely proportional with the speed of the electron:

$$\sigma_{ECD} \approx \frac{v_{e-i}}{n_e.V_e} \qquad (2.1)$$

where $\nu_{e\text{-}i}$ is the frequency of a single ion collision with electrons, n_e is the concentration of electrons and V_e is the electron velocity.

Increase of electron capture cross section can be achieved by using low-energy electrons (i.e.: electron's kinetic energy < 0.2 eV) which leads to an increase of fragment ion abundances (figure 2.1) [31,32].
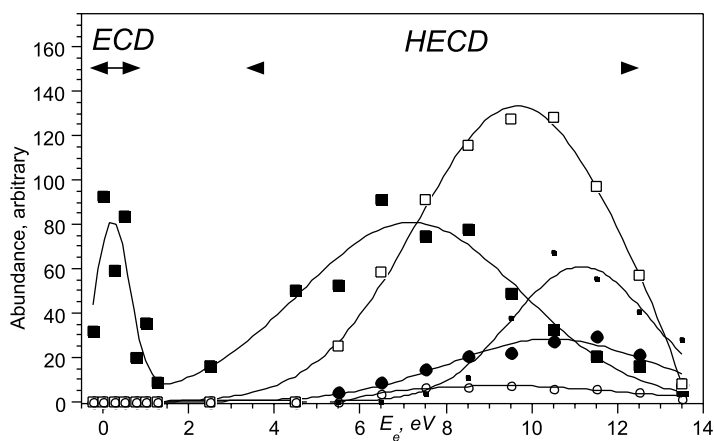
Figure 2.1 Fragment ion abundances versus electron energy E_e for 250 ms irradiation of molecular cations of the SRP peptide: 2+ ion, ■ N-C bond cleavages, □ peptide C-N cleavage, o $z_4^{+\bullet}$ fragments, ● $w_4^{+\bullet}$ fragments; 1+ ion, ▪ peptide C-N bond cleavage. Reproduced with permission from reference 32.

On the other hand the electron capture cross section increases with the square of the charge [31]. Another aspect is the landing site of the electron on the ion. Because electron – ion interaction is primarily Coulombic, the most likely case is that the electron will be captured by a proton. Electron capture could also occur at the adjacent NH group that has high gas-phase basicity and in this case, the electron capture event is followed by prompt dissociation. The third possibility is the electron capture by other positively charged groups. Thus, the electron could be captured far from the location of the proton with subsequent transfer of the electron to the

sites with the highest gas-phase basicity which leads to the formation of a hydrogen radical. Formation of the H• was observed experimentally by H• loss from charge-reduced species. The electron capture process proceeds through a series of Rydberg states together with a conversion of the recombination energy into vibrational energy or dissipation through photon emission. However, the Coulombic recombination energy is insufficient to cause any type of fragmentation if the energy is distributed into all vibrational modes of the molecule, suggesting that ECD proceeds via a non-ergodic mechanism [33,44].

2.3.2 The recombination energy

Electron capture results in release of a certain amount of recombination energy into the molecule. An estimation of the recombination energy (RE) depends on the ionization energy (IE) of the hydrogen atom, the proton affinity (PA) of the molecule with (n-1) protons and the hydrogen affinity (HA) of the molecule with (n-1) protons:

$$\text{RE} = 13.6 \text{ eV} - \text{PA } [M+(n-1)H]^{(n-1)+} + \text{HA } [M+(n-1)H]^{(n-1)+} \qquad (2.2)$$

The proton affinity has values between 8 and 10.6 eV while the hydrogen affinity of the even-electron species is typically less than 1 eV. Several estimations of the recombination energy between an electron and a solvated proton in a typical peptide have been reported in literature. These values lie in the range of 5–7 eV for a multiply protonated protein according to McLafferty *et al.* [34] or in the range of 4-7 eV accordingly to Zubarev *et al.* [33]. Theoretical calculations made by Turecek *et al.* [35] using doubly charged peptide ions give a value for the ion-electron recombination energy of 4.1 eV to form an ammonium radical in ground state. If this recombination energy follows an internally vibrational redistribution, the energy per degree of freedom would not be enough to cleave the N-C_α bound. However, the fact that ECD leads to the cleavage of the N-C_α bond points to a very localized phenomenon.

This is consistent with the fact that the labile groups from modified peptides are preserved in ECD. The observation that labile groups like PTM`s are not lost in ECD and the fact that high sequence coverage is obtained for large polypeptides without cleavage selectivity lead to the idea that ECD is a non-ergodic process. Non-ergodicity means that the cleavage occurs before intramolecular vibration energy redistribution. In spite of many experimental evidence that supports this statement a theoretical study made by Turecek [36] indicates that $N-C_{\alpha}$ bond cleavages in peptide ketyl radicals and cation-radicals are extremely facile reactions. This makes it unnecessary to invoke non-ergodicity in order to explain the cleavage of strong $N-C_{\alpha}$ bonds while the weak ones are kept intact.

2.3.3 $N-C_{\alpha}$ bond cleavage

Comparative with other dissociation methods that use infrared or collisional activation to generate *b* and *y* fragments, in electron capture dissociation mainly *c·* and *z·* ions are formed due to the cleavage of the $N-C_{\alpha}$ bond (scheme 3.1). Mainly two reasons explain why ECD does not lead to the scission of the peptide bond. The first one is that the peptide-bond cleavage during vibrational excitation occurs through intermediates which require a long time (up to milliseconds) [37] to be formed. Therefore, in this case, peptide-bond fragmentation is an ergodic process. Compared with vibrational excitation, ECD is supposed to occur on a time scale less then 10^{-12} s, which implies instant backbone scission (a non-ergodic behaviour). A second reason is based on the mechanism of the ECD. While in vibrational excitation the ions are even-electron species, in ECD fragmentation occurs through intermediates that are hydrogen-abundant radical cations. Theoretical calculations shows that capture of the hydrogen radical by the carbonyl oxygen form transient species which have a low activation barrier [36,38].
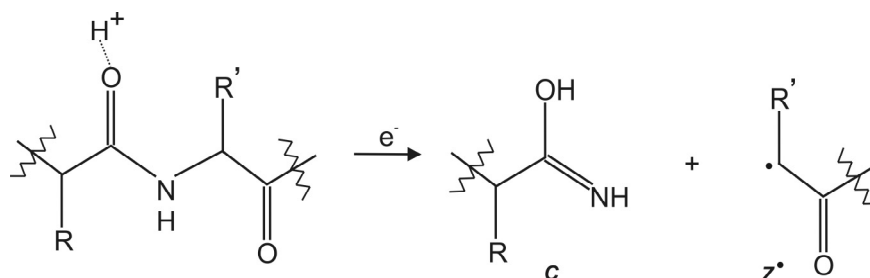
Scheme 3.1: The formation of *c* and *z*[•] fragment ions in protonated species

Alternatively, the hydrogen radical can be captured by the amide nitrogen to form hypervalent species which fragments without an energy barrier [39]. Experimental evidence, which supports this mechanism, is the observation of ECD fragments with addition of a hydrogen atom.

Theoretical attempts to elucidate the mechanism of ECD investigated the role of the positive charge in this mechanism. A computational study made by Simons at al. showed that Coulombic stabilization of the peptide amide π^* orbitals by protons or other positive charges makes them favourable for exothermic electron attachment followed by cleavage of the nearby N-C$_\alpha$ bond [30]. Syrstad and Turecek explored recently the effects of positive charge on the properties of ammonium and amide radicals in order to clarify the energetics of ECD. Based on computational results, they proposed the amide superbase mechanism in which the presence of the proton increases the electron affinity of the amide group and leads to exothermic electron capture to form a long-lived electronic state of a valence type. The captured electron increases the basicity of the amide carbonyl oxygen that can exothermically abstract a proton from an amino acid residue to form an aminoketyl radical that immediately dissociates through N-C$_\alpha$ cleavage. These authors also suggest that the amide superbase mechanism can act in conjunction with a hot hydrogen atom like mechanism. Even some experimental results can be explained with the proposed scenarios for N-C$_\alpha$ cleavage the mechanism of electron capture dissociation still remains a hotly debated subject [15,33,40].

2.3.4   Disulfide bond cleavage

A unique feature of ECD is that it extensively cleaves disulfide bonds in proteins. For many years, the presence of disulfide bonds represented a major obstacle in MS^n to achieve high sequence coverage [41]. Zubarev *et al.* showed that the most abundant fragments produced in ECD corresponds to the cleavage of the disulfide bonds with retention of the hydrogen atom on these fragments (scheme 3.2) [15].

$$H^\bullet$$
$$R-S-S-R' \longrightarrow R-SH \ + \ {}^\bullet S-R'$$
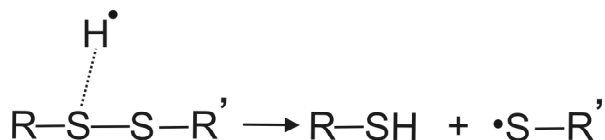
Scheme 3.2: The mechanism of disulfide bond cleavage in ECD.

Recently, it has been demonstrated that ECD of lantibiotics results in peptide backbone fragments and abundant dissociation products corresponding to the scission of the monosulfide bridge which allows their localization [28]. Because the proton affinity of the monosulfide group is 1 eV lower than that of the carbonyl group, the efficient cleavage of the disulfide bond can be explained by its higher $H^\bullet$ affinity. The presence of the radical site and the exothermicity of proton neutralization and $H^\bullet$ capture leads to disulfide bond cleavage. Direct electron capture to the S-S link is unlikely and therefore the S-S cleavage seems to be due to high $H^\bullet$ affinity [15]. Another possible explanation for preferred disulfide bond cleavage in ECD was proposed by Brauman [ref 23 in [15]]. The electron is captured on a high-n Rydberg state, which is expected to be long-lived. This intermediary state has a favourable intersystem crossing state with an S-S dissociative state. The proposal advanced by Brauman is still under further investigation.

2.3.5 Other cleavages observed in ECD

Another possibility, which can result from electron capture of the protonated amide nitrogen, is the formation of *y* fragments and unstable *b*˙ species that subsequently lose CO and forms *a*˙ ions (scheme 3.3). Abundant CO losses from doubly protonated *b* ions subjected to ECD have been reported by Haselmann *et al.* [42]
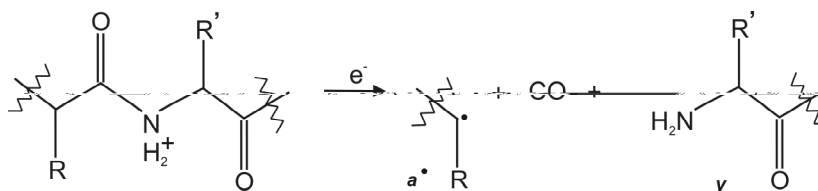
Scheme 3.3: The formation of *a*˙ and *y* fragment ions in protonated species. R and R' correspond to side chain group of a specific aminoacid.

ECD spectra usually are dominated by *c* and *z* type fragments, however, in some cases quite abundant *b* ions could be found in these spectra. A recent investigation of the causes which determine the presence of *b* ions in ECD spectra concluded that both charge carrier and peptide structure are responsible for this unexpected fragmentation pathway [43].

A particularity of ECD is that it does not lead to the formation of abundant internal fragmentation. This facilitates interpretation of ECD spectra because cleavage of the peptide/protein backbone release only fragments which contains one of the termini. On the other hand, generation of internal fragments would require secondary backbone scission. This has lower probability for occurence because the charge reduced species has an electron capture cross section that is considerably lower. However, secondary cleavages have been reported in ECD of linear [44] and cyclic peptides [45] under the form of side chain losses from the primary backbone fragments, *c* and *z*˙ ions from cleavage of the proline residue or loss of

backbone regions from cyclic peptides. Secondary cleavages in ECD are usually attributed to the formation of radical sites through electron capture. These odd-electron species easily dissociate because they are much more unstable than even-electron species.

The practical utility of producing secondary fragments resides in their diagnostic value. For instance, the group of professor Zubarev showed that that secondary fragmentation produced in ECD could lead to the formation of *w*-type ions in the fragmentation pattern which allows to distinguish isomeric residues such as Ile and Leu [32,44,46]. Moreover, fine tuning of the experimental parameters like electron energy, flux and irradiation time can greatly enhance secondary fragmentation [47,48].

Other types of dissociation products, currently observed in ECD, are the result of the cleavages in the side chains of amino acids and leads to neutral mass losses. These could be generated either from primary or secondary cleavages. Investigation of the identity of side chain losses associated neutral losses of 44 Da, 59 Da and 101 Da to the presence of arginine in the amino acid composition of the protein while C_3H_6S and $C_4H_{11}N$ are indicative for the presence of methionine and lysine, respectively. Other characteristic neutral losses are $C_4H_6N_2$ for histidine and CH_3NO for asparagine/glutamine [49]. Their diagnostic value has been confirmed on several peptides having the aforementioned amino acids at different position in the peptide sequence. This non-negligible pathway following ECD can help the analyst to correctly assign the amino acid composition of an unknown peptide/protein.

2.4   ECD applied to proteomics

All the ECD features described above contribute to the increase of sequence coverage, a requirement highly demanded by proteomics. Application of ECD to the field of proteomics was then a straightforward step. Folding and unfolding studies have also been performed using ECD [50,51].

In addition to proteomics, ECD has been used to "sequence" polyethylene glycols [52], peptide nucleic acids [53], polyglycols [54], polyester amide oligomers[55] and oligodeoxynucleotides [56].

The ECD experimental work on different biomolecular species modified by the addition of labile groups revealed another remarkable feature of this dissociation technique. ECD has been shown to retain labile modifications and therefore is extremely useful in identifying and localizing post-translational modifications (PTM`s). Biomolecules that contain PTM`s are wide spread in nature and in some cases they have been associated with different diseases. Using conventional dissociation methods these labile modifications are preferentially lost when the internal energy of the ion population is increased to induce cleavages. This makes it difficult to determine their location. The fact that PTM`s are preserved during ECD lead to the assumption that ECD is a non-ergodic dissociation technique (i.e. the cleavage occurs before the recombination energy is completely randomized all over the molecule) [14]. However, theoretical studies showed that it is not necessary to invoke non-ergodicity in ECD because N-C_α bond cleavage is extremely facile in peptide ketyl radicals and cation-radicals [36,38]. There is still an ongoing debate on mechanistic and energetic aspects of ECD.

Experimental work on fundamental aspects of ECD is presented in chapter 3. Fundamental research, both theoretical and experimental, tries to provide a better understanding of the phenomena involved in ECD in order to enable its application to structural studies.

2.4.1 ECD of protonated (poly)peptides

Understanding the structure and functions of peptides and proteins at cellular level is one of the main goals of proteomics. Such studies lead to a better understanding of the cell function and help researchers to better address different diseases of present day concern (Alzheimer, Parkinson, cancer, etc.). To learn more about the molecular background of diseases it is needed to characterize different levels of proteins in the cell including posttranslational modifications,

protein complexes, and proteins conformation. Posttranslational modifications are associated with many diseases. Accumulation of knowledge about the presence or location of the PTM can have diagnostic and therapeutic implications. Conventional methods currently applied in MS/MS produce fragmentation through collision with a target or by multiple photon absorptions. Slow heating techniques can identify the labile modifications through specific mass losses but hardly can establish PTM`s location. ECD has been proven to be a useful technique to study these modified peptides and proteins.

ECD applied to peptides and proteins can produce abundant $[M+nH]^{(n-1)+\bullet}$ ions. These are precursor ions that capture one electron and do not dissociate. It could also be backbone fragments, linked together through non-covalent bonds (see paragraph 2.5.2). A dissociation channel frequently observed in ECD spectra corresponds to small neutral losses from these charged species. $H^{\bullet}$ or NH_3 losses from $[M+nH]^{(n-1)+\bullet}$ ions are quite abundant in ECD spectra and in some cases can be even the major product ions [57,58]. In general, the most intense fragments in ECD correspond to the cleavage of the $N-C_{\alpha}$ bond which results in *c* and *z* type fragments [14]. A minor fragmentation channel in ECD of peptides and proteins is the formation of *a*$^{\bullet}$ and *y* fragment ions. Even if ECD results in extensive sequence coverage, usually this does not include the cleavage of N-terminal site of proline [14]. In one unusual case, *c*/*z*$^{\bullet}$ fragments from the proline residue have been reported in literature [59]. Unexpectedly, ECD of cyclic peptides and proteins produce backbone fragments upon a single electron capture [45,60]. An explanation for this observation was given by O`Connor *et al.* based on a radical reaction cascade mechanism [45]. They postulated that the primary cleavage generates α-carbon radical site which propagates along the protein backbone and initiates series of free radical rearrangements which cause backbone and side chain cleavages. Another particularity of ECD is the preferential cleavage of the C-terminus to tryptophan residues [59].

2.4.2 ECD on intact proteins and protein complexes

These remarkable features mentioned above makes ECD an ideal technique for top-down proteomics. Using ECD, McLafferty *et al.* obtained extensive sequence coverage: 75 out of 103 interresidue bonds were cleaved for cytochrome c and 67 out of 75 for ubiquitin [31]. Another structural study reported complete sequence coverage for two proteins of 1.3 and 2.2 kDa [61]. Similar behaviour has been observed for smaller proteins with a less compact structure [62]. For other bigger proteins, application of ECD only results in abundant charge reduced species without significant backbone fragments. McLafferty proposed that ECD in fact cleaves the peptide backbone but the backbone fragments are kept together by intramolecular non-covalent interactions. Nevertheless, a recent ECD study in our group on non-covalent gp31 co-chaperonin complex containing 21 protons shows a preferential cleavage of the non-covalent bond. Such an observation is in contrast with the commonly known ECD behaviour (i.e: preservation of non-covalent bonds) and indicates that the conformation of the protein plays a crucial role in ECD [63].

To circumvent non-covalent bonding of backbone fragments, the ions subjected to electron irradiation are heated before, during, or after ECD to destroy their higher order structure. This technique is known as activated ion – electron capture dissociation (AI-ECD) and include activation with a nitrogen gas pulse, infrared irradiation, and blackbody irradiation [64]. Several studies made on 17, 29, 30 and 42 kDa proteins showed that AI-ECD results in increased sequence coverage compared to ECD without ion activation. For instance, ECD of a 17 kDa protein resulted in the cleavage of the 33 interresidue bonds out of 153 while AI-ECD increased this ratio at 99/153. Horn *et al.* reported a dramatic increase of reaction product abundance using AI-ECD on the 29 kDa protein carbonic anhydrase. ECD alone does not result in any backbone fragmentation of this protein while AI-ECD cleaves at 116 from 256 sites [64]. McLafferty and co-workers developed a variant of this technique by colliding low energy electrons (0.15 – 15 eV) with gas before ion introduction to the ICR cell. The resulting plasma conditions leads to a significant increase in fragmentation efficiency. Under these conditions a

single scan ECD spectra of carbonic anhydrase revealed peaks corresponding to cleavage at 183 from 258 possible sites [65, 66].

ECD is also applicable to study protein folding because of its very fast fragmentation reactions. Hence, the fragments produced in ECD represent a snapshot of the conformational heterogeneity of the gas phase protein ions. The role of conformational heterogeneity on the fragments produced in ECD will be discussed in detail in chapter 3 of this thesis. Other techniques such as CID destroy non-covalent bonding and thereby disrupt gas phase protein structure. Thermal protein unfolding of the 9+ charge state ions of cytochrome c was analyzed by Horn *et al.* by ECD [50]. Monitoring the kinetic intermediates, they showed that unfolding of these ions proceeds through unfolding of up to 13 backbone regions with melting temperatures from $<25^0$ until 140^0 C. Such a dynamic mixture of several conformers that fold through a variety of pathways to the most stable conformers is consistent with both the "folding funnel" model and with the unfolding mechanism via intermediates that partially retains their native structure. Folding and unfolding process was scrutinized by Breuker *et al.* with ECD for 5+ to 13+ charge states of gaseous bovine ubiquitin ions (Figure 2.2) [51]. Their results confirmed the ion mobility studies that suggest that the unfolding is a three-state process in the gas phase.
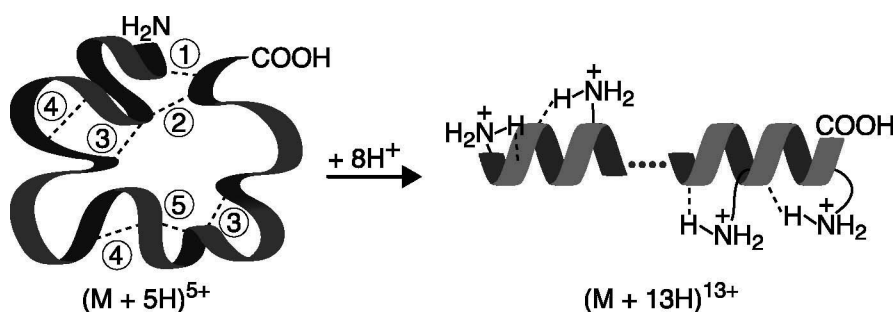

Figure 2.2 Unfolding of the 13+ ubiquitin ions in gas phase. Reproduced with permission from reference 51.

In another study, McLafferty and co-workers, using ECD and photofragment spectroscopy, investigated the influence of the charge state on the protein structure [67]. Those results on ubiquitin gas phase ions indicate that helical structure is predominant in high charge state (10+ to 13+) ions while lower charge states (6+ to 9+) have terminal helical regions arranged antiparallel and non-covalently bounded to a central helix.

2.4.3   Posttranslational modifications studied with ECD

The first application of ECD to the study of labile posttranslational modifications was made by Kelleher *et al.* on 28-residue peptides containing γ-carboxylated glutamic acid residues [68]. IRMPD or CID of these peptides results in ejection of γ-CO_2 moieties before cleavage of the peptide backbone. When ECD was employed, the generated *c* fragments preserved the CO_2 group allowing direct localization of this labile modification. Based on these findings, Niiranen *et al.* succeeded to localize γ-carboxyglumatic acid residues in osteocalcin subforms [69]. ECD can also be used to localize sulfonation in peptides. A 21-mer peptide containing a sulfated cysteine residue showed loss of the sulfate group when subjected to slow heating techniques in MS/MS. In contrast, ECD of the peptide produces some H_2O and H_2SO_3 from the precursor but none from the backbone fragments [16].

ECD was used to study glycosylation that is one of the most prevalent posttranslational modifications. Mirgorodskaya *et al.* investigated several O-glycopeptides using ECD [70]. For each peptide, ECD produced abundant *c* fragments that retained the *N*-acetylgalactosamine (GalNac) group. The *z*$^\bullet$ fragments in general retained the modification and together with the *c* fragments showed that the modification could be mapped by ECD. Later it has been shown by Haselmann *et al*. that ECD applied to a 60 and a 25-residue peptide that contain six GalNAc monosaccharides allowed determine of their location [71]. A less common modification, namely *O*-linked fucosylation was also investigated by ECD. Quite recently, Macek *et al.* demonstrated that ECD is the most suitable technique

for rapid and unambiguous identification of the sites of *O*-fucosylation in modified peptides [72].

Another type of modification is *N*-linked glycosylation that occurs at asparagines residues and is widely present in nature being involved in many biological functions such as cellular recognition. Häkansson *et al.* obtained complementary structural information of an *N*-glycosylated peptide through IRMPD and ECD. IRMPD proved to be of diagnostic value by defining the glycan components and the branching pattern while ECD revealed the peptide sequence and sites of modifications [73,74].

Phosphorylation and dephosphorylation of proteins play a pivotal role in biological systems. Tandem mass spectrometry, including ECD of phosphorylated peptides, allowed facile and unambiguous determination and localization of the phosphorylated amino acids [68,75]. Moreover, AI-ECD provided the first direct characterization of the heterogeneously phosphorylated protein ß-casein (~24 kDa) without the need of enzymatic digestion and subsequent chromatographic separation [76].

2.4.4 ECD applied to peptides complexed with divalent metal cations

Primarily, mass spectrometric studies reported in the literature have been made on protonated species. On the other hand, many biomolecules became biologically active when they form complexes with different metal ions. The ECD literature includes only a few studies on these types of complexes. It is unclear what the ECD mechanism is in these cases. Cerda *et al.* applied for the first time ECD to polyethyleneglycol (PEG) complexed with sodium ions [52]. They showed that ECD of $[PEG_{24}+2Na^+]$ produce backbone fragments but less fragmentation than for doubly protonated PEG_{24}. This indicates that the ECD mechanism in metalated polyethers is similar to that for doubly protonated species. Moreover, the fact that ECD of $[PEG_{24}+2Na^+]$ produces a smaller number of fragments compared to $[PEG_{24}+2H^+]$ is consistent with the fact that sodiated species have a much lower

recombination energy compared with protonated species. Interestingly, ECD spectra of $[PEG_{24}+2Na^+]$ contain also dissociation products that do not incorporate the neutralized Na atom. Zubarev *et al.* in ECD of angiotensin II complexed with Zn^{2+} have observed similar behaviour. Even if far less backbone fragments are produced from this complex compared with ECD of doubly protonated analogue, they are typical ECD fragments, namely *c*, *z*, *a* and *y* [33]. This means that the metal cation serves as original landing site for electron with subsequently transfer of the electron to other parts of the molecule. However, a very different ECD behaviour is observed for cytochrome c 15+ ions that contain a heme group with Fe^{3+}. The region around the heme group containing Fe^{3+} remains immune to ECD and the most intense peak in the spectrum corresponds to $[M+15H]^{14+\bullet}$. CID of the $[M+15H]^{14+\bullet}$ ions yields 13+ ions without the heme group which are more abundant than in the CID spectrum of the $[M+14H]^{14+}$ ions. Another particularity of these spectra is that CID of $[M+15H]^{14+\bullet}$ gave singly charged $[heme+H^+]$ (m=617 Da) while CID of $[M+14H]^{14+}$ gave $heme^+$ (m=616 Da) [31]. These results are consistent with the transfer of the $H^\bullet$ to the heme group followed by fragmentation or can suggest possible electron capture to the Fe^{3+} without further dissociation.

Another aspect, which derives from these results, is related to the location of the metal ion. As will be shown in chapter 3, for protonated species, the ECD cleavages reflect the location of the proton. For metalated species, there are just a few studies that pay attention to the possibility of localizing the metal ion in complexes with ECD. A correlation of the ECD products from $[PEG_{24}+2Na^+]$ ions with the structures proposed by Bowers and coworkers [77], suggest that the ECD products could reflect the original gas phase structure of the ions [52].

For nonapeptide oxytocin complexed with different transition metal cations, there are strikingly different ECD fragmentation patterns compared with that corresponding to ECD of the doubly protonated ions [78]. However, for oxytocin complexes containing Ni^{2+}, Co^{2+} and Zn^{2+} the ECD spectra result in abundant *c*/*z*$^\bullet$ and *a*$^\bullet$/*y* backbone cleavages and ECD characteristic S-S and S-C bond cleavages. A strikingly different situation is observed for $[oxytocin+Cu^{2+}]$ whose ECD spectra display fragments similar with those observed in low-energy ECD.

Therefore, it was proposed that the captured electron is involved in Cu^{2+} reduction to Cu^+. The redistribution of the recombination energy would explain the observed low-energy CID-type fragmentation.

In a recent ECD study made on substance P containing a proton and a divalent metal cation (Mg^{2+}, Ca^{2+}, Sr^{2+}, Ba^{2+} and Mn^{2+}, Fe^{2+}, Co^{2+}, Ni^{2+}, Cu^{2+}, Zn^{2+}), Håkansson *et al.* observed a larger number of product ions than in previous ECD on doubly charged metal-containing peptides. ECD of Mg-Ba, Mn, Fe and Zn-containing complexes produced *c* and *z*• fragments with and without the metal ion. ECD of Co- and Ni-containing complexes produced abundant backbone fragments corresponding to cleavage of the C-terminal methionine residue (probably the metal ion binding site). In a stark contrast with these results, Cu-containing complexes displayed an atypical ECD behaviour through formation of *b* and *y* fragments. They concluded that some of the ECD fragments produced in this type of complexes could be explained both within the hot hydrogen atom mechanism and mechanisms involving electron capture into excited states. They explain the drastically different fragmentation patterns observed for Co, Ni and Cu-complexes based on their higher propensity for nitrogen (as opposed to oxygen) binding. In addition, these results seem to indicate that at least part of the ECD behaviour is correlated with the second ionization energy [40].

2.5 ECD instrumental setups

ECD remains a technique used almost exclusively in FTICR-MS even if attempts exist to implement this technique to other types of mass spectrometres, like radio-frequency (RF) 3D quadrupole ion trap (QIT) [79] or RF linear 2D quadrupole ion trap (QIT) [80]. The main hindrance in ECD implementation to other type of mass spectrometers, as those mentioned above, comes from the fact that for ion traps radio frequency (RF) electrostatic fields are used, instead of static magnetic or electric fields. With this RF fields the thermal energy of the electrons is maintained constant, with respect to the ions, just for a very short period of time (less then a microsecond) and they are not trapped. Therefore, creating ECD

conditions as in FTICR-MS is technically challenging. Experimental evidence has been recently reported with ECD in RF ion trap [79, 80] but the fragmentation efficiency is small compared with ECD performed in FTICR-MS.

Even in FTICR-MS, ECD efficiency, in terms of fragmentation rate, is low compared to the efficiency of other dissociation techniques, like (SORI)-CID, IRMPD or BIRD. The enhancement of ECD efficiency and shortening of the irradiation time still remains the main objectives in instrumental development dedicated to this dissociation technique. In the early years, ECD was performed using a directly heated filament as source of electrons [14]. The electron beam cross-section supplied by this filament is not jus small in diameter ($<< 1$ mm^2) but also the energy of the electrons has more broad distribution due to the variation of the electrical potential along the heated filament. Moreover, with a thin electron beam is hard to obtain a good overlap with the ion cloud. As a consequence obtaining satisfactory ECD spectra in this case requires irradiation times in the range of seconds which makes ECD a rate-limiting step in tandem MS and severely restricts on-line coupling of ECD with chromatographic separation techniques for high throughput proteomics.

A much bigger electron beam is obtained by replacing the directly heated filament with an indirectly heated electron gun (dispenser cathode) [81]. This device has much larger emitting area (> 1 mm^2), which realizes a better overlap between the electron beam and the ion cloud. The energy distribution of the electrons is much narrower as the surface temperature of the cathode is much lower. With this type of electron gun, the ECD efficiency was increased and the irradiation time was brought in the milliseconds time scale [81]. Recently, it has been shown that reflecting electrons through the ICR cell, efficient ECD could be obtained with just 500μs irradiation times and the technique is known as multipass ECD [82]. A further study highlighted the fact that ECD efficiency varies periodically with the magnetron motion of the ion cloud [83].

A factor limiting ECD efficiency is the possibility that the *c* and *z* fragments can be kept together through non-covalent bonding. Pre-excitation of the parent ion through collision activation (CA) or infrared irradiation in order to break these non-covalent bonds reduces the possibilities that the backbone fragments to remain

linked together after the irradiation event. This ion heating before or during ECD also increases the conformation heterogeneity of the ion cloud by denaturing the protein. The technique is known as activated ion ECD (AI-ECD) and has been shown to provide extensive sequence information on both backbone termini [64]. Short irradiation times used in IRMPD and the absence of the collision gas makes the combination between ECD and IRMPD to be the desired option in proteomics because assure high-throughput and extensive sequence coverage. Chapter 4 presents a brief overview of the successful attempts to combine these two dissociation techniques in ICR cell and propose a novel configuration that allows simultaneous introduction of the electron and the infrared beam in the ICR cell using an unmodified indirectly heated electron gun. The high-resolution offered by FTICR-MS instrumentation together with facilities for combined ECD and IRMPD and proteomics dedicated software make such a setup a powerful tool for protein identification and localization of post-translational modifications.

2.6   ECD related processes

So far, ECD is applicable for polycations only because a singly charged cation would neutralize after a single electron capture and therefore could not be detected. Under experimental conditions that use electrons with energies higher then 10 eV, similar to Tandem Ionization Mass Spectrometry (TIMS) [84,85], it has been shown that is possible to induce cleavage of the molecular backbone [86]. In TIMS a second ionization event is accomplished by electron impact of polypeptide cations or dianions that results in $[M+nH]^{(n+1)\bullet}$ radical cations or $[M-2H]^{-\bullet}$ radical anions, respectively. Positively charged radical cations produced by TIMS could subsequently capture low-energy electrons and forms electronically excited $[M+nH]^{n+\bullet}$ ions which rapidly dissociate. This process was termed electron excitation dissociation (EED) and allows the detection of dissociation products from singly protonated precursor ions as such it is applicable to polypeptide ions generated by MALDI. EED produce mainly *a* and *c* ions with the backbone

cleavage sites complementary to those from ECD or CID. A major drawback of EED is its low efficiency due tot the limited production rate of radical dications.

In the case of anionic species, capture of low energy electrons has low probability to occur due to Coulombic repulsion. However, ECD with 10-30 eV electrons applied to the sulphide peptide caerulin dications produced by TIMS resulted in abundant CO_2 and SO_3 losses from the parent ion together with backbone *a*, *c* and *z* fragments that give nearly complete sequence coverage. Most of the fragments retained the sulfate group that allows the determination of their location. It has been shown that production of backbone fragments is more efficient when the energy of the electrons exceeds 20 eV. These energetic electrons induce electron detachment that leads to the creation of holes. Recombination of a hole with one negative charge produces electronic excitation followed by dissociation. The technique was termed electron detachment dissociation (EDD). As in ECD, the fragments produced by EDD retain posttranslational modifications. In addition to *a*, *c* and *z* fragments produced with EDD, also internal fragments are formed indicating the deposition of a significant amount of internal energy. Although EDD is a promising technique for structural studies of labile species, the fragmentation efficiency is low.

Electronic excitation of multiply charged cations could also be initiated in ECD when the energy of the electrons is higher then 1 eV. Hence, ECD exhibits a local maximum for electron kinetic energies of $\approx$10eV. Because electron capture causes rapid dissociation, some of the fragments could still be in an electronically excited state, which later relaxes radiatively or via secondary fragmentation. The process is known as hot electron capture dissociation (HECD) and has the ability to distinguish the isomeric leucine and isoleucine residues due to the formation of *w* ions from primary $z^{\bullet}$ ions. Also, the fragments produced by HECD, yield high sequence coverage and retains posttranslational modifications [87,88]. These features are of great utility for protein *de novo* sequencing and protein identification.

Techniques like ECD, HECD, EED and EDD, all use an electron gun as a source of electrons to perform ion-electron reactions. Recently, a new dissociation technique to sequence peptides was developed wherein the electrons are supplied by gas-phase anions in ion-ion reaction with multiply protonated cations. The technique is

known as Electron Transfer Dissociation (ETD) [87,89,90] and use fragmentation pathways similar as in ECD to cleave the molecular backbone. ETD has utility for sequence analysis of peptides from complex mixtures and is particularly useful for characterization of peptides that contains PTM`s allows to identify and localize them. In addition, ETD technique is implemented in quadrupole ion trap instruments that are much affordable in price and maintenance costs than FTICR-mass spectrometers.

References

(1)   Petsko, G. A.; Ringe, D. Annu. Rev. Biophys. Biomol. Struct. **1984**, 13, 331-371.

(2)   Bax, A. Annu. Rev. Biochem. **1989**, 58, 223-256.

(3)   Wuthrich, K. J. Biol. Chem. **1990**, 265, 22059-22062.

(4)   Clore, G. M.; Gronenborn, A. M. Annu. Rev. Biophys. Biophys. Chem. **1991**, 20, 29-63.

(5)   Kelly, S. M.; Price, N. C. Biochim. Biophys. Acta **1997**, 1338, 161-185.

(6)   Li, R.; Woodward, C. Protein Sci. **1999**, 8, 1571-1591.

(7)   Englander, S. W. Annu. Rev. Biophys. Biomol. Struct. **2000**, 29, 213-238.

(8)   Winger, B. E.; Light-Wahl, K. J.; Rockwood, A. L.; Smith, R. D. J. Am. Chem. Soc. **1992**, 114, 5897.

(9)   Covey, T.; Douglas, D. J. J. Am. Soc. Mass Spectrom. **1993**, 4, 616-623.

(10)   Kemper, P. R.; Bowers, M. T. J. Am. Soc. Mass Spectrom. **1990**, 1, 197-207.

(11)   Wyttenbach, T.; von Helden, G.; Bowers, M. T. J. Am. Chem. Soc. **1996**, 118, 8355-8364.

(12)   Shelimov, K. B.; Clemmer, D. E.; Hudgins, R. B.; Jarrold, M. F. J. Am. Chem. Soc. **1997**, 119, 2240-2248.

(13)   Wu, Q.; Vanorden, S.; Cheng, X. H.; Bakhtiar, R.; Smith, R. D. Anal. Chem. **1995**, 67, 2498-2509.

(14)   Zubarev, R. A.; Kelleher, N. L.; McLafferty, F. W. J. Am. Chem. Soc. **1998**, 120, 3265.

(15)   Zubarev, R. A.; Kruger, N. A.; Fridriksson, E. K.; Lewis, M. A.; Horn, D. M.; Carpenter, B. K.; McLafferty, F. W. J. Am. Chem. Soc. **1999**, 121, 2857-2862.

(16)   Kelleher, N. L.; Zubarev, R. A.; Bush, K.; Furie, B.; Furie, B. C.; McLafferty, F. W.; Walsh, C. T. Anal. Chem. **1999**, 71, 4250-4253.

(17)   Oh, H.; Breuker, K.; Sze, S. K.; Ge, Y.; Carpenter, B. K.; McLafferty, F. W. Proc. Natl. Acad. Sci. U.S.A. **2003**, 99, 15863-15868.

(18)   Kaplan, J. Phys. rev. **1931**, 38, 1048-1051.

(19)   Campbell, W. W. Astrophys J. **1895**, 2, 162.

(20)   Vekey, K.; Brenton, G. A.; Beynon, J. H. J. Phys. Chem. **1986**, 90, 3569-3577.

(21)   Curtis, J. M.; Vekey, K.; Brenton, A. G.; Beynon, J. H. Org. Mass Spectrom. **1987**, 22, 289.

(22)   Guan, Z.; Kelleher, N. L.; O`Connor, P. B.; Aaserud, D. J.; Little, D. P.; McLafferty, F. W. *Int. J. Mass Spectrom. Ion Proc.* **1996**, 157/158, 357-364.

(23)   Gauthier, J. W.; Trautman, T. R.; Jacobsen, D. B. *Anal. Chim. Acta* **1991**, 246, 211-225.

(24)   Loo, J. A.; Udseth, H. R.; Smith, D. R. *Rapid Comm. Mass Spectrom.* **1988**, 2, 207-210.

(25)   Senko, M. W.; Speir, P. J.; McLafferty, F. W. *Anal. Chem.* **1994**, 66, 2801-2808.

(26)   Little, D. P.; Spier, P. J.; Senko, M. W.; O'Connor, P. B.; McLafferty, F. W. *Anal. Chem.* **1994**, 66, 2809-2815.

(27)   Price, W. D.; Paul, D. S.; Williams, E. R. *Anal. Chem.* **1996**, 68, 859-866.

(28)   Kleinnijenhuis, A. J.; Duursma, M. C.; Breukink, E.; Heeren, R. M. A.; Heck, A. J. R. *Anal. Chem.* **2003**, 75, 3219-3225.

(29)   Anusiewicz, I.; Berdys-Kochanska, J.; Simons, J. *J. Phys. Chem. A* **2005**, 109, 5801-5813.

(30)   Sobczyk, M.; Anusiewicz, I.; Berdys-Kochanska, J.; Sawicka, A.; Skurski, P.; Simons, J. *J. Phys. Chem. A* **2005**, 109, 250-258.

(31)   Zubarev, R. A.; Horn, D. M.; Fredricksson, E. K.; Kelleher, N. L.; Kruger, N. A.; Lewis, M. A.; Carpenter, B. K.; McLafferty, F. W. *Anal. Chem.* **2000**, 72, 563-573.

(32)   Kjeldsen, F.; Haselmann, K. F.; Budnik, B. A.; Jensen, F.; Zubarev, R. A. *Chem. Phys. Lett.* **2002**, 356, 201-206.

(33)   Zubarev, R. A.; Haselmann, K. F.; Budnik, B. A.; Kjeldsen, F.; Jensen, F. *Eur. J. Mass Spectrom.* **2002**, 8, 337-349.

(34)   McLafferty, F. W.; Horn, D. M.; Breuker, K.; Ge, Y.; Lewis, M. A.; Cerda, B. A.; Zubarev, R. A.; Carpenter, B. K. *J. Am.Soc. Mass Spectrom.* **2001**, 245-249.

(35)   Turecek, F.; Syrstad, E. A. *J. Am. Chem. Soc.* **2003**, 125, 3353-3369.

(36)   Turecek, F. *J. Am. Chem. Soc.* **2003**, 125, 5954-5963.

(37)   Tsaprailis, G.; Nair, H.; Wysocki, V. H.; Zhong, W.; Futrell, J. J.; Summerfield, S. G.; Gaskel, S. *J. Am. Chem. Soc.* **1999**, 121, 5142-5154.

(38)   Turecek, F.; Syrstad, E. A.; Seymour, J. L.; Chen, X.; Yao, C. *J. Mass Spectrom.* **2003**, 38, 1093-1104.

(39)   Zubarev, R. A. *Mass Spectrom. Rev.* **2003**, 22, 57-77.

(40)   Liu, H.; Hakansson, K. *J. Am. Soc. Mass Spectrom.* **2006**, 17.

(41)   Wells, J. M.; Stephenson, J. L.; McLuckey, S. A. *Int. J. Mass Spectrom.* **2000**, 203, A1-A9.

(42)   Haselmann, K. F.; Budnik, B. A.; Zubarev, R. A. *Rapid Comm. Mass Spectrom.* **2000**, 14, 2242-2246.

(43)   Cooper, H. J. *J. Am. Soc. Mass Spectrom.* **2005**, 16, 1932-1940.

(44)   Cooper, H. J.; Hudgins, R. R.; Hakansson, K.; Marshall, A. G. *Int. J. Mass Spectrom.* **2003**, 228, 723-728.

(45)   Leymarie, N.; Costello, C. E.; O'Connor, P. B. *J. Am. Chem. Soc.* **2003**, 125, 8949-8958.

(46)   Kjeldsen, F.; Haselmann, K. F.; Sørensen, E. S.; Zubarev, R. A. *Anal. Chem.* **2003**, 75, 1267-1274.

(47)   Haselmann, K. F.; Budnik, B. A.; Kjeldsen, F.; Nielsen, M. L.; Olsen, J. V.; Zubarev, R. A. *Eur. J. Mass Spectrom.* **2002**, 8, 117-121.

(48)   Tsybin, Y. O.; Witt, M.; Baykut, G.; Hakansson, P. Rapid Comm. Mass Spectrom. **2004**, 18, 1607-1613.

(49)   Cooper, H. J.; Hudgins, R. R.; Hakansson, K.; Marshall, A. G. J. Am. Soc. Mass Spectrom. **2002**, 13, 241-249.

(50)   Horn, D. M.; Breuker, K.; Frank, A. J.; McLafferty, F. W. J. Am. Chem. Soc. **2001**, 123, 9792-9799.

(51)   Breuker, K.; Oh, H.; Horn, D. M.; Cerda, B. A.; McLafferty, F. W. J. Am. Chem. Soc. **2002**, 124, 6407-6420.

(52)   Cerda, B. A.; Horn, D. M.; Breuker, K.; Carpenter, B. K.; McLafferty, F. W. EJMS **1999**, 5, 335-338.

(53)   Olsen, J. V.; Haselmann, K. F.; Nielsen, M. L.; Budnik, B. A.; Nielsen, P. E.; Zubarev, R. A. Rapid Comm. Mass Spectrom. **2001**, 15, 969-974.

(54)   Cerda, B. A.; Breuker, K.; Horn, D. M.; McLafferty, F. W. J. Am. Soc. Mass Spectrom. **2001**, 12, 565-570.

(55)   Koster, S.; Duursma, M. C.; Boon, J. J.; Heeren, R. M. A.; Ingemann, S.; van Benthem, R. A. T. M.; de Koster, C. G. J. Am. Soc. Mass Spectrom. **2003**, 14, 332-341.

(56)   Häkansson, K.; Hudgins, R. R.; Marshall, A. G.; O`Hair, R. A. G. J. Am. Soc. Mass Spectrom. **2003**, 14, 23-41.

(57)   Breuker, K.; Oh, H. B.; Cerda, B. A.; Horn, D. M.; McLafferty, F. W. EJMS **2002**, 8, 177-180.

(58)   Kleinnijenhuis, A. J.; Heck, A. J. R.; Duursma, M. C.; Heeren, R. M. A. J. Am. Soc. Mass Spectrom. **2005**, 16, 1595-1601.

(59)   Kruger, N. A.; Zubarev, R. A.; Carpenter, B. K.; Kelleher, N. L.; Horn, D. M.; McLafferty, F. W. Int. J. Mass Spectrom. **1999**, 182/183, 1-5.

(60)   Lin, C.; O'Connor, P. B.; Cournoyer, J. J. J. Am. Soc. Mass Spectrom. **2006**, 17, in press.

(61)   Kruger, N. A.; Zubarev, R. A.; Horn, D. M.; McLafferty, F. W. Int. J. Mass Spectrom. Ion Proc. **1999**, 787, 787-793.

(62)   Cooper, H. J.; Case, M. A.; McLendon, G. L.; Marshall, A. G. J. Am. Chem. Soc. **2003**, 125, 5331-5339.

(63)   Geels, R. B. J.; van der Vies, S. M.; Heck, A. J. R.; Heeren, R. M. A. Anal. Chem. **2006**, in press.

(64)   Horn, D. M.; Ge, Y.; McLafferty, F. W. Anal. Chem. **2000**, 72, 4778-4784.

(65)   Sze, S. K.; Ge, Y.; Oh, H. B.; McLafferty, F. W. Proc. Natl. Acad. Sci. U.S.A. **2002**, 99, 1774-1779.

(66)   Sze, S. K.; Ge, Y.; Oh, H. B.; McLafferty, F. W. Anal. Chem. **2003**, 75, 1599-1603.

(67)   Oh, H.; Breuker, K.; Sze, S. K.; Ge, Y.; Carpenter, B. K.; McLafferty, F. W. Proc. Natl. Acad. Sci. U.S.A. **2002**, 99, 15863-15868.

(68)   Kelleher, N. L.; Zubarev, R. A.; Bush, K.; Furie, B. C.; McLafferty, F. W.; Walsh, C. T. Anal. Chem. **1999**, 71, 4250-4253.

(69)   Niiranen, H.; Budnik, B. A.; Zubarev, R. A.; Auriola, S.; Lapinjoki, S. J. Chromatogr. A **2002**, 962, 95-103.

(70)   Mirgorodskaya, E.; Roepstorff, P.; Zubarev, R. A. Anal. Chem. **1999**, 71, 4431-4436.

(71) Haselmann, K. F.; Budnik, B. A.; Olsen, J. V.; Nielsen, M. L.; Reis, C. A.; Clausen, H.; Johnsen, A. H.; Zubarev, R. A. Anal. Chem. **2001**, 73, 2998-3005.

(72) Macek, B.; Hoofsteenge, G.; Peter-Katalinic, J. Rapid Comm. Mass Spectrom. **2001**, 15, 771-777.

(73) Hakansson, K.; Cooper, H. J.; Emmet, M. R.; Costello, C. E.; Marshall, A. G.; Nilsson, C. L. Anal. Chem. **2001**, 73, 4530-4536.

(74) Häkansson, K.; Chalmers, M. J.; Quinn, J. P.; McFarland, M. A.; Hendrickson, C. L.; Marshall, A. G. Anal. Chem. **2003**, 75, 3256.

(75) Stensballe, A.; Jensen, O. N.; Olsen, J. V.; Haselmann, K. F.; Zubarev, R. A. Rapid Comm. Mass Spectrom. **2000**, 14, 1793-1800.

(76) Shi, S. D.-H.; Hemling, M. E.; Carr, S. A.; Horn, D. M.; Lindh, I.; McLafferty, F. W. Anal. Chem. **2001**, 73, 19-22.

(77) von Helden, G.; Wyttenbach, T.; Bowers, M. T. Science **1995**, 267, 1483-1485.

(78) Kleinnijenhuis, A. J.; Mihalca, R.; Heeren, R. M. A.; Heck, A. J. R. Int. J. Mass Spectrom. **2006**, 253, 217-224.

(79) Silivra, O. A.; Kjeldsen, F.; Ivonin, I. A.; Zubarev, R. A. J. Am. Soc. Mass Spectrom. **2005**, 16, 22-27.

(80) Baba, T.; Hashimoto, Y.; Hasegawa, H.; Hirabayasi, A.; Waki, I. Anal. Chem. **2004**, 76, 4263-4266.

(81) Tsybin, Y. O.; Hakansson, P.; Budnik, B. A.; Haselmann, K. F. Rapid Comm. Mass Spectrom. **2001**, 15, 1849-1854.

(82) McFarland, M. A.; Chalmers, M. J.; Quinn, J. P.; Hendrickson, C. L.; Marshall, A. G. J. Am. Soc. Mass Spectrom. **2005**, 16, 1060.

(83) Tsybin, Y. O.; Hendrickson, C. L.; Beu, S. C.; Marshall, A. G. Int. J. Mass Spectrom. **2006**, 225-256, 144-149.

(84) Zubarev, R. A.; Nielsen, M. L.; Budnik, B. A. Eur. J. Mass Spectrom. **2000**, 6, 235-240.

(85) Budnik, B. A.; Zubarev, R. A. Chem. Phys. Lett. **2000**, 316, 19-23.

(86) Budnik, B. A.; Haselmann, K. F.; Zubarev, R. A. Chem. Phys. Lett. **2001**, 342, 299-302.

(87) Coon, J. J.; Syka, J. E. P.; Scwartz, J. C.; Shabanowitz, J.; Hunt, D. F. Int. J. Mass Spectrom. **2004**, 236, 33-42.

(88) Coon, J. J.; Ueberheide, B.; Syka, J. E. P.; Dryhurst, D. D.; Ausio, J.; Shabanowitz, J.; Hunt, D. F. Proc. Natl. Acad. Sci. U.S.A. **2005**, 102, 9463-9468.

(89) Syka, J. E. P.; Coon, J. J.; Schroeder, M. J.; Shabanowitz, J.; Hunt, D. F. Proc. Natl. Acad. Sci. U.S.A. **2004**, 9528-9533.

(90) Coon, J. J.; Shabanowitz, J.; Hunt, D. F.; Syka, J. E. P. J. Am. Soc. Mass Spectrom. **2005**, 16, 880-882.

Chapter 3

Electron capture dissociation at low temperatures reveals selective dissociations

Romulus Mihalca[1], Anne J. Kleinnijenhuis[1,2], Liam A. McDonnell[1], Albert J. R. Heck[2] and Ron M. A. Heeren[1,2*]

[1]**FOM Institute for Atomic and Molecular Physics (AMOLF), Kruislaan 407, 1098 SJ Amsterdam, The Netherlands**
[2]**Department of Biomolecular Mass Spectrometry, Bijvoet Center for Biomolecular Research, Utrecht Institute for Pharmaceutical Sciences, Utrecht University, Sorbonnelaan 16, 3584 CA Utrecht, The Netherlands**

Abstract

Electron capture dissociation at 86 K of the linear peptide substance P produced just two backbone fragments, whereas at room temperature eight backbone fragments were formed. Similarly, with the cyclic peptide gramicidin S, just one backbone fragment was formed at 86 K but five at room temperature. The observation that some backbone scissions are active and others inactive, when all involve N-C_α cleavages and have a high rate constant, indicates that the more specific fragments at low temperatures reflects the reduced conformation heterogeneity at low temperatures. This is supported by reduced or inactive hydrogen loss, a channel that has previously been shown to be affected by conformation. The conclusion that the ECD fragments are a snapshot of the conformational (intramolecular solvation shell) heterogeneity helps explain how the relative intensities of ECD fragments can be different on different instrument and highlights the common theme in methodologies used to increase sequence coverage, namely an increase in the conformational heterogeneity of the precursor ion population.

3.1   Introduction

Electron capture dissociation (ECD)[1-4] employs reactions of multiprotonated peptides/proteins with low energy electrons to generate peptide fragments. The high sequence coverage and the ability to retain labile groups after ECD have allowed posttranslational modifications (PTMs) and point mutations (PMs) in peptides and proteins to be both identified and localised. Such performance is of great value for the analysis of the proteome, particularly that of diseased organisms. PTMs and PMs are widespread and are frequently associated with disease,[5-7] for example over 80 different point mutations have been found in transthyretin (most of which lead to autosomal disorders)[8].

To be able to fully characterize such modified proteins, 100 % sequence coverage is required (so-called top-down proteomics). Several methods have been developed to increase the sequence coverage of ECD, which can be grouped into either infrared illumination[9-11] or collisional activation[12]. These methods increase the average internal energy of the ions, which also affects the conformation of these gas-phase ions[13].

There is experimental and theoretical evidence that ECD is directed by the internal solvation of the (neutralized) proton.[9,14-18] If the reaction progresses faster than the electron-proton recombination energy is randomised and thermal fluctuations are small, specific fragments would be expected from a single (frozen) conformer, reflecting the solvation shell, specific for that conformation, surrounding the neutralised proton. Thermal fluctuations that result in a dynamic solvation shell but not conformational change (local fluctuations rather than a global change), would produce a greater number of fragments. Finally, multiple conformations as well as thermal fluctuations would produce yet more fragments. Because the methods used to increase the sequence coverage of ECD all increase the internal energy of the ions, and so affect the conformation of the gas-phase ions, the greater sequence coverage could simply reflect the greater conformational heterogeneity (and "thermal" motion) of the activated ion population. To investigate the importance of conformational heterogeneity on the fragments produced by ECD, we have performed ECD at 86 K. If the extent of fragmentation is governed by the conformational heterogeneity, less but more specific fragments will be obtained at 86 K.

Here we report significant changes in ECD spectra at low temperatures compared with those at near room temperature performed on a linear and a cyclic peptide under otherwise identical conditions.

3.2   Experimental

Gas phase ions of the linear peptide Substance P (RPKPQQFFGLM) and the cyclic peptide Gramicidin S (VOLFPVOLFP) were generated using electrospray ionisation (20 μM in 1:1 H_2O:acetonitrile + 1 % formic acid) and injected into a Fourier transform ion cyclotron resonance mass spectrometer (FTMS) equipped with an electron gun and a temperature-controlled cell.[19] Following isolation of the $[M + 2H]^{2+}$ ions using a stored waveform inverse Fourier transform pulse[20] the precursor ions were left to equilibrate at the requested temperature for 50 s before undergoing a 400 ms ECD event. To investigate the temperature dependence of ECD, experiments were performed on ion-populations thermalized near room temperature and at 86 K. These represent the two temperatures under which most ECD experiments are performed and an extremely low temperature (the lowest temperature amenable to out experimental set-up) that would detect any temperature dependence.

3.3   Results and discussion

Substance P was chosen because it is a linear peptide that under normal conditions (room temperature) produces many backbone fragments. ECD of substance P at 308 K produced seven c fragments (c_{4-10}) and a weak $z_9^{\bullet}$ fragment, in agreement with previous studies[21]. Under otherwise identical conditions, except performing the experiment at 86 K, the c_4, c_5, c_6, c_8, c_9 and $z_9^{\bullet}$ fragments were not detected. Only the c_7 and c_{10} fragments were observed at 86 K. Figure 3.1 shows a comparison of these two spectra, the disappearance of six of the eight fragments is readily apparent.

Figure 3.2 shows three representative examples in more detail, the c_5 and c_9 fragments that both disappeared at 86 K and the c_{10} fragments that remained. The top row shows the fragment spectra at 308 K and the bottom the analogous

spectra at 86 K. It is clear that a smaller number of fragments were detected at 86 K.

ECD is thought to occur close to the charge-reduced protonation sites through internal solvation of the proton and H transfer after electron capture.[2,16-18] (Note: it was recently suggested that electron capture could occur prior to proton transfer[22], the results shown here cannot distinguish between these two possibilities). The fragments formed by these fast mechanisms would be expected to be sensitive to the conformational heterogeneity of the molecule and, extrapolating, the fragments formed by an ion population would be sensitive to the conformational heterogeneity of the ion packet.
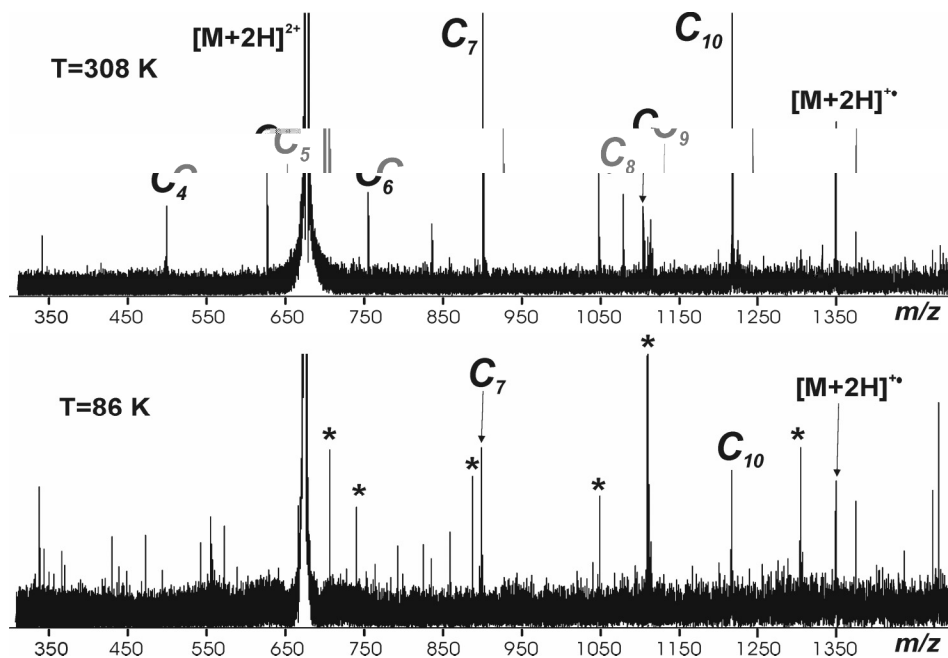
Figure 3.1 Comparison of the ECD spectra of the [M+2H]$^{2+}$ ion of substance P at 308 K (a) and 86 K (b). Both spectra are the average of 50 scans.
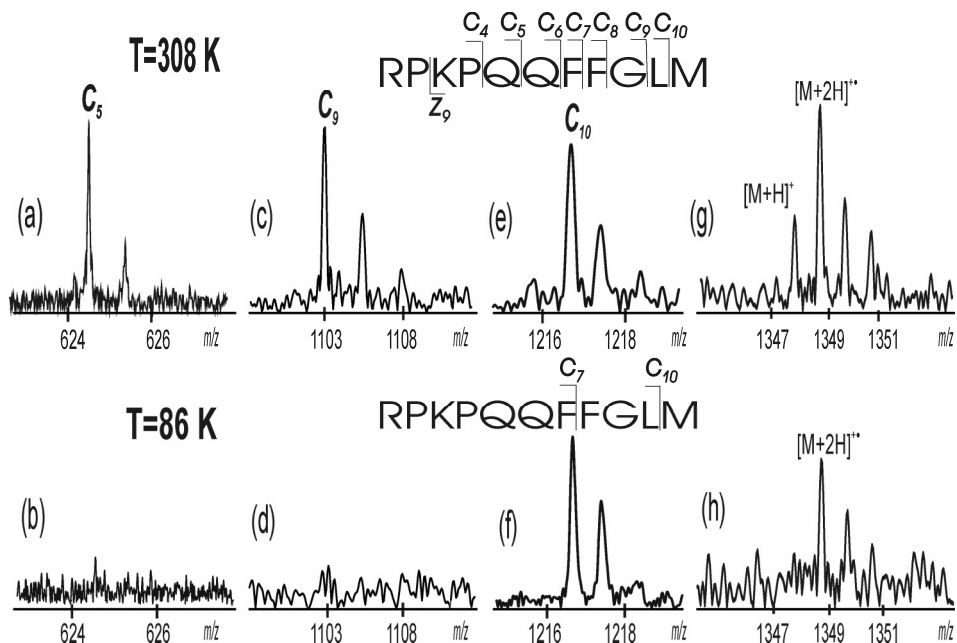
Figure 3.2 c_5 fragment of substance P after ECD at (a) 308 and (b) 86 K; c_9 fragment of substance P after ECD at (c) 308 and (d) 86 K; c_{10} fragment of substance P after ECD at (e) 308 and (f) 86 K; [M+H]$^+$ and [M+2H]$^{+\bullet}$ cluster at (g) 308 and (h) 86 K.

At higher temperatures (or after collisional / radiative activation) the number of conformations and the thermal fluctuations are larger. Consequently, more fragments are expected at higher temperatures (internal energies). Figure 3.1 shows that the fragments obtained after ECD of substance P at 86 K and 308 K fit this scenario, namely more fragments are obtained at higher temperatures because of the larger conformational space occupied by the molecule. The sensitivity of the fragments formed by ECD to the conformation population also explains why the relative abundances of the c fragments have differed on different instruments. The following relative intensities have all been reported $c_5 > c_4 > c_6 > c_7 > c_8 > c_9 > c_{10}$ [23], $c_5 > c_6 > c_7 > c_4 > c_9 > c_{10} > c_8$ [11] and $c_{10} > c_7 > c_9 > c_8 > c_6 > c_5 >> c_4$ [24]. The different fragment intensities could reflect the different conformation populations present. The conformation population is influenced by the final internal

energy distribution of the ions, which can be altered during ionisation, ion transport through the mass spectrometer and ion trapping in the ICR cell (where ECD occurs). These parameters are almost certainly different for experiments performed on different instruments operated by different people.

A common reaction pathway found in ECD experiments is loss of a hydrogen atom (the reduced proton). Different degrees of hydrogen loss have been attributed to conformational change[25]. In support of the above conformation explanation for the different fragments detected at 308 and 86 K, it was found that the hydrogen loss channel was active at the higher temperature but not at the lower temperature (Figure 3.2). All of the above observations are consistent with the premise that the reaction pathways followed after electron capture, and thus the fragments obtained, reflect the conformational heterogeneity of the trapped ions. It is encouraging that the fragments obtained at 86 K appear to correlate with the structure calculated by Bowers and workers for the gas-phase $[M+2H]^{2+}$ ion of substance P, in which the part of the peptide backbone involved in internal solvation includes the amino acids whose scission leads to the c_7 and c_{10} fragments[26]. Intramolecular solvation of the protonated lysine is ≈ 40 kJ mol^{-1} more stable (enthalpically) than solvation of the other protonation site (arginine) and the enthalpic contribution increasingly dominates the conformer population at lower temperatures (and thus the intramolecular solvation shells that determine which fragments are obtained).

The ability to cleave N-C$_\alpha$ bonds but retain labile groups after ECD and the time-scales of other recombination-dissociation reactions lead to the postulate that ECD is a non-ergodic process, that dissociation occurs prior to energy randomisation[2]. However, more recent studies have concluded that, for these radical reactions, non-ergodicity does not need to be invoked because of the low activation barriers of the backbone cleavages[27]. For substance P the total internal energy after ECD is 3.9 (4.6) and 6.2 (6.9) eV, for neutralization of the lysine (arginine) protonation site at 86 and 308 K, respectively. These internal energies are sufficient for unimolecular rate constants $> 10^5$ s^{-1} when distributed throughout the molecule[27]. The question as to whether the smaller number of fragments at 86 K reflects the lower conformational heterogeneity before energy randomisation or

after requires further study to determine the energies associated with the conformational changes that lead to different fragments. Future plans include performing temperature resolved ion mobility studies to determine the internal energies associated with these conformational changes.

ECD of Gramicidin S (VOLFPVOLFP) at 86 K also showed differences from that performed near room temperature. At 313 K three types of fragments were detected: small molecule losses, five backbone cleavages (labeled B1-5 in Figure 3) and side chain losses, in agreement with previous studies[28]. At 86 K a smaller number of each type of fragment was detected, for example just one backbone fragment (labeled B1 in Figure 3.3). Because Gramicidin S is cyclic, these backbone fragments require two cleavages from a single electron-capture event and are thought to arise from a free-radical cascade[28]. While it is pertinent to contemplate whether the reduced number of fragments is atributable to the radical cascade terminating earlier at the lower internal energies at 86 K, considering the low activation barriers of these gas-phase radical reactions[18,27] it is not sufficient without invoking a conformational argument. As with the substance P results, the smaller number of fragments is consistent with a smaller conformer population and reduced thermal fluctuations. This is also supported by the observation that the hydrogen loss channel was significantly attenuated at 86 K (Figure 3.3).

Recently Iavarone *et al* reported that the number of *c* fragments obtained from ECD of the synthetic peptide AcHN-(AKAAK)$_3$A-NH$_2$ was insensitive to temperature from room temperature up to 150 °C. This was interpreted as indicating that the products are "…not due to effects of tertiary structure."[29] This behavior is in stark contrast to the cold temperature results reported here and several previous studies. Breuker et al. have reported increased sequence coverage of ubiquitin by heating throughout the same temperature range[9], Håkansson et al. and Tsybin et al. have increased the number of fragments by heating the ion cloud with an infrared laser[10,11], Horn et al. have increased the sequence coverage by using collisional activation to heat the ion cloud[30], and in addition to temperature dependent ECD, Adams et al. found that a single D-amino acid substitution, which is known to affect solution-phase secondary and tertiary structure, significantly affected the ECD fragments obtained[16].
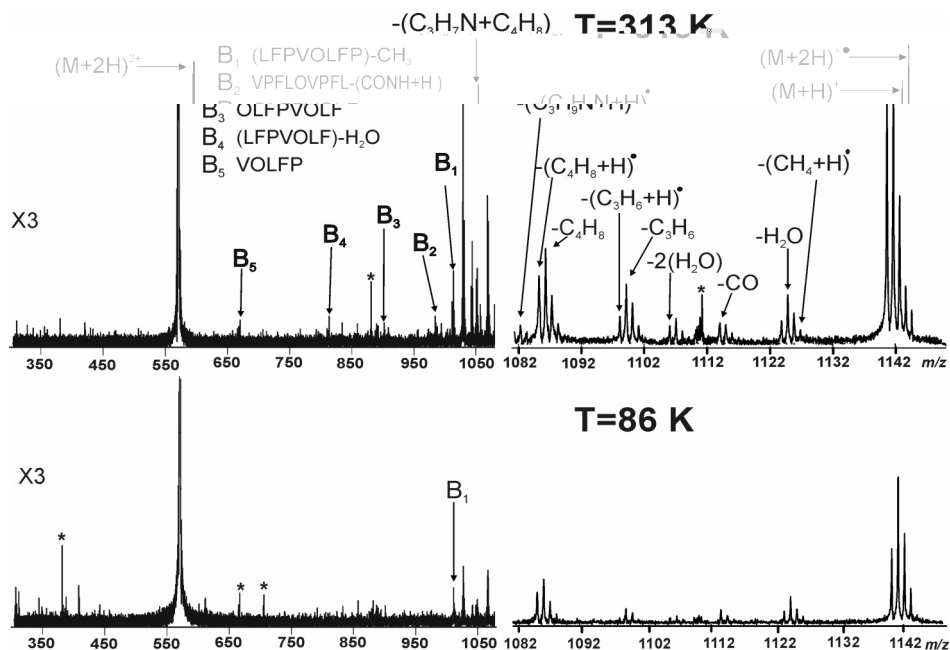
Figure 3.3 A comparison of gramicidin S ECD fragments at 313 K and 86 K. The B fragments correspond to backbone fragments. Both spectra are the average of 25 scans.

The different behavior seen by Iavarone reflects the unusual nature of the peptide used in their study. This peptide has previously been shown to exhibit an unusually stable helix, especially in non-polar solvents (high vacuum is also non-polar)[31]. Increased helix formation has been associated with a smaller number of ECD fragments because the carbonyl groups that would otherwise solvate the (neutralized) proton and lead to N-C_α scission are involved in the hydrogen-bond network that stabilizes the helix. Consequently it is the unusual stability of the helix in this peptide that is probably responsible for the limited number of ECD fragments, throughout the temperature range investigated. In this regard the results of Iavarone et al. would provide further support for the crucial role of conformation in ECD.

All of the results discussed above demonstrate that the fragments produced by ECD of multiprotonated peptides / proteins are significantly influenced by the conformations of the gas phase ions because this determines which groups are involved in the intramolecular solvation of the (neutralized) proton. The results presented here show that, at 86 K, ECD generates much fewer fragments than at room temperature, for both substance P and gramicidin S. This reflects the reduced conformational heterogeneity at lower temperatures, not least because the low activation barriers associated with gas-phase radical reactions makes any argument based on reaction rates problematic. Such conformational arguments are consistent with observations of increased sequence coverage using techniques that heat the ion population and provide an explanation why the relative intensities of ECD fragments can be different on different instruments. For increased sequence coverage these results indicate that it is advisable to heat (energize) the ion population in order to obtain a heterogeneous conformation population. When analyzing biomolecules that contain labile post-translational modifications this should be performed with due care in order to ensure that these labile groups are retained. Such modifications are associated with many diseases and ECD provides an exceptional methodology for identifying and localizing these modifications. With sufficient care a balance can be reached in which the ion-population is energized enough for extensive sequence information but the labile modifications are retained[10,12,32].

3.4   Conclusions

Electron capture dissociation at 86 K of the linear peptide substance P and the cyclic peptide gramicidin S generated significantly fewer fragments than at room temperature. It is inferred that these more specific fragments reflect the conformational heterogeneity of the ion population because the reactions are still fast at 86 K (> 10^5 s^{-1} for the common ECD channels) and directed by intramolecular hydrogen bonds, and the similarity of the channels for fragments that were active and inactive make any alternative explanation implausible. At

higher temperatures a greater number of conformations as well as larger thermal fluctuations leads to more fragments. Changes to the degree of hydrogen loss, a reaction pathway previously shown to be influenced by conformation, support this assertion. Moreover the specific substance P fragments at 86 K are consistent with preferential intramolecular solvation of the lysine.

The results presented here indicate how the conformation (solvation shell) population of the ion packet affect the relative intensities of the fragments and sequence coverage. This last aspect is important because the most attractive feature of ECD is its ability to identify and localize post-translational modifications to proteins, which are associated with many of the diseases of present day concern (Alzheimer's, Parkinson's and cancer).

Acknowledgements

Addendum

In a personal communication in 2004, Turecek, F. writes as follows: "B3-PMP2/6-311++G(2d,p) calculations of ionization energies give IE_a = 3.00 eV for the ε-ammonium radical from N_α-acetyl-lysine amide and IE_a = 3.53 eV for the guanidinium radical from N_α-acetyl-arginine amide. The vertical recombination energies are somewhat lower, RE_v = 2.84 and 2.44 eV for the lysine and arginine cations, respectively. The coulomb contribution to recombination energy in doubly charged RPKPKQQFFGLM has been calculated from fully optimized structures (by PM3) of RPK-NH2 motifs combined with Mulliken and NPA charge distributions

with the B3LYP/6-31G* wave function. The more stable conformer with internally solvated Lys side chain has $E_{coulomb}$ = 0.60-0.73 eV (NPA and Mulliken populations, respectively). The less stable conformer (DE = +24 kJ mol^{-1}) with internally solvated Arg side chain has $E_{coulomb}$ = 0.85 eV. Thus, the total recombination energy in a Lys-solvated [RPKPKQQFFGLM + 2H]$^{2+}$ conformer should be close to 3.00 + 0.7 = 3.7 eV for electron capture at the Lys residue and 3.53 + 0.7 = 4.23 eV for electron capture at the Arg residue.

Using previous data for peptide heat capacities, [RPKPKQQFFGLM + 2H]$^{2+}$ is estimated to have 0.2 and 2.5 eV internal energy (H_T) at 86 and 308 K, respectively. Upon adding the electron recombination energy, the "cold" Lys-reduced ion will have a total of 0.2 + 3.7 = 3.9 eV internal energy, corresponding to an effective temperature of 385 K. The "ambient" ion will have 2.5 + 3.7 = 6.2 eV, corresponding to 495 K. The Arg-reduced ions will be slightly more energetic, 4.6 and 6.9 eV for the "cold" and "ambient" systems, corresponding to 415 and 520 K, respectively."

References

(1)   R. A. Zubarev; N. A. Kruger; E. K. Fridriksson; M. A. Lewis; D. M. Horn; B. K. Carpenter; F. W. McLafferty J. Am. Chem. Soc. **1999**, 121, 2857-2862.

(2)   R. A. Zubarev Mass Spectrom. Rev. **2003**, 22, 57-77.

(3)   R. A. Zubarev; D. M. Horn; E. K. Fredricksson; N. L. Kelleher; N. A. Kruger; M. A. Lewis; B. K. Carpenter; F. W. McLafferty Anal. Chem. **2000**, 72, 563-573.

(4)   R. A. Zubarev; N. L. Kelleher; F. W. McLafferty J. Am. Chem. Soc. **1998**, 120, 3265.

(5)   Y. Ge; M. ElNaggar; S. K. Sze; H. B. Oh; T. P. Begley; F. W. McLafferty; H. Boshoff; C. E. Barry III J. Am. Soc. Mass Spectrom. **2003**, 14, 253-261.

(6)   S. Hanash Nature **2003**, 422, 226-232.

(7)   J. Pierson; J. I. Norris; H.-R. Aerni; P. Svenningsson; R. M. Caprioli; P. E. Andrén J. Proteome Res. **2004**, 3, 289-295.

(8)   L. H. Connors; A. M. Richardson; R. Theberge; C. E. Costello Amyloid-Journal Protein Folding Disorder **2000**, 7, 54-69.

(9)   K. Breuker; H. Oh; D. M. Horn; B. A. Cerda; F. W. McLafferty J. Am. Chem. Soc. **2002**, 124, 6407-6420.

(10)   K. Håkansson; M. J. Chalmers; J. P. Quinn; M. A. McFarland; C. L. Hendrickson; A. G. Marshall Anal. Chem. **2003**, 75, 3256-3262.

(11) Y. O. Tsybin; M. Witt; G. Baykut; F. Kjeldsen; P. Håkansson Rapid Comm. Mass Spectrom. **2003**, 17, 1759-1768.
(12) S. K. Sze; Y. Ge; H. Oh; F. W. McLafferty PNAS **2002**, 99, 1774-1779.
(13) M. F. Jarrold Annu. Rev. Phys. Chem. **2000**, 51, 179-207.
(14) H.-B. Oh; K. Breuker; S. K. Sze; Y. Ge; B. K. Carpenter; F. W. McLafferty PNAS **2002**, 99, 15863-15868.
(15) Y. M. E. Fung; L. Duan; T.-W. D. Chan Eur. J. Mass Spectrom. **2004**, in press.
(16) C. M. Adams; F. Kjeldsen; R. A. Zubarev; B. A. Budnik; K. F. Haselmann J. Am. Soc. Mass Spectrom. **2004**, 15, 1087-1098.
(17) K. F. Haselmann; B. A. Budnik; F. Kjeldsen; N. C. Polfer; R. A. Zubarev Eur. J. Mass Spectrom. **2002**, 8, 461-469.
(18) F. Turecek; E. A. Syrstad; J. L. Seymour; X. Chen; C. Yao J. Mass Spectrom. **2003**, 38, 1093-1104.
(19) X. Guo; M. Duursma; A. Al-Khalili; L. A. McDonnell; R. M. A. Heeren Int. J. Mass Spectrom. **2004**, 231, 37-45.
(20) A. G. Marshall; T. C. L. Wang; T. L. Ricca J. Am. Chem. Soc. **1985**, 107, 7893-7897.
(21) J. Axelsson; M. Palmblad; K. Håkansson; P. Håkansson Rapid Comm. Mass Spectrom. **1999**, 13, 474-477.
(22) E. A. Syrstad; F. Turecek 52nd ASMS Conference on Mass Spectrometry, Nashville, TN, 2004.
(23) T.-W. D. Chan; W. H. H. Ip J. Am. Soc. Mass Spectrom. **2002**, 13, 1396-1406.
(24) M. A. McFarland; R. R. Hudgins; K. Hakansson; C. L. Hendrickson; A. G. Marshall 50th ASMS Conference on Mass Spectrometry and Allied Topics, Orlando, Florida, 2002.
(25) K. Breuker; H. Oh; B. A. Cerda; D. M. Horn; F. W. McLafferty Eur. J. Mass Spectrom. **2002**, 8, 177-180.
(26) A. C. Gill; K. R. Jennings; T. Wyttenbach; M. T. Bowers Int. J. Mass Spectrom. **2000**, 195/196, 685-697.
(27) F. Turecek J. Am. Chem. Soc. **2003**, 125, 5954-5963.
(28) N. Leymarie; C. E. Costello; P. B. O'Connor J. Am. Chem. Soc. **2003**, 125, 8949-8958.
(29) A. T. Iavarone; K. Paech; E. R. Williams Anal. Chem. **2004**, 76, 2231-2238.
(30) D. M. Horn; Y. Ge; F. W. McLafferty Anal. Chem. **2000**, 72, 4778-4784.
(31) S. Marqusee; V. H. Robbins; R. L. Baldwin PNAS **1989**, 86, 5286-5290.
(32) M. J. Chalmers; K. Håkansson; R. Johnson; R. Smith; J. Shen; M. R. Emmett; A. G. Marshall Proteomics **2004**, 4, 970-981.

Chapter 4

Combined infrared multiphoton dissociation and electron-capture dissociation using co-linear and overlapping beams in Fourier transform ion cyclotron resonance mass spectrometry

Romulus Mihalca[1], Yuri E. M. van der Burgt[1], Liam A. McDonnell[1], Marc Duursma[1], Iliya Cerjak[1], Albert J. R. Heck[2] and Ron M. A. Heeren[1,2*]

[1]FOM Institute for Atomic and Molecular Physics (AMOLF), Kruislaan 407, 1098 SJ Amsterdam, The Netherlands
[2]Department of Biomolecular Mass Spectrometry, Bijvoet Center for Biomolecular Research, Utrecht Institute for Pharmaceutical Sciences, Utrecht University, Sorbonnelaan 16, 3584 CA Utrecht, The Netherlands

Abstract

A novel set-up for Fourier transform ion cyclotron resonance mass spectrometry (FT-ICRMS) is reported for simultaneous infrared multiphoton dissociation (IRMPD) and electron-capture dissociation (ECD). An unmodified electron gun ensures complete, on-axis overlap between the electron and the photon beams. The instrumentation, design, and implementation of this novel approach are described. In this configuration, the IR beam is directed into the ICR cell using a pneumatically actuated mirror inserted into the ion-optical path. Concept validation was made using different combinations of IRMPD and ECD irradiation events on two standard peptides. The ability to perform efficient IRMPD, ECD, and especially simultaneous IRMPD and ECD using lower irradiation times is demonstrated. The increase in primary sequence coverage, with the combined IRMPD and ECD set-up, also increases the confidence in peptide and protein assignments.

4.1.   Introduction

Proteomics is an indispensable technology in the molecular description of life's organization. As proteins carry out most biological activities in a cell or organism[1], it is essential to characterize their structure, expression distribution and interactions. Over the past decade, mass spectrometry (MS) has become the method of choice for the systematic analysis of a proteome. It has enabled protein identification and quantification, protein profiling and the characterization of protein interactions and modifications. Nevertheless, MS-based proteomics still faces significant challenges[1,2], such as the improvement of tandem mass (MS/MS) spectra in order to decrease the amount of false positives in peptide and protein assignments. Here we describe an instrumental development to improve the quality and information content of MS/MS spectra.

A common method of protein identification uses partial sequence information of one or more proteolytic peptides[1,3,4]. This sequence-tag strategy

involves proteolysis of the protein mixture, followed by chromatographic separation of peptides and MS/MS. The peak lists from such MS/MS spectra are then submited to a database for protein identification.

The confidence of the assignment increases with the amount of sequence information and the mass accuracy of the measurement. The high mass accuracy provided by Fourier transform ion cyclotron resonance mass spectrometry (FTICR-MS) is the principal reason for it currently being the method of choice for proteomics investigations[4]. With suitable control, FTICRMS can provide mass accuracies consistently under 2 ppm, and the majority under 1 ppm[5-7]. While the new Orbitrap can also provide accurate mass capabilities[8], the process of FTICRMS permits the analyst to use a wide variety of tandem mass spectrometry techniques. Collision-activated dissociation (CAD)[9] [10], infrared-multiphoton dissociation (IRMPD)[11] [12], ultra-violet photo-dissociation (UV-PD)[13] [14], and electron-capture dissociation (ECD)[15] [16-19] can all be used to obtain sequence information. The identity and relative intensities of the product ions are dependent on which technique is used and how it is applied. This flexibility has been exploited to the extent that entire proteins have been sequenced using a combination of these MS/MS techniques, even including the position of post-translational modifications (PTMs)[20].

For the typical sequence-tag proteomics experiments, involving a separation step, MS/MS must be performed on a time scale compatible with the separation. A scan duration of less than 2 s would allow the MS/MS spectra to be obtained from several co-eluting peptides (assuming liquid chromatography (LC) peak duration of 10 - 30 s). IRMPD and ECD are both well-established, easy to implement and have time-scales compatible with LC/MS proteomics.

1)   IRMPD –Irradiation heating times are usually 10^2 to 10^3 ms. Peptide and protein ions undergo fragmentation typical of slow vibrational activation[21]. Labile PTMs are generally lost prior to backbone cleavage and efficient backbone cleavage forms intense *b* and *y* ions. The mass losses due to the loss of a labile group, such as a glycan or phosphate, can be used to indicate the presence of that group[19]. Occasionally, the position of the modification can be determined from established biochemical rules. In comparison with ECD, IRMPD allows

fragmentation of singly charged ions and provides N-terminal cleavages of the proline residue.

2)   ECD – involves the capture of low-energy electrons by multiply charged molecular-related ions of peptides and proteins, e.g. $[M+nH]^{n+}$. ECD can provide extensive sequence information and is the only technique to retain labile side groups such as PTMs[22]. Consequently it is the only MS technique able to identify *and* locate PTMs. This ability led to early reports speculating that ECD might be a non-ergodic process[15]. The gentle nature of ECD has been further demonstrated by the observation that non-covalent interactions can limit the degree of fragmentation observed with ECD. More abundant product ions and more extensive sequence information are obtained by gently heating the ions during ECD using collisional[23] or IR[24] activation.

It is desirable to have simultaneous access to ECD and IRMPD. However, both techniques are optimised when the electron/IR beam has complete overlap with the ion cloud in the ICR cell. Figure 4.1(a) shows a schematic of a typical FTICR instrument, including the distribution of an ion cloud. As can be seen, the ions are transferred from an external ion source by ion-optical elements to the ICR cell, which is situated in the center of a strong magnet. Here, ions form an ellipsoid along the axis of the ICR cell. Co-axial irradiation of this ion packet by the electron beam *and* the IR beam is complicated by the ion optics on the front side of the ICR, consequently previous attempts have concentrated on introducing both beams from the rear. Figures 4.1(b) – 4.1(e) show the solutions to date, but which all compromise the degree of overlap with the ion cloud for at least one of the beams.

The first attempts to apply the complementary capabilities of ECD and IRMPD were made by Håkansson *et al.*[19] for the structural characterization of several posttranslational modified peptides. A directly heated filament placed off-axis with simultaneous use of an on-axis IR laser beam (Figure 4.1(b)). This configuration allowed efficient IRMPD but satisfactory ECD spectra required long irradiation times, up to 30 s, because of poor overlap between the ion cloud and the small electron beam produced by the filament cathode.
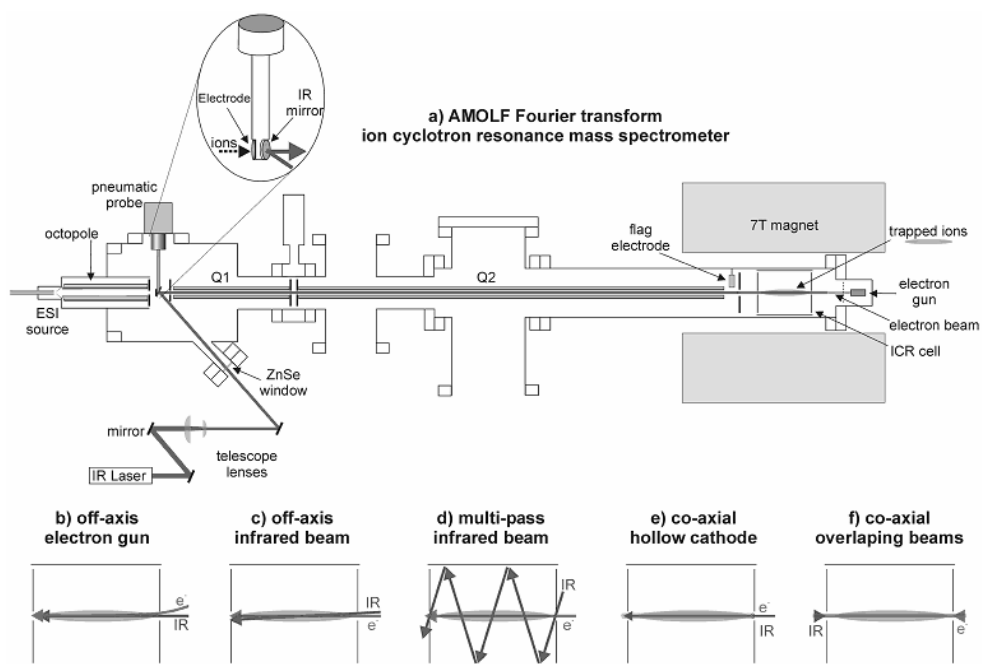
Figure 4.1 A schematic diagram (not to scale) of the FOM`s 7T FTICR-MS set-up for performing simultaneous on-axis IRMPD and ECD in the ICR cell (a). The inset highlights the pneumatic probe used to reflect the IR beam through the ion optics in to the ICR cell. Bottom (b-f) shows different reported configurations used to combine ECD and IRMPD in FTICR-MS.

The broader electron beam produced by an indirectly heated dispenser cathode, provides more overlap and thus increased ECD efficiency; however, performance is still sensitive to position, decreasing rapidly when the electron gun is moved more then a few millimeters off-axis.

Alternative designs have positioned the electron gun on-axis and the IR beam slightly off-axis (Figs. 4.1(c) and 4.1(d))[24]. Using this configuration more abundant product ions have been reported. Nevertheless, overlap of the IR beam with ion cloud is incomplete. Recently Tsybin et al. implemented a ring cathode in which the IR laser passes through the center of the ring (Fig 4.1 (e))[25]. Short irradiation times for combined IRMPD and ECD provided more than 60% sequence coverage of the peptide HNP-1. In the strong magnetic field, the electron beam

maintains the ring cross section of the cathode throughout the ICR cell. ECD efficiency could be increased by increasing the effective interaction volume. This can be achieved by using sidekick tapping or ion-excitation with an off-resonance excitation. However, such excitation would reduce IR overlap.

All the instrumental configurations mentioned above compromise the degree of overlap between the ion cloud and either the IR or electron beam. The common cause is the combined introduction of the IR and electron beam from the rear end of the ICR cell.

Here we report a novel FT-ICRMS set-up for combined on-axis ECD and IRMPD in the ICR cell, in which both beams have complete overlap with the ion cloud (Figs 4.1(a) and (f)), using a standard dispenser cathode. An IR mirror, attached to a guided pneumatic probe, is inserted between ion-optical elements to reflect the IR beam along the axis of the instrument and into the ICR cell. Geometrical design ensures good overlap between the electron beam, IR beam and ion cloud. A detailed description of this new device is presented followed by validation of the approach.

4.2.   Design and experimental

4.2.1 Experimental set-up

All the experiments were performed using a heavily modified Bruker APEX 7.0eT FTICR mass spectrometer equipped with an infinity cell, a 7 T super-conducting magnet and an electron source located behind the ICR cell. Figure 1(a) shows a schematic of the instrument. The ions generated by an electrospray ionization (ESI) source are accumulated in an octopole ion trap prior to being transferred to the ICR cell via two quadrupole ion guides. As can be seen, there is a clear optical path through the quadrupole ion guides and into the ICR cell. It is evident from this figure that once an IR beam is aligned through the cell and quadrupole ion guides, and the electron source has been positioned for maximum current (using the movable 'flag electrode' on the opposite side of the cell), the

geometry dictates that the beams are co-axial and will overlap with the ions contained in the center of the ICR cell.

The key to this approach is the ability to direct the IR beam through the quadrupole ion guides after the ions have been transferred to the ICR cell, specifically, the ability to align the IR laser beam along the axis, and the reproducibility of this optimum alignment. With these concerns in mind, a pneumatic probe has been designed that inserts an IR first-surface mirror in front of the quadrupole ion guides, includes a mechanical auto-alignment mechanism and allows the user to fine-tune the position and angle of the IR mirror.

4.2.2 Pneumatic probe

After ion transfer to the ICR cell an IR mirror, attached to the pneumatic probe, is inserted between ion optical elements to redirect the IR beam into the center of the ICR cell. The schematic of the instrument (Figure 4.1(a)) indicates the paths of the IR beam and electron beam. Behind the IR mirror, an electrically isolated metallic plate is also attached to the probe. While the probe is inserted, it is used to monitor the current emitted from the octopole.

Figure 4.2 details the principal elements of the probe. The probe is a stainless steel rod, to which the IR first-surface mirror and the electrically isolated electrode are attached. The mirror has been designed to redirect an incident laser beam through 49.8° azimuthal onto the ion-optical axis (this angle was defined by the available vacuum flanges).

A first surface mirror reflects light from its front surface. The use of a first-surface mirror avoids the secondary reflections of a standard mirror (reflection occurs from the front surface and rear coating) and the beam displacement due to refraction through the glass of the mirror.

Accurate positioning of the 'in' position of the IR mirror and the high reproducibility of this final position are based on a mechanical auto-alignment mechanism. Figure 4.2 also illustrates this mode of action. The probe is rigidly attached to a mounting that sits upon 3 lockable micrometer screws. Retraction of

the probe by the pneumatic actuator lifts this entire assembly: the probe, the mounting and the 3 micrometer screws. The bottoms of these screws consist of small metallic spheres, or engaging balls.

When the probe is released, the three engaging balls enter three corresponding v-shaped grooves (Figure 4.2(b)). A small rod ensures that the engaging balls enter the grooves and atmospheric pressure ensures that these spheres sit at the base of these grooves. Consequently, the lateral position of the probe is defined and reproducible.

Variation of the three micrometer screws provides up to 10 mm axial translation freedom and up to 2.5° freedom in the two elevation angle of the probe, Θand Φ (Figure 4.2). A fourth micrometer screw can be used to rotate the plate containing the three v-shaped grooves by up to ± 5 ° azimuthal (Ψ in Figure 4.2). Accordingly, these four micrometer screws allow all three angles and the axial position of the probe to be fine-tuned.

When the probe is retracted, the mirror and mount with the three micrometer screws are lifted by a pneumatic actuator, thereby not affecting the inserted position of the probe. A guide ensures the smooth motion of the probe through the duration of its insertion and extraction. Prior to the probe being mounted, the stability of the positioning system was tested using a HeNe alignment laser over a 4 m working distance. The position of the laser spot was found to be identical after hundreds of shots. Further use has confirmed the stability of the probe for extended periods of time. Similar devices have been reported to provide a mean angular error of 3µR[26].

a) Pneumatic probe

pneumatic
actuator

v-shaped
grooves

b) Retracted probe

probe
mount

micrometer
screws

guide

lectrode

probe

IR mirror

e

c) Inserted probe

steering rod

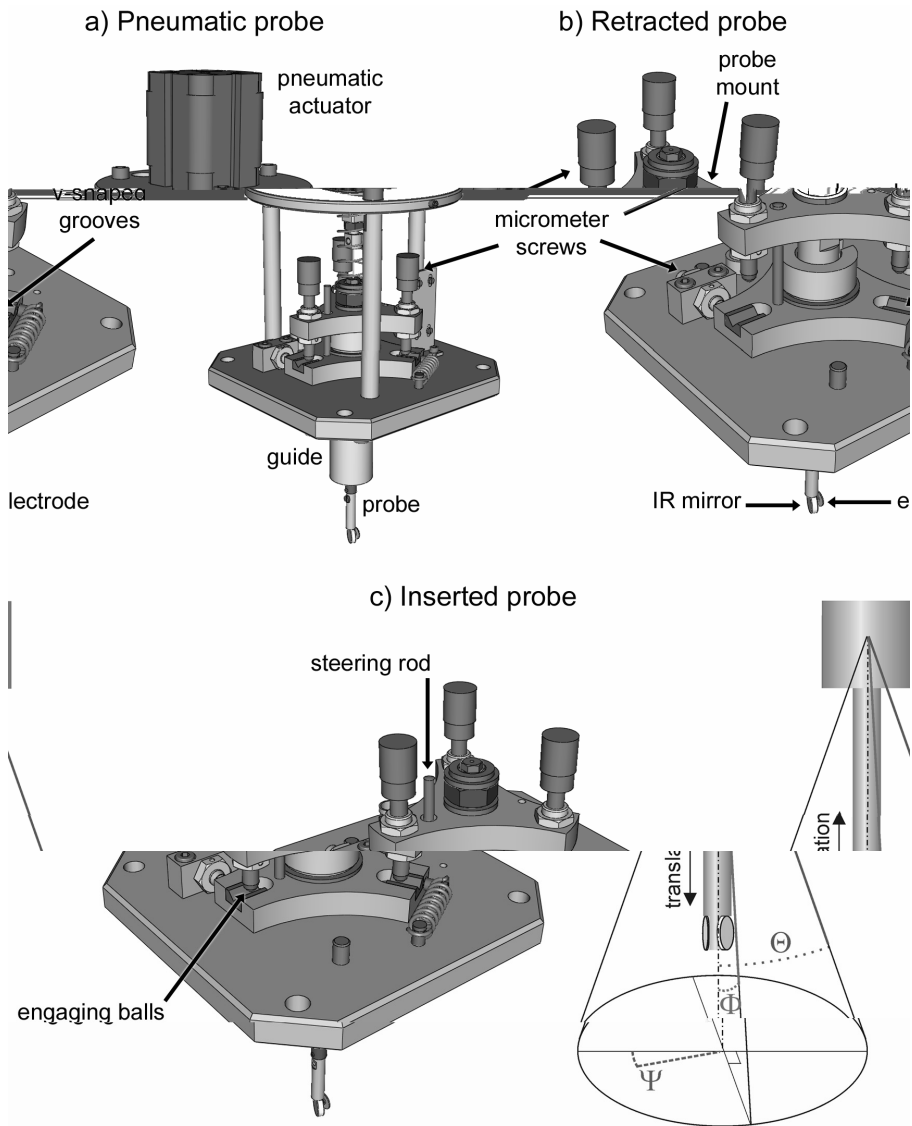engaging balls

translation

Θ

Φ

Ψ

Figure 4.2 Detailed view of the pneumatic probe (a). The four parts could be distinguished: pneumatic actuator, positioning system, guiding part and the probe itself. The positioning system and the mode of action of the pneumatic probe is illustrated: the retracted position (b) and the inserted position (c). It is also included a diagrammatic presentation of the angular freedom of the probe (c).

4.2.3 Infrared irradiation

IRMPD and the simultaneous IRMPD and ECD experiments were performed using a 10.6 μm CO_2 laser (model J48-2, Synrad, Mukiteo, WA, USA). The continuous laser pulses were activated with a TTL trigger generated by the in-house software AWE 1.5.22. Laser powers of 2 – 2.5 W (measured after the ICR cell) and pulse durations of 50 – 1500 ms have provided efficient IR activation. For improved transmission, a telescope was used to reduce the diameter of the IR beam to approximately 1.2 mm prior to it entering the mass spectrometer through a ZnSe window (see Figure 4.1 (a)).

4.2.4 Electron irradiation

An indirectly heated cathode (HeatWave, Watsonville, CA, USA) was used for the production of 320 nA of 0.45 eV electrons. When not in use, electron irradiation was prevented by positively biasing the dispenser cathode and applying a retarding potential to a grid located 5 mm in front of the cathode (for efficient electron extraction during ECD this grid was switched to +10 V).

4.2.5 Mass spectrometry

Substance P and melittin were purchased from Sigma Aldrich and used without further purification. Solutions of 20 μM in 69:29:2 methanol:water:acetic acid were electrosprayed using New Objective Picotips™ at 20 μLh^{-1}. Figure 4.3 shows a (not-to-scale) schematic of the experimental sequence.

Ions produced by the ESI source were accumulated for 30 ms in the accumulation octopole[27] and subsequently ejected into the ICR cell. Multiply charged cations were trapped in the infinity ICR cell using Ar as trapping gas Side-kick trapping was avoided to ensure the ions remained on-axis but this lengthened the experimental sequence to ≈5 s (without trapping gas, experiments can be

performed in 1-2 s). The ions of substance P, [M+2H]$^{2+}$ at *m/z* = 674.372, and melittin, [M+4H]$^{4+}$ at *m/z* = 712.196, were isolated using a stored waveform inverse Fourier transformed (SWIFT) excitation pulse[28].
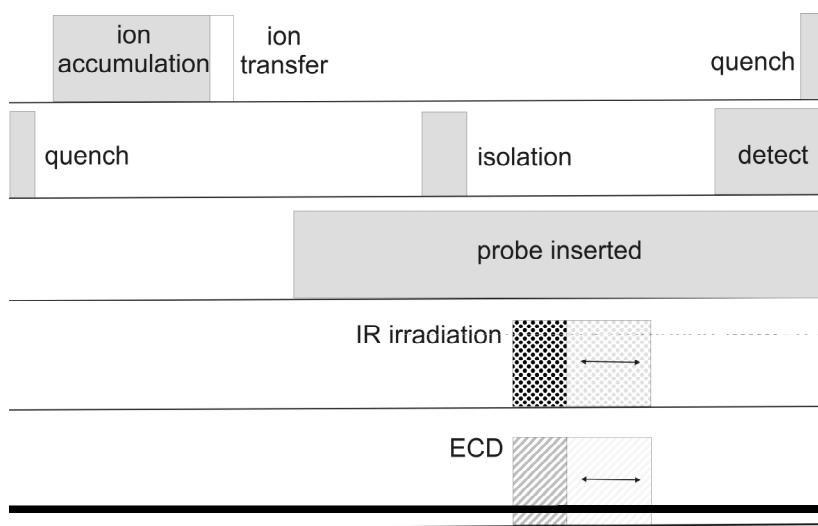

Figure 4.3 Schematic of the experimental sequence

4.3.   **Results and discussion**

Two well-characterized peptides, substance P and melittin, were used to determine the performance of our set-up. After isolation of the precursor ions, [M+2H]$^{2+}$ for substance P and [M+4H]$^{4+}$ for melittin, MS/MS-experiments were carried out with varying electron- and photon-irradiation times. All other experimental parameters were kept constant to enable the comparison of independent experiments with simultaneous electron and photon irradiation.

4.3.1 Independent and simultaneous ECD and IRMPD of Substance P

In the independent ECD-experiment of substance P the optimum electron-irradiation time with respect to the number of fragments and their signal intensities was experimentally determined at 1.5s (±0.1s). In agreement with previous results, seven c fragments, (c_4-c_{10}), and one weak z fragment, z_9, were observed (Figure 4.4)[18 29,30].

As expected, due to the presence of two prolines, c_1 and c_3 were not observed. Thus, sequence coverage of 80% corresponds to the maximum that is achievable from typical ECD fragmentation of substance P. In the independent IRMPD experiment of substance P the optimal photon irradiation time was determined at 0.5s (±0.1s) based on sequence coverage (data not shown). Generally, the fragment signal intensities in IRMPD spectra were higher than in the ECD spectra. Following IRMPD, six b ions (b_2, b_5-b_8, b_{10}) and two y ions (y_8, y_9) of substance P were seen. In addition, several ions due to secondary cleavages, *i.e.* small neutral mass losses and internal fragments, were detected. Without including these lower abundance ions the sequence coverage from the independent IRMPD experiment was 70%. As can be seen in Figure 4.4, simultaneous IRMPD and ECD of doubly protonated substance P yielded all fragments that were produced in independent ECD and IRMPD experiments. The combination of all typical ECD fragments with the y fragments results in a sequence coverage of 90% of substance P. The c and z ions in the simultaneous experiment were slightly less abundant than in independent ECD spectrum.
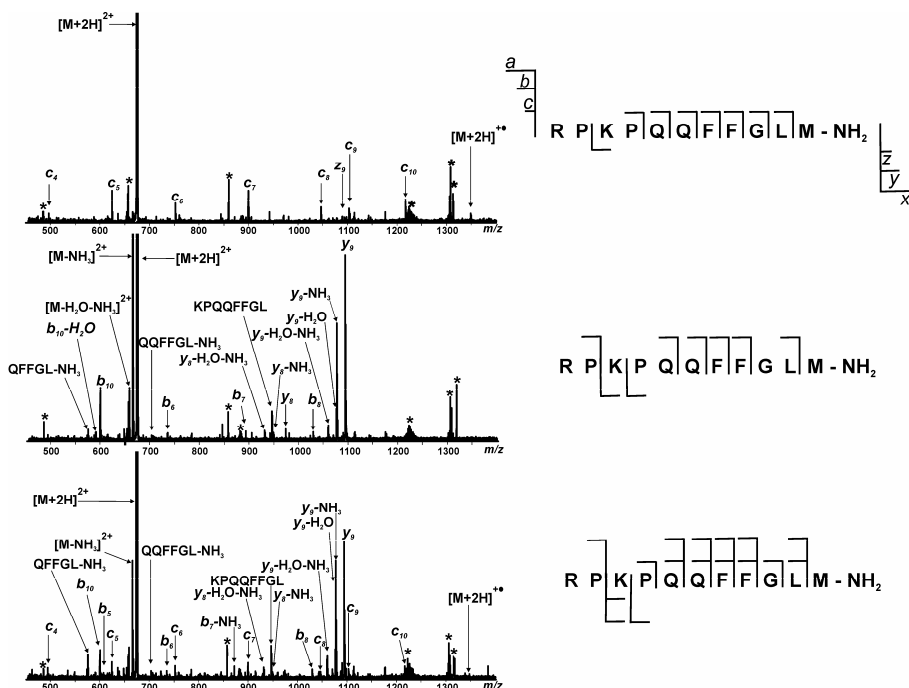
Figure 4.4 MS/MS spectra of the [M+2H]$^{2+}$ of substance P subjected to: ECD (top), IRMPD (middle) and simultaneous on-axis IRMPD and ECD (bottom). Asterisk denotes noise. Each spectrum results from the accumulation of 50 scans.

4.3.2   Independent and simultaneous ECD and IRMPD of melittin

In the ECD experiment of quadruply protonated melittin, lower electron-irradiation times, 0.5 s, were necessary because electron-capture efficiency increases with the square of the charge[16]. A typical ECD-spectrum of melittin is shown in Figure 4.5.
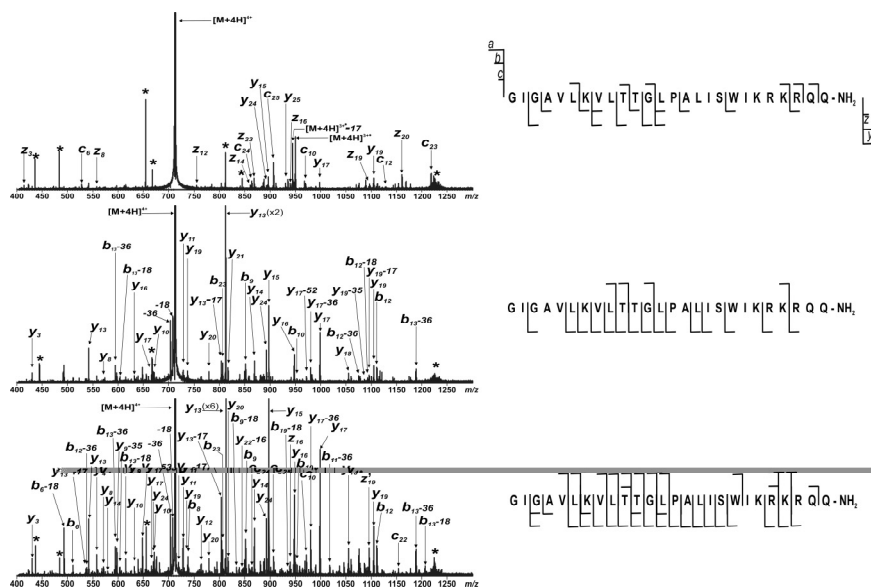
99

Figure 4.5 MS/MS spectra of the $[M+4H]^{4+}$ ions of bee venom melittin subjected to: ECD (top), IRMPD (middle) and simultaneous on-axis IRMPD and ECD (bottom). Asterisk denotes noise. Increased sequence coverage is obtained in simultaneous on-axis IRMPD and ECD (88%) compared with independent ECD (52%) or IRMPD (60%). Each spectrum results from the accumulation of 25 individual scans.

Here, six c (c_9, c_{10}, c_{12}, c_{23}-c_{25}), eight z (z_3, z_8, z_{12}, z_{14}, z_{16}, z_{19}, z_{20}, z_{23}) and five y ions (y_{14}, y_{15}, y_{17}, y_{19}, y_{24}) were detected after 0.5s of electron irradiation, as well as two triply protonated reduced species ($[M+4H]^{3+\bullet}$ and $[M+4H]^{3+\bullet}$–NH_3). Most of these c, z and y fragments are consistent with previous results[31]. In total, these 19 ECD ions result in 52% sequence coverage. When melittin is subjected to IRMPD for 0.5s, four b ions (b_9, b_{10}, b_{12}, b_{23}) and 19 y ions (y_3, y_5, y_8, y_{10}, y_{11}, y_{13}-y_{21}, y_{24}) are observed. The resulting sequence coverage from these ions is 60%. In addition, multiple ions that result from neutral losses from b and y ions are present. As was the case for substance P, the IRMPD fragments of melittin are more abundant than the ECD fragments. In all experiments product ion abundances were calculated relative to the precursor ion. After simultaneous IRMPD and ECD of melittin for 0.5s three c ions (c_{10}, c_{22}, c_{25}), four z ions (z_{24}, z_{23}, z_{16}, z_{14}), 11 b ions

(b_5, b_6, b_8 - b_{13}, b_{19}, b_{22}, b_{23}) and 22 *y* ions (y_3, y_4, y_5, y_8-y_{21}, y_{24}) are observed (Figure 4.5). This results in 88% sequence coverage, which is significantly higher than in the independent experiments at similar irradiation times (52% for ECD and 60% for IRMPD). However, compared with the independent experiments, some *c* and *z* ions disappeared and new *b* and *y* ions are generated. Additionally, ions that result from neutral losses from *b* and *y* fragments are significantly higher. To a lesser extent this change in fragmentation pathways was also seen in the simultaneous experiment of substance P. Possibly the ion cloud in the ICR cell is focused by the electron beam, resulting in a larger fraction of the precursor ions overlapping with the IR beam and thus more abundant *b* and *y* ions. IR dissociation of *c* and *z* ions would lower their abundances, as observed in the simultaneous IRMPD and ECD experiments. An alternative explanation for the increase of the relative abundance of *b* and *y* ions in the simultaneous experiments is capture of one or two electrons of the $[M+4H]^{4+}$ precursor, followed by typical *b*/*y* fragmentation upon IR irradiation[32]. This pre-activation of the IRMPD reaction pathways is in agreement with the observed decrease in the abundance of the reduced triply charged ion $[M+4H]^{3+\bullet}$ upon constant ECD irradiation and increasing IR irradiation times.

4.3.3 Irradiation times versus sequence coverage

The effects of the electron- and photon-irradiation times on the number of fragments and the resulting sequence coverage of melittin are plotted in Figure 4.6. The maximum sequence coverage of melittin using ECD was 56%, using IRMPD 76% and in the simultaneous IRMPD and ECD experiment 88%. Using simultaneous irradiation this maximum was reached at 0.5s, which was faster than IRMPD (0.55s) or ECD (0.8s). Furthermore, it is clear that simultaneous irradiation results in a higher number of fragments than in the independent experiments. Note that at 0.8s the increase in the number of fragments in the simultaneous experiment does not result in higher sequence coverage. It is the number of *primary sequence fragments* that is important, as they provide the specific

sequence information. The number of *primary sequence fragments* even begins to decrease at 0.9s due to secondary fragmentation, thus defining an optimal irradiation time in a simultaneous experiment.
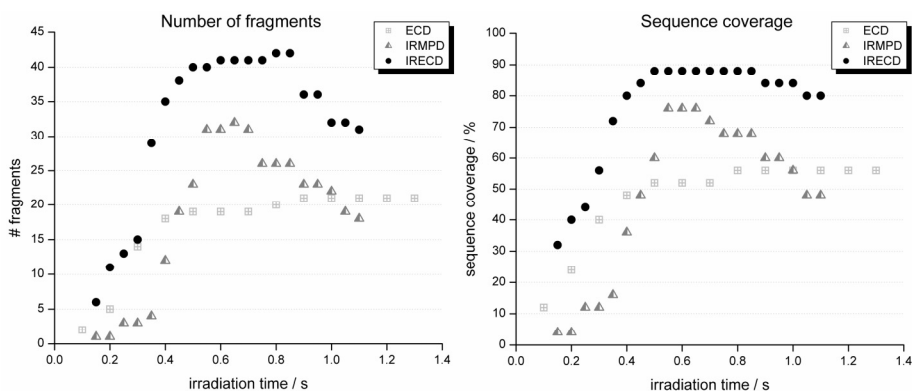

Figure 4.6 Plot of the number of fragments (left) and sequence coverage (right) vs. irradiation time for ECD, IRMPD and simultaneous on-axis IRMPD and ECD of melittin.

Simultaneous electron and photon irradiation of mellitin (and substance P) increases the sequence coverage in one MS/MS spectrum. In the set-up reported here it is possible to perform on-axis ECD and IRMPD of isolated ions in both independent experiments as well as in the simultaneous ones using irradiation times that are compatible with the time-scales of eluting LC peptides. This flexibility increases the information content of peptide tandem mass spectra for the two standard peptides used in this study.

4.4 Conclusions

We have presented an FTICR-MS set-up that allows simultaneous on-axis IRMPD and ECD in the ICR cell. In this instrumental configuration a pneumatic probe was inserted in the ion-optical path that enables on-axis IR irradiation of the ion cloud from the front of the ICR cell simultaneously with electron irradiation, provided by a standard dispenser cathode from the rear of the ICR cell. This set-up results in a better overlap between the IR beam, electron beam and the ion cloud.

Simultaneous ECD and IRMPD resulted in a significant increase in product ions and thus sequence coverage of substance P and melittin. The increased abundance of the *b* and *y* ions, and the dependence of this abundance on the order of IR and electron irradiation, is interpreted as ion cloud focusing by the electron beam concentrating the ion cloud on-axis and within the IR beam. This increased overlap allows shorter irradiation times. The flexibility to carry out both independent and combined ECD and IRMPD experiments, and the shorter time-scales of the combined experiments, are highly desirable for proteomics investigations because they increase the information content of the MS/MS spectra.

Acknowledgements

References

(1)   R. Aebersold; M. Mann Nature 2003, 422, 198-207.
(2)   M. M. Hanno Steen Nature Reviews. Molecular Cell Biology 2004, 5, 699-711.

(3)   J. Bergquist; M. Palmblad; M. Wetterhall; P. Håkansson; K. Markides Mass Spectrom. Rev. 2002, 21, 2-15.

(4)   B. Bogdanov; R. D. Smith Mass Spectrom. Rev. 2004, 24, 168-200.

(5)   J. E. Bruce; G. A. Anderson; J. Wen; R. Harkewicz; R. D. Smith Anal. Chem. 1999, 71, 2595-2599.

(6)   J. E. Bruce; G. A. Anderson; M. D. Brands; L. Pasa-Tolic; R. D. Smith J. Am. Soc. Mass Spectrom. 2000, 11, 416-421.

(7)   B. Spengler J. Am. Soc. Mass Spectrom. 2004, 15, 703-714.

(8)   Q. Hu; R. J. Noll; H. Li; A. Makarov; M. Hardman; R. G. Cooks J. Mass Spectrom. 2005, 40, 430.

(9)   J. W. Gauthier; T. R. Trautman; D. B. Jacobsen Anal. Chim. Acta 1991, 246, 211-225.

(10)   M. W. Senko; P. J. Speir; F. W. McLafferty Anal. Chem. 1994, 66, 2801-2808.

(11)   D. P. Little; P. J. Spier; M. W. Senko; P. B. O'Connor; F. W. McLafferty Anal. Chem. 1994, 66, 2809-2815.

(12)   W. Li; C. L. Hendrickson; M. R. Emmet; A. G. Marshall Anal. Chem. 1999, 71, 4397-4402.

(13)   W. D. Bowers; S.-S. Delbert; R. L. Hunter; J. Robert T. McIver J. Am. Chem. Soc. 1984, 106, 7288-7289.

(14)   E. R. Williams; J. J. P. Furlong; F. W. McLafferty J. Am. Soc. Mass Spectrom. 1990, 1, 288-294.

(15)   R. A. Zubarev; N. L. Kelleher; F. W. McLafferty J. Am. Chem. Soc. 1998, 120, 3265.

(16)   R. A. Zubarev; D. M. Horn; E. K. Fredricksson; N. L. Kelleher; N. A. Kruger; M. A. Lewis; B. K. Carpenter; F. W. McLafferty Anal. Chem. 2000, 72, 563-573.

(17)   R. A. Zubarev Mass Spectrom. Rev. 2003, 22, 57-77.

(18)   K. Hakansson; M. R. Emmett; C. L. Hendrickson; A. G. Marshall Anal. Chem. 2001, 73, 3605-3610.

(19)   K. Hakansson; H. J. Cooper; M. R. Emmet; C. E. Costello; A. G. Marshall; C. L. Nilsson Anal. Chem. 2001, 73, 4530-4536.

(20)   A. J. Forbes; S. M. Patrie; G. K. Taylor; Y. B. Kim; L. H. Jiang; N. L. Kelleher Proc. Natl. Acad. Sci. U.S.A. 2004, 101, 2678-2683.

(21)   S. A. McLuckey; D. E. Goeringer J. Mass Spectrom. 1997, 32, 461-474.

(22)   N. L. Kelleher; R. A. Zubarev; K. Bush; B. Furie; B. C. Furie; F. W. McLafferty; C. T. Walsh Anal. Chem. 1999, 71, 4250-4253.

(23)   D. M. Horn; Y. Ge; F. W. McLafferty Anal. Chem. 2000, 72, 4778-4784.

(24)   K. Hakansson; M. J. Chalmers; J. P. Quinn; M. A. McFarland; C. L. Hendrickson; A. G. Marshall Anal. Chem. 2003, 75, 3256.

(25)   Y. O. Tsybin; M. Witt; G. Baykut; F. Kjeldsen; P. Håkansson Rapid Comm. Mass Spectrom. 2003, 17, 1759-1768.

(26)   M. P. Koster 1998, Constructieprincipies voor het nauwkeurig bewegen en positioneren, Twente University Press, Enschede, 1998, 211.

(27)   I. M. Taban; L. A. McDonnell; A. Rompp; I. Cerjak; R. M. A. Heeren Int. J. Mass Spectrom. 2005, 244, 135-143.

(28)   S. Guan; A. G. Marshall Int. J. Mass Spectrom. Ion Proc. 1996, 157/158, 5-37.

(29)   J. Axelsson; M. Palmblad; K. Hakansson; P. Hakansson Rapid Comm. Mass Spectrom. 1999, 13, 474.

(30)   R. Mihalca; A. J. Kleinnijenhuis; L. A. McDonnell; A. J. R. Heck; R. M. A. Heeren J. Am. Soc. Mass Spectrom. 2004, 15, 1869.

(31)   N. C. Polfer; K. F. Haselmann; R. A. Zubarev; P. R. R. Langridge-Smith Rapid Comm. Mass Spectrom. 2002, 16, 936-943.

(32)   A. J. Kleinnijenhuis; A. J. R. Heck; M. C. Duursma; R. M. A. Heeren J. Am. Soc. Mass Spectrom. 2005, 16, 1595-1601.

Chapter 5

Disulfide bond cleavages observed in SORI-CID of three nonapeptides complexed with divalent transition metal cations

Romulus Mihalca[1], Yuri E. M. van der Burgt[1], Albert J. R. Heck[2] and Ron M. A. Heeren[1,2*]

[1]FOM Institute for Atomic and Molecular Physics (AMOLF), Kruislaan 407, 1098 SJ Amsterdam, The Netherlands
[2]Department of Biomolecular Mass Spectrometry, Bijvoet Center for Biomolecular Research,
Utrecht Institute for Pharmaceutical Sciences, Utrecht University, Sorbonnelaan 16, 3584 CA Utrecht, The Netherlands

Abstract

Tandem MS sequencing of peptides that contain a disulfide bond is often hampered when using a slow heating technique. We show that complexation of a transition metal ion with a disulfide bridge containing nonapeptide yields very rich tandem mass spectra, including fragments that involve the cleavage of the disulfide bond up to 56% of the total product ion intensity. On the contrary, MS/MS of the corresponding protonated nonapeptides results predominantly in fragments from the region that is not involved in the disulfide bond. Eleven different combinations of three nonapeptides and three metal ions were measured using Fourier transform ion cyclotron resonance mass spectrometry (FTICR-MS) using sustained off-resonance irradiation collision induced dissociation (SORI-CID). All observed fragments are discussed with respect to four different types of product ions: neutral losses, *b/y*-fragmentation with and without disulfide bond cleavage, and losses of internal amino acids without rupture of the disulfide bridge. Furthermore, it is shown that observed complementary fragment pairs obtained from peptide-metal complexes can be used to determine the region of the binding site of the metal ion. This approach offers an efficient way to cleave disulfide-bridged structures using low energy MS/MS, which leads to increased sequence coverage and more confidence in peptide- or protein assignments.

5.1   Introduction

Fourier transform ion cyclotron resonance mass spectrometry (FTICR-MS) offers a collection of techniques for identification and structural investigation of a large variety of biomolecules in the gas phase [1]. Such studies require both information obtained from high mass accuracy measurements and tandem mass spectrometry (MS^n) strategies [2]. The high mass accuracy and sensitivity of FTICR-MS enable peptide identifications with high confidence in the analysis of complex peptide mixtures in a typical proteomics set-up. Moreover, most tandem MS

techniques currently used for peptide fragmentation are compatible with FTICR mass spectrometers. The amount and quality of information obtained from these MS[n] spectra is strongly related to the identity, relative abundance, and the number of product ions. In this paper we report on unexpected fragmentation pathways of three similar nonapeptides using a so-called slow heating fragmentation technique [3]. The most unexpected fragments observed in these rich tandem mass spectra result from different cleavages of a disulfide bridge between the two cysteines. It will be shown that complexation of these peptides with transition metal ions results in enhancement of this effect.

5.1.1 Slow heating techniques for tandem MS

Tandem mass spectrometry (MS[n]) is an indispensable tool to structurally characterize a selected precursor ion by analyzing its dissociation products. The most common method for ion fragmentation is collision-induced dissociation (CID), often used for sequencing tryptic peptides obtained in a proteomics experiment. However, for sequencing peptides and proteins with a higher molecular mass (>2 kDa) CID is not an ideal method. For these purposes, slow heating techniques can be advantageous. With these techniques the internal energy of a molecule is slowly increased to initiate molecular fragmentation. FTICR mass spectrometers are extremely suitable for the application of slow heating techniques such as infrared multiphoton dissociation (IRMPD) [4], blackbody infrared dissociation (BIRD) [5,6], ultraviolet photon dissociation (UVPD) [7-10], surface induced dissociation (SID) [11-14], on-resonance collision induced dissociation (CID) [15] or sustained off-resonance induced dissociation (SORI-CID) [16-18]. These techniques are referred to as "slow heating" because the trapped gas-phase ions are collided with relatively low kinetic energies to induce ion activation and fragmentation. In SID the internal energy is increased through collision of the ion of interest with a static target [12-14,19,20], whereas in on-resonance CID and SORI-CID the collision target is mobile *i.e.* neutral atoms of an inert gas like Ar or He are pulsed into the ICR cell. In SORI-CID the selected precursor is periodically excited and de-excited by applying, in the

presence of a collision gas, a low-amplitude radio-frequency pulse slightly off-resonance (-1500Hz) compared to the cyclotron frequency of the selected ion [21]. During this process the ions undergo multiple collisions with the neutral atoms of the collision gas. In each collision event a part of the kinetic energy of the ion is converted into internal energy. In this way the internal energy of the excited ions can be modulated, thus enabling the study of the lowest energy fragmentation pathways. Compared with on-resonance excitation, the collision energy in SORI-CID is much lower because of the lower kinetic energy of the ions. Another advantage over CID is that in SORI-CID the fragments are produced close to the axis of the cell allowing a more efficient detection of the dissociation products. With IRMPD, BIRD, and UVPD the trapped ions are dissociated by irradiation with an infrared (IRMPD) or an ultraviolet (UVPD) laser beam or they are activated through absorption of infrared photons (BIRD) from a heated ICR cell. Similar to the SORI experiment, the energy after multiple photon absorption is redistributed through intramolecular vibrations. The dissociation essentially follows the same type of fragmentation pathways as using collisionally-based dissociation techniques.

5.1.2 Disulfide bond cleavages in mass spectrometry

It is well known that disulfide bonds play an important role in defining and stabilizing the secondary and tertiary structure of folded proteins [22]. Many biologically relevant peptides contain one or more intramolecular disulfide bonds between different cysteine residues. Tandem MS sequencing of peptides that contain disulfide bonds is often hampered when using slow heating techniques. For example, CID of multiply protonated insulin with two intramolecular linkages results in incomplete sequence coverage [23]. In general, sequencing of multiply protonated peptides with intramolecular disulfide bonds is limited to backbone fragments that do not contain the disulfide linkage. This reduces the amount of information which can be extracted using such MS^n techniques. A common approach to overcome this problem is to reduce and alkylate the disulfide bonds prior to MS^n analysis. This preparation step is time consuming and, therefore, not desirable for high-

throughput proteomics applications. Moreover, the site-specific information on the exact location of the S-S bond linkages is lost following reduction. Another approach of analyzing cysteine-bridged peptides is using high-energy CID [24,25], MALDI in-source decay [26,27] or post-source decay [26-29], or MALDI combined with ion trap mass spectrometry [30]. In addition, ion trap mass spectrometry has been used both in positive [23] and negative [31] mode to study peptides/proteins that contain disulfide linkages. A powerful method for dissociation of multiply charged proteins that contain disulfide bridges is electron capture induced dissociation (ECD) introduced by McLafferty and co-workers [32,33]. It has been shown that ECD has the potential for cleaving and mapping disulfide bonds present in peptides and proteins [34, 35]. Currently, ECD is implemented only on FTICR instruments, whereas compatibility with three-dimensional quadrupole ion traps would make it a more accessible fragmentation technique [36,37]. ECD of peptides requires multiple protonation which can be difficult to be achieve. To overcome this hurdle, metal ions can be used as charge carriers in peptides. Moreover, the presence of a certain metal ion may be pivotal for the biologic activity of the peptide. Often the secondary and/or tertiary structure of a peptide (or protein) is changed by a co-factor such as a metal ion or a small nucleotide. A well-known example is the hormone oxytocin, for which the presence of a transition metal cation like Cu or Zn is essential for binding to its cellular receptor. ECD efficiency does not increase using a metal ion, however it has been shown that metalated peptides provide complementary ECD fragments compared to protonated species [38,39]. In line with this is a recent study on substance P in which complexation with divalent metals resulted in very rich ECD spectra of triply charged species [38,39]. Structural investigation of oxytocin complexed with different divalent transition metal ions showed remarkable differences in the ECD spectra [40]. Here, the observed specific fragmentation pathways for different charge carriers possibly result from structural differences between the oxytocin-metal ion complexes. For oxytocin complexed with Ni^{2+}, Co^{2+}, or Zn^{2+} the most abundant ECD fragments included the cleavage of the disulfide bond. However, the [oxytocin+Cu^{2+}] complex showed mainly b' type ions that did not result from cleavage of the disulfide bond. In the latter case 15% of the fragments included a disulfide bond cleavage whereas for other oxytocin-

metal ion complexes 60-70% of the fragments included one cysteine residue only. This atypical ECD behaviour of the [oxytocin+Cu^{2+}] complex inspired us to investigate this compound with a slow heating technique such as SORI-CID in more detail.

5.1.3 Rationale of this work

In this work the SORI-CID fragmentation pathways of three different nonapeptides containing one disulfide bond are studied. The effect of complexation with different divalent transition metal cations compared with protonated peptide will be discussed in terms of cleavage efficiency of the disulfide bond. Further, it will be investigated whether the differences between the measured tandem mass spectra can be correlated to possible conformational changes in the peptide due to the presence of a metal ion. Oxytocin (OT, CysTyrIleGlnAsnCysProLeuGly) was chosen as a model compound for these studies based on the remarkable results from earlier work [40].

Two peptide analogs were chosen to explore possible structural correlations or differences, namely vasopressin (VS, CysTyrPheGlnAsnCysProArgGly) and Thr4-Gly7-oxytocin (TGOT, CysTyrIleThrAsnCysGlyLeuGly). All three peptides contain a disulfide bridge between the cysteines at positions 1 and 6 and are amidated at the C-terminus. Usually, for OT the peptide region that is closed by the disulfide bond is called the tocin ring and the remaining part is referred to as the tail. The tocin ring is a rather rigid structure, whereas the tail is flexible. In this paper, the terms "tocin ring" and "tail" will also be used for describing regions of the other two nonapeptides due to the structural similarities with oxytocin. Both oxytocin and vasopressin exert various hormonal effects. Oxytocin is responsible for elicit contraction of uterus smooth muscle at term and of myoepithelial cells that surround the alveoli of the mammary gland during lactation [41]. Oxytocin also plays a decisive role in the affiliation process in mammals like maternal behaviour and infant separation distress [42]. Vasopressin facilitates water re-absorption by the kidney and the contraction of

smooth muscle cells in arteries [41, 43]. Moreover, more recent studies showed that these peptides are involved in numerous cognitive processes such as memory and learning [41]. Oxytocin and vasopressin are biologically activated by essential elements like metal ions (Zn^{2+}, Ni^{2+}, or Co^{2+}). The presence of the divalent metal ion could drastically change the peptide conformation with implications in the binding process of these peptides to their receptors. The role of these metal ions for the interaction process of oxytocin with its receptor was highlighted earlier [44, 45]. It has been shown that binding of oxytocin to its receptor is enhanced in the increasing order of Zn^{2+}, Ni^{2+}, and Co^{2+} but is negligible is the presence of Cu^{2+} [43]. However, it has not been elucidated whether the metal ion interacts first with the peptide, the receptor, or with both.

5.2   Experimental

5.2.1. Mass Spectrometry

All the experiments were performed using a heavily modified Bruker APEX 7.0eT FTICR mass spectrometer equipped with a 7 T superconducting magnet and an infinity cell. The ions generated by an electrospray ion source are accumulated (300-500 ms) in an octopole ion trap [46] prior to being transferred to the ICR cell via two quadrupole ion guides. Argon was used for gas assisted dynamic trapping of the ions. High resolution mass spectra revealed that all of the nonapeptides complexed with divalent metal cations resulted in parent ions of the type [peptide+metal]$^{2+}$. The full isotopic cluster of a doubly charged parent ion was isolated using a stored waveform inverse Fourier transformed (SWIFT) excitation pulse [47]. In some cases, an additional SWIFT isolation was applied to avoid noise signals at the lower mass range. Fragmentation of protonated and divalent metal containing peptides was carried out using SORI-CID [16]. The isolated ion clusters were excited kinetically using a SORI pulse with 250 cycles at a frequency -1500 Hz away from the cyclotron frequency of the isolated ion. For fragmentation, argon collision gas was pulsed into the cell at a pressure range of 10^{-7} mbar. During

detection the pressure in the ICR cell was less than 10^{-9} mbar. All experimental parameters were controlled using software and hardware developed in-house as part of the continual evolution of this proteomics / fundamental studies instrument [48, 49]. Data analysis was carried out both manually and automatically using in-house developed processing tools [50].

5.2.2   Sample preparation

All three nonapeptides, namely oxytocin (OT), Thr4Gly7oxytocin (TGOT), and Arg8vasopressin (VS), were purchased from Sigma Aldrich and used without further purification. All three peptides contain a disulfide bond between Cys-1 and Cys-6 and are amidated at the C-terminus. Sample solutions of 49:49:2 water:methanol:acetic acid at a concentration of 20 μM were prepared. Freshly prepared complexes of the peptides with Ni^{2+}, Zn^{2+} and Cu^{2+} were obtained using the corresponding acetate salt of the metal ion in 25 times excess in the absence of acetic acid. Electrospray ionisation was carried out using New Objective Picotips™ at 500 nl/min and an electric potential difference of approximately 2100 V.

5.3   Results and discussion

5.3.1   Nomenclature

The assignment and designation of peptide fragments is based on Roepstorff-Fohlman-Biemann nomenclature [51-53]. All observed backbone cleavages in the three studied nonapeptides are typical *b* or *y*, in which the charge is retained at the N- or the C-terminus, respectively. For calculation of the exact masses of the fragments for each cysteine residue, one hydrogen atom is subtracted because of the disulfide bridge. Backbone fragments that result from cleavage between residues 1 up to 6 ("tocin ring") require additional cleavage of the disulfide bridge.

Basically, this disulfide bridge can be cleaved at three different positions. The "regular" fragment ion results from S-S cleavage. Two other types are referred to as "+S or –S" when the backbone bond is cleaved in combination with an S-C bond. These fragment ions thus contain either two or zero sulphur atoms. In principle, the fragment ions observed in the tandem mass spectra of nonapeptides complexed with Zn^{2+}, Ni^{2+}, or Cu^{2+} retained the metal ion. It will be mentioned explicitly when this is not the case (see Table 2). Finally, the internal fragments resulting from multipoint cleavages in the backbone of the parent ion [54, 55] or the dissociation products are denoted with the three-letter code of the amino acid that is lost.

5.3.2. Four different types of product ions in SORI-CID spectra

For each of the three nonapeptides, three different tandem MS spectra (SORI-CID after SWIFT-isolation of the doubly charged parent ion) were obtained after complexation with Zn^{2+}, Ni^{2+}, or Cu^{2+} ions. Similarly, MS/MS was carried out on doubly protonated oxytocin (OT) and vasopressin (VS). In the case of Thr4GlyOxytocin (TGOT) the doubly protonated species was not observed in the mass spectrum, probably due to the absence of basic amino acids. Thus eleven SORI-CID spectra were obtained. These will be discussed according to the different types of product ions as depicted in Figure 5.1. Each product ion results either, from a neutral loss or a typical *b/y*-fragmentation, or a combination thereof. In addition, certain product ions require the cleavage of the disulfide bridge, which occurs either at S-S or at C-S. Basically, four main types of product ions are observed in the spectra. The first results from single or multiple neutral loss of NH_3, H_2O, or CO from the parent ion (I). The second follows "regular" *b/y*-fragmentation of the peptide backbone tail (II), resulting in observed product ions b_6, b_7, b_8, y_3, and y_2. The third type results from *b/y*-fragmentation in the tocin ring, including a cleavage of the disulfide bridge (III). As was explained earlier (section 5.3.1), this fragmentation pathway results in observed fragments such as b_4, b_4+S, y_7, or y_4-H_2S. These product ions are rather unexpected, since disulfide bonds usually are

not affected by slow heating techniques. The fourth and last type of product ions here considered also requires multipoint cleavages (IV), as is the case for fragmentation of type III. Here, one or more internal amino acids are lost from the parent through typical *b/y*-cleavages, whereas the disulfide bridge remains intact. Such losses are observed from both the tocin ring and the tail. Complementary, in most cases of multiple residue loss these internal amino acids are observed in the spectrum (*e.g.* [Tyr+Ile]$^+$ or [Tyr+Ile+Thr]$^+$). The sequence of events to result at type I, II, III, or IV ions is chosen arbitrarily in Figure 5.1. The results from all eleven SORI-CID spectra are summarized in Figure 5.2. In Table 5.1, all the identified product ions are categorized according to the four types of fragmentation pathways. The intensity of each product ion was determined from all corresponding peak intensities in the isotope cluster. In the case of a Ni^{2+}- or Cu^{2+}-complexed peptide at least three isotopes were observed in one cluster, whereas in the case of Zn^{2+} at least four peaks were taken into account. Thus, the obtained intensities are shown relative to the total intensity of all assigned product ions. The total number of assigned fragments in each MS/MS spectrum varied between 16 and 55. In most of the assignments the mass accuracy was below 5 ppm. Mass accuracies between 5 and 15 ppm were usually due to significant intensity differences (more than 100-fold) between the fragments used for calibration and the ion of interest. Also shown in Table 1 are the assigned fragments as a percentage of the total product ion intensity (%PII). For most species more than 75% of PII is assigned. For VS+Cu^{2+}, OT+Zn^{2+} and TGOT+ Zn^{2+} a significant amount of PII was not assigned (48%, 40% and 42%, respectively), mostly because of overlap with other isotope clusters in the mass spectrum (an example is shown in Figure 5.3, see section 5.3.3.). Moreover, it is evident that the typical isotope profiles of the transition metals add complexity to the spectrum. In the following sections the SORI-CID results will be discussed with respect to the four types of product ions depicted in Figure 5.1.
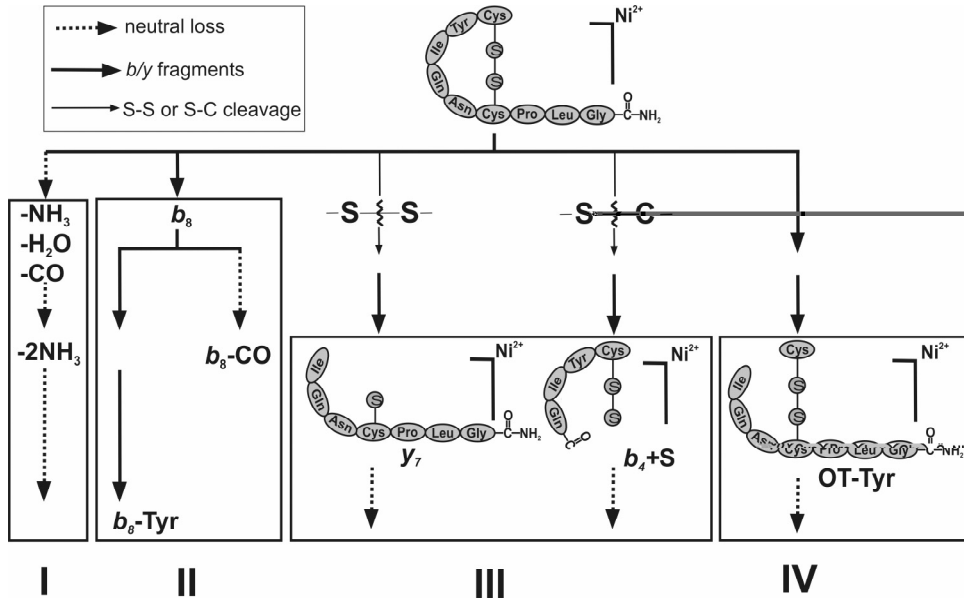
Figure 5.1 Overview of different types of product ions observed in SORI-CID spectra of protonated or metal-complexed nonapeptides. As an example, a few of the product ions observed upon SORI-CID of oxytocin complexed with Ni^{2+} are shown. Note that the sequence of events is chosen arbitrarily, *e.g.* "b_8-CO" may also result from the loss of CO followed by *b/y*-fragmentation. The ion "OT-Tyr" may fragment further to "b_8-Tyr" via *b/y*-fragmentation.
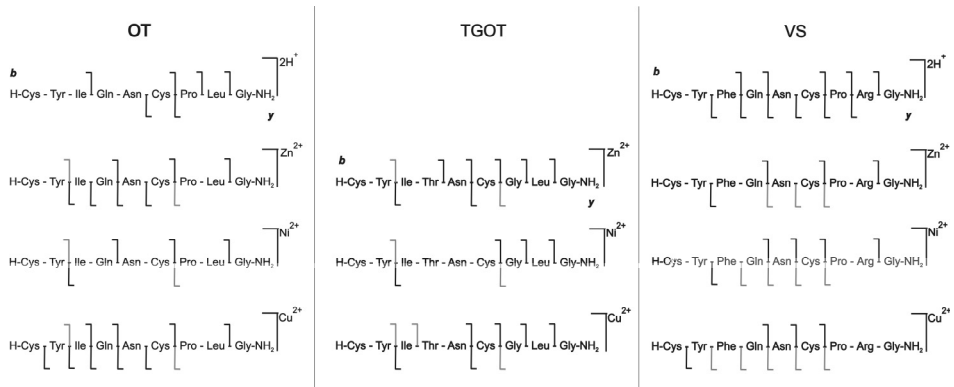

Figure 5.2 Summary of all fragments observed in eleven different SORI-CID spectra

(i)   Small neutral losses from the parent ion (I)

Single or multiple losses of small neutral species (NH_3, H_2O, and CO) from the parent ion are observed in all eleven spectra, however with significant variation in relative abundances (see type I product ions in Table 5.1). For OT and TGOT the highest total peak intensity of neutral losses is observed in the Ni^{2+}-complexed peptide and a low total peak intensity in the Cu^{2+}-complex, whereas for VS the opposite is true. As is clear from Figure 5.1, small neutral losses are also observed from product ions of type II, III, or IV. In total, this additional loss accounts for 10-50% of thus resulting ions, which remain categorized as *b/y*-fragments (type II, III, or IV). Notably, in the MS/MS spectrum of VS+Cu^{2+} the loss of H_2S is observed in different product ions (*i.e.* M-H_2S, M-(H_2S+NH_3) and M-(H_2S+NH_3+H_2O)). This results from a rather unexpected cleavage of the disulfide bond, which will be discussed in more detail in section 3.2.3.

(ii)   "Regular" b/y-product ions from the peptide backbone tail (II)

Fragmentation of the backbone tail through *b/y*-cleavages accounts for 20% (OT+Cu^{2+}) to 64% (OT+2H^{2+}) of PII (see type II product ions in Table 5.1). The two protonated species (OT and VS) show the highest relative amount of tail fragments due to the absence of type III ions (see also section 5.3.2. iv.). The observed fragments in the peptide backbone tail are b_6, b_7, b_8, y_3, and y_2. Note that in none of the eleven different spectra did *all* of these ions occur at once. Complete series of *b*-ions from the tail are observed in all spectra from TGOT that is complexed with a metal ion. Due to the presence of proline in OT and VS it is expected that b_6 and y_3 ions dominate the type II product ions. This effect is illustrated in Table 5.2, where the intensities of b_6 and y_3, and the sum of all remaining type II ions are depicted as the percentage of the total product ion intensity.

Peptide	assigned fragments (no.)	assigned fragments (%PII)	I (neutral loss)	II (tail *b*/*y*)	III (ring *b*/*y*)	IV (internal loss)
[OT+2H⁺]	41	99	23	64	1	12
[OT+Zn²⁺]	25	60	10	45	37	8
[OT+Ni²⁺]	20	86	44	45	8	3
[OT+Cu²⁺]	55	87	16	20	50	14
[T OT+Zn²⁺]	36	58	19	24	56	1
[T OT+Ni²⁺]	26	75	51	34	14	1
[T OT+Cu²⁺]	34	76	7	30	51	12
[VS+2H²⁺]	40	93	16	61	1	22
[VS+Zn²⁺]	16	80	12	47	40	1
[VS+Ni²⁺]	17	79	9	48	43	0
[VS+Cu²⁺]	28	52	26	21	53	0

Table 5.1 Product ion intensities in SORI-CID spectra of three different nonapeptides.

Peptide	b_6	y_3	all other type II ions (tail b/y)
[OT+2H$^+$]	13	4	47
[OT+Zn^{2+}]	26	16	3
[OT+Ni^{2+}]	29	12	4
[OT+Cu^{2+}]	4	3	13
[T OT+Zn^{2+}]	4	2	18
[T OT+Ni^{2+}]	12	5	17
[T OT+Cu^{2+}]	3	1	26
[VS+2H^{2+}]	36	18	7
[VS+Zn^{2+}]	14	15	18
[VS+Ni^{2+}]	19	27	2
[VS+Cu^{2+}]	16	5	0

Table 5.2 Product ion intensities of b_6 and y_3 compared to other type II fragments. The numbers in this table indicate the percentage of PII.

As is clear from Table 5.2, this effect of proline is observed in OT+Zn^{2+} and OT+Ni^{2+}. Remarkably, in both OT+2H^{2+} and OT+Cu^{2+} fragment ions b_7 and b_8 dominate or at least contribute significantly to the tail fragments. These findings can be explained as a result of different structural conformations of OT upon complexation with different metal cations. In contrast to OT, for all species of VS the ions b_6 and y_3 dominate the tail fragments. In the case of VS+Zn^{2+} also intense b_8-ions are observed. In all species of TGOT the ions b_6 and y_3 appear in the SORI-CID spectra. These ions are not dominating the tail fragments, which is expected due to the change of proline in glycine at position 7. For all metal-

complexed nonapeptides the y_3-fragment appears in the SORI-CID spectrum as a singly protonated ion. The only exception is OT+Cu^{2+}, where both protonated and metal-containing y_3 are observed in the spectrum in a ratio of 7:1. From this observation of protonated y_3-ions it is concluded that the metal cation is complexed with amino acids between 1 and 6. This is in agreement with the fact that in all spectra of metal-complexed nonapeptides the b_6-ion contains the doubly charged metal cation. The location of the metal cation in the peptide complex will be discussed in more detail in section 5.3.3. Finally, in some spectra internal amino acid loss from a b_8-ion is observed (OT+Cu^{2+}, OT+Ni^{2+}, OT+2H$^+$). One example is described in Figure 1, *i.e.* b_8-Tyr. It cannot be determined whether this product ion results from first b_8-formation and then loss of Tyr, or the reverse order, or a combination of these two possibilities.

(iii)   Cleavage of the disulfide bridge (III)

As is indicated in Figure 5.1, product ions of type III require a two-step process. Both a *b/y*-fragmentation in the tocin ring and cleavage of the disulfide bridge is necessary for the formation of b_2, b_3, b_4, b_5, y_8, y_7, y_6, y_5, and y_4, and derivatives thereof (such as b_4+S). From Table 5.1 it can be seen that SORI-CID fragmentation of the two protonated species hardly yields any ion of type III. This is in agreement with earlier studies, in which it was found that disulfide bridges hamper peptide sequencing using MS/MS methods (see also section 5.1.2). Surprisingly, when complexed with Cu^{2+} or Zn^{2+} all three nonapeptides yield significant amounts of product ions of type III (varying from 37% to 56% of PII). As a result these SORI-CID spectra are richer than those of doubly protonated precursor ions and thus show greater peptide sequence coverage. In addition, the location of the disulfide bridge is reflected in the product ions. In the case of complexes with Ni^{2+} type III ions are less abundant for OT and TGOT (8% and 14% respectively), whereas for VS+Ni^{2+} 43% of PII results from cleavages of the disulfide bridge. This increase in cleavage efficiency of the disulfide bond is likely the result of conformational differences between the different metal-complexed

peptides. Earlier, we also observed remarkable differences in ECD spectra of metal-complexed OT dependent on the type of metal ion used [40]. Furthermore, it is known that the conformation of oxytocin changes upon complexation with different metal cations [45]. Also, the biological activity of oxytocin depends strongly on the type of transition metal cation [44], which relates intuitively to the conformation of the metal-complexed peptide. Finally, the loss of H_2S is observed in metal-complexed peptides, both from the parent ion (VS+Cu^{2+}, see also 5.3.2. i) and from *b*- or *y*-ions from the tocin ring (b_3, b_4, b_5, b_6, y_5, y_4).

(iv)   Loss of internal amino acids via *b*/*y*-fragmentation (IV)

Product ions of type IV result from sequential *b*- and *y*-ion formation. When this two-step process occurs in the tocin ring both the "lost" internal amino acid(s) and the remaining M-(internal loss) can be expected in the MS/MS spectrum, provided that the disulfide bridge remains intact. Such ions are actually observed in five of the SORI-CID spectra here discussed and account for 8% to 14% of PII. In the case of protonated VS the intensity is even 22%, mainly due to an abundant fragment ion pair [M-(Phe+Gln+H^+)]$^+$ / [Phe+Gln+H^+]$^+$. Both single and multiple amino acid losses from the parent are seen, where the latter process results in complementary product ions such as [Tyr-Ile]$^+$ or [Tyr-Ile-Thr]$^+$. These complementary fragments are detected as protonated species and never contain a metal cation. This fragmentation pathway is discussed in more detail in section 5.3.3. Furthermore, from Table 5.1 it can be seen that VS complexed with metal ions hardly yields any type IV ions upon SORI-CID. This fragmentation pathway also holds for Ni^{2+}–complexed OT and TGOT and TGOT+Zn^{2+}.

5.3.3 Localization of the transition metal ion in the peptide complex

In all of the discussed SORI-CID spectra of the nine metal-complexed species, multiple product ions are present that do not contain the metal cation. Only in a few cases, the absence of the metal ion is clear from the isotopic distribution of the fragment ion. When the absence of the metal ion cannot be determined unambiguously due to overlap between different clusters and low intensities of isotopes at lower masses, the assignments are based on mass accuracy. As an example, the SORI-CID spectrum of OT+Cu^{2+} is shown in Figure 5.3.
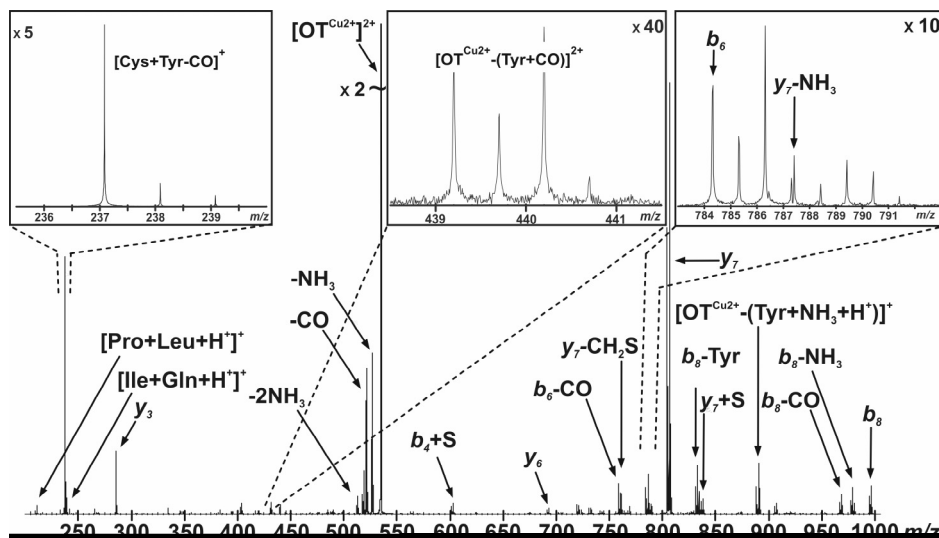
Figure 5.3 SORI-CID spectrum of OT+Cu^{2+} obtained after SWIFT-isolation of the doubly charged Cu^{2+}–complexed nonapeptide. Note that all ions contain a Cu^{2+}–ion, except for [Cys+Tyr-CO]$^+$ and y_3.

The isotope profile of the ion at *m/z* 237 is in good agreement with a distribution lacking Cu^{2+}, whereas at *m/z* 439 a clear Cu^{2+}–like isotope profile is observed. The magnification in Figure 5.3 at *m/z* 784 shows an example of overlapping clusters in

a SORI-CID spectrum (mentioned in section 5.3.2.). We hypothesize that fragments that lack the metal ion have a significant role in determining the location of the metal in the peptide complex in the gas phase. Moreover, corresponding fragments that contain the metal ion corroborate these data. To test this idea, the OT+Zn^{2+} species is chosen because earlier work was carried out on the localization of the metal ion in this peptide complex [44, 45]. Using molecular modelling it was found that the metal ion coordinates to amino acids in the tocin ring (Tyr-2, Ile-3, Gln-4, and Cys-6), and also may have interaction with amino acids from the tail (Pro-7 and Leu-8) [45]. In Figure 5.4 two strong fragment ion pairs can be seen, namely b_2/y_7 and b_6/y_3.
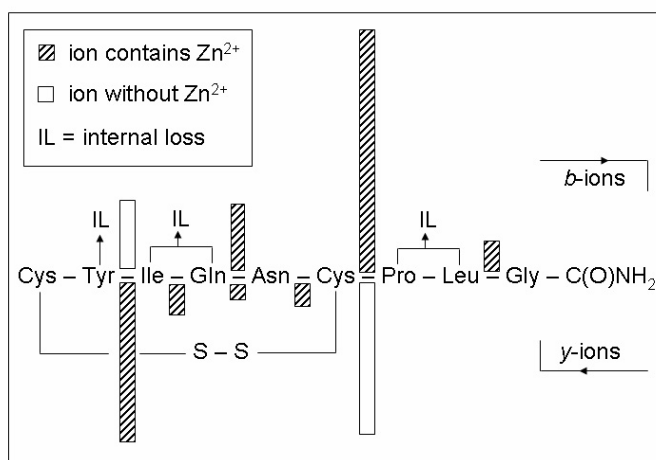
Figure 5.4 Overview of fragment ions obtained from SORI-CID of OT+ Zn^{2+}. The length of the bars correlates linearly with the ion intensity.

In the first pair the Zn^{2+} remains on the *y*-ion, whereas in the second Zn^{2+} is present in the *b*-ion cluster. From these pairs it follows that is preferably interacts with Ile-3, Gln-4, Asn-5 and/or Cys-6 in the tocin ring. Additional *y*-fragments in this part of the peptide (y_4-y_6) are of low intensity, therefore unambiguous localization of Zn^{2+} is not

possible from these ions. Internal losses of amino acids are observed from fragment ions in the mass spectrum that do not contain Zn^{2+}. This suggests that these amino acids are not, or at least not preferentially, involved in the Zn^{2+}–complexation in the tocin ring. This would leave Asn-5 and Cys-6 for interaction with Zn^{2+}, however an intense b_4–ion containing the metal is observed. This b_4–ion actually is a "b_4+S" fragment, implying that Zn^{2+} remains on the b_4–part when the two sulphurs from the disulfide bridge are also included. Hence, all data points towards the presence of Zn^{2+} in the tocin ring. Additional fragments that result from this part of the peptide indicate interaction of the metal ion with Ile-3, Gln-4, Asn-5 and/or Cys-6. In all other metal-complexed nonapeptides the typical fragment ion pair b_6/y_3 is highly abundant in the SORI-CID spectra, implying the presence of the metal ion in the tocin ring. The b_2/y_7 pair is present in all species of OT and TGOT, however the b_2–ion is not present in the spectra of VS. In the case of OT+Cu^{2+} both protonated and metal-containing y_3 are observed in the spectrum (ratio 7 to 1, see also 5.3.2. ii). In addition, the b_6–ion is present both with and without the Cu^{2+}-ion (ratio 11 to 1). This strongly indicates a mixture of two different species, *i.e.* one species with Cu^{2+} attached to the tail and one with Cu^{2+} coordinating in the tocin ring.

5.4   Conclusions

It was shown that SORI-CID of a disulfide bridge containing nonapeptide (OT, TGOT or VS) complexed with a divalent transition metal ion (Ni^{2+}, Cu^{2+} or Zn^{2+}) resulted in four types of dissociation products. First, small neutral mass losses from the parent accounted for 7% up to 51% of the product ion intensity. Surprisingly, VS+Cu^{2+} showed the loss of H_2S as a neutral. Second, for all species high intensities of backbone fragments resulting from cleavage of the tail region were observed (20% - 64% PII). For all metalated peptides the b_6/y_3 ion pair suggested the presence of the metal ion in the tocin ring. Thirdly, SORI-CID spectra of Zn^{2+} or Cu^{2+}–complexed peptides showed abundant cleavages of the disulfide bond (37% - 56%). In the Ni^{2+}–complexed peptides of OT and TGOT

these ions are of lower intensities, whereas in the protonated species rupture of the disulfide bridge was observed only in trace amounts. This observed cleavage of the disulfide bridge upon complexation of a divalent transition metal ion to a peptide is likely a result of induced conformational changes. Finally, in five out of eleven different species single or multiple internal residue losses were observed (8% - 22% PII). It was shown that these internal losses in combination with fragment ion pairs can be used to localize of the complexation of the metal ion. The results presented here highlight the advantages of using transition metal-cationized complexes for sequencing disulfide bridged structures of peptides (and proteins) using slow heating techniques such as SORI-CID. This aspect is important because numerous biologically relevant peptides and proteins contain one or more disulfide bonds that often hamper MS/MS sequencing of amino acids in the bridged region.

Acknowledgements

References

(1)   Bogdanov, B.; Smith, R. D. Mass Spectrom. Rev. **2004**, 24, 168-200.
(2)   Aebersold, R.; Mann, M. Nature **2003**, 422, 198-207.
(3)   McLuckey, S. A.; Goeringer, D. E. J. Mass Spectrom. **1997**, 32, 461-474.
(4)   Little, D. P.; Spier, P. J.; Senko, M. W.; O'Connor, P. B.; McLafferty, F. W. Anal. Chem. **1994**, 66, 2809-2815.
(5)   Price, W. D.; Schnier, P. D.; Williams, E. R. Anal. Chem. **1996**, 68, 859-866.
(6)   Dunbar, R. C.; McMahon, T. B. Science **1998**, 279, 194-197.
(7)   Bowers, W. D.; Delbert, S.-S.; Hunter, R. L.; Robert T. McIver, J. J. Am. Chem. Soc. **1984**, 106, 7288-7289.

(8)   Williams, E. R.; Furlong, J. J. P.; McLafferty, F. W. J. Am. Soc. Mass Spectrom. **1990**, 1, 288-294.

(9)   Thompson, M. S.; Cui, W.; Reilly, J. P. Angew. Chem. **2004**, 43, 4791-4794.

(10)   Fung, Y. M. E.; Kjeldsen, F.; Silivra, O. A.; Dominic Chan, T. W.; Zubarev, R. A. Angew. Chem. **2005**, 44, 6399-6403.

(11)   Tsaprailis, G.; Nair, H.; Somogyi, A.; Wysocki, V. H.; Zhong, W.; Futrell, J. H.; Summerfield, S. G.; Gaskell, S. J. J. Am. Chem. Soc. **1999**, 121, 5142-5154.

(12)   Laskin, J.; Denisov, E.; Futrell, J. H. Int. J. Mass Spectrom. **2002**, 219, 189-201.

(13)   Laskin, J.; FutrelL, J. H. Mass Spectrom. Rev. **2003**, 158.

(14)   Laskin, J.; Futrell, J. H. J. Am. Soc. Mass Spectrom. **2003**, 14, 1340-1347.

(15)   Senko, M. W.; Speir, P. J.; McLafferty, F. W. Anal. Chem. **1994**, 66, 2801-2808.

(16)   Gauthier, J. W.; Trautman, T. R.; Jacobsen, D. B. Anal. Chim. Acta **1991**, 246, 211-225.

(17)   Heck, A. J. R.; de Koning, L. J.; Pinkse, F. A.; Nibbering, N. M. M. Rapid Comm. Mass Spectrom. **1991**, 5, 406-414.

(18)   Senko, M. W.; Speir, J. P.; McLafferty, F. W. Anal. Chem. **1994**, 66, 2801-2808.

(19)   Williams, E. R.; Henry, K. D.; McLafferty, F. W.; Shabanowitz, J.; Hunt, D. F. J. Am. Soc. Mass Spectrom. **1990**, 1, 413-416.

(20)   Laskin, J.; Futrell, J. H. Mass Spectrom. Rev. **2005**, 24, 135-167.

(21)   Mirgorodskaya, E.; O`Connor, P. B.; Costello, C. E. J. Am. Soc. Mass Spectrom. **2002**, 13, 318-324.

(22)   Creighton, T. E. BioEssay **1988**, 8, 57-63.

(23)   Wells, J. M.; Stephenson, J. L.; McLuckey, S. A. Int. J. Mass Spectrom. **2000**, 203, A1-A9.

(24)   Bean, M. F.; Carr, S. A. Analytical Biochemistry **1992**, 201, 216-226.

(25)   Stults, J. T.; Bourell, J. H.; Canovadavis, E.; Ling, V. T.; Larame, G. R.; Winslow, J. W.; Griffin, P. R.; Rinderknecht, E.; Vandlen, R. L. Biomed. Environment. Mass Spectrom. **1990**, 19, 655-664.

(26)   Jones, M. D.; Patterson, S. D.; Lu, H. S. Anal. Chem. **1998**, 70, 136-143.

(27)   Jones, M. D.; Hunt, J.; Liu, J. L.; Patterson, S. D.; Kohno, T.; Lu, H. S. Biochem. **1997**, 36, 14914-14923.

(28)   Patterson, S. D.; Katta, V. Anal. Chem. **1994**, 66, 3727-3732.

(29)   Zhou, J.; Ens, W.; Poppe-Schriemer, N.; Standing, K. G.; Westmore, J. B. Int. J. Mass Spectrom. **1993**, 126, 115-122.

(30)   Qin, J.; Chait, B. T. Anal. Chem. **1997**, 1997, 4002-4009.

(31)   Chrisman, P. A.; McLuckey, S. A. J. Prot. Res. **2002**, 1, 549-557.

(32)   Zubarev, R. A.; Kelleher, N. L.; McLafferty, F. W. J. Am. Chem. Soc. **1998**, 120, 3265.

(33)   Zubarev, R. A.; Kruger, N. A.; Fridriksson, E. K.; Lewis, M. A.; Horn, D. M.; Carpenter, B. K.; McLafferty, F. W. J. Am. Chem. Soc. **1999**, 121, 2857-2862.

(34)   Ge, Y.; Lawhorn, B. G.; ElNaggar, M.; Strauss, E.; Park, J.-H.; Begley, T. P.; McLafferty, F. W. J. Am. Chem. Soc. **2002**, 124, 672-678.

(35)   Kleinnijenhuis, A. J.; Duursma, M. C.; Breukink, E.; Heeren, R. M. A.; Heck, A. J. R. Anal. Chem. **2003**, 75, 3219-3225.

(36)   Silivra, O. A.; Kjeldsen, F.; Ivonin, I. A.; Zubarev, R. A. J. Am. Soc. Mass Spectrom. **2005**, 16, 22-27.

(37)   Baba, T.; Hashimoto, Y.; Hasegawa, H.; Hirabayasi, A.; Waki, I. Anal. Chem. **2004**, 76, 4263-4266.

(38)   Zubarev, R. A.; Haselmann, K. F.; Budnik, B. A.; Kjeldsen, F.; Jensen, F. Eur. J. Mass Spectrom. **2002**, 8, 337-349.

(39)   Liu, H.; Hakansson, K. J. Am. Soc. Mass Spectrom. **2006**, 17, xxx.

(40)   Kleinnijenhuis, A. J.; Mihalca, R.; Heeren, R. M. A.; Heck, A. J. R. Int. J. Mass Spectrom. **2006**, 253, 217-224.

(41)   Barberis, C.; Tribollet, E. Crit. Rev. Neurobiol. **1996**, 10, 119-154.

(42)   Gimpl, G.; Fahrenholz, F. Physiol. Rev. **2001**, 81, 629-683.

(43)   Barberis, C.; Mouillac, B.; Durroux, T. J. Endocrin. **1998**, 156, 223-229.

(44)   Pearlmutter, A. F.; Soloff, M. S. J. Bio. Chem. **1979**, 254, 3899-3906.

(45)   Liu, D.; Seuthe, A. B.; Ehrler, O. T.; Zhang, X.; Wyttenbach, T.; Hsu, J. F.; Bowers, M. T. J. Am. Chem. Soc. **2005**, 127, 2024-2025.

(46)   Taban, I. M.; McDonnell, L. A.; Rompp, A.; Cerjak, I.; Heeren, R. M. A. Int. J. Mass spectrom. **2005**, 244, 135-143.

(47)   Guan, S.; Marshall, A. G. Int. J. Mass Spectrom. Ion Proc. **1996**, 157/158, 5-37.

(48)   Römpp, A.; Taban, I. M.; Mihalca, R.; Duursma, M. C.; Mize, T. H.; McDonnell, L. A.; Heeren, R. M. A. Eur. J. Mass Spectrom. **2005**, 11, 443-456.

(49)   Mize, T. H.; Taban, I. M.; Duursma, M. C.; Seynen, M.; Konijnenburg, M.; Vijftigschild, A.; Doornik, C. v.; Rooij, G. v.; Heeren, R. M. A. Int. J. Mass spectrom. **2004**, 235, 243-253.

(50)   van der Burgt, Y. E. M.; Taban, I. M.; Konijnenburg, M.; Biskup, M.; Duursma, M.; Heeren, R. M. A.; van Nieuwpoort, R. V.; Bal, H. E.; Rompp, A. J. Am. Soc. Mass Spectrom. **2006**, submitted.

(51)   Roepstorff, P.; Fohlman, J. Biomed. Mass Spectrom. **1984**, 11, 11.

(52)   Biemann, K. Annu. Rev. Biochem. **1992**, 61, 977-1010.

(53)   Steen, H.; Mann, M. Nature Rev. **2004**, 5, 699-711.

(54)   Hunt, D. F.; Yates, J. R.; Shabanowitz, J.; Winston, S.; Hauer, C. R. Proc. Natl. Acad. Sci. U.S.A. **1986**, 83, 6233-6237.

(55)   Paizs, B.; Suhai, S. Mass Spectrom. Rev. **2005**, 24, 508-548.

Chapter 6

ECD behaviour of disulfide bond containing peptides is determined by the type of divalent metal cation

Romulus Mihalca[1], Yuri E. M. van der Burgt[1], Albert J. R. Heck[2] and Ron M. A. Heeren[1,2*]

[1]**FOM Institute for Atomic and Molecular Physics (AMOLF), Kruislaan 407, 1098 SJ Amsterdam, The Netherlands**
[2]**Department of Biomolecular Mass Spectrometry, Bijvoet Center for Biomolecular Research, Utrecht Institute for Pharmaceutical Sciences, Utrecht University, Sorbonnelaan 16, 3584 CA Utrecht, The Netherlands**

Abstract

Three nonapeptides (oxytocin, vasopressin and Thr4Gly7oxytocin) containing a disulfide bridge were subjected to electron capture dissociation (ECD) in protonated form or complexed with divalent transition metal ions to probe their structural features. ECD leads to facile cleavage of the disulfide bond in doubly protonated nonapeptides oxytocin and vasopressin and generates high sequence coverage. Complementary fragments are observed in ECD spectra of these two nonapeptides when they are complexed with divalent transition metal ions (e.g. Zn^{2+}, Ni^{2+} or Cu^{2+}). Metal ion addition is especially useful for peptides like Thr4Glyoxytocin that hardly form protonated species in gas-phase. We show that for these three nonapeptides the types of the observed ECD fragments are strongly related with the identity of the metal ion. The ECD behaviour of these species shows differences and similaritites. Ni^{2+} -complexes dissociates in ECD mainly through ring cleavage while enhanced scission of the tail region is noticed for Cu^{2+}-complexes. The difference of two amino acids in the primary structure of these nonapeptides is expected to result in significantly different ECD spectra. However, common features like production of *c/z*-ions for Zn^{2+}-complexes and *b*-ions for Cu^{2+}-complexes were remarked. Such behaviour can be indicative for structural similarities between different species.

6.1   Introduction

In a relatively short period, electron capture dissociation (ECD) has proven its great value in the mass spectrometric (MS) analysis of biomolecules such as peptides and proteins [1-4]. With both the development of FTICR instrumentation and the introduction of electron-transfer dissociation (ETD) [5, 6] it is expected that electron capture events will play an important role in future proteomics experiments. The fact that ECD does not necessarily result in cleavage of the weakest peptide bonds has made this fragmentation technique a powerful

alternative to the widely-used collision induced dissociation (CID) methods. ECD data of peptides is often complementary to spectra obtained from traditional MS/MS methods [7], and results in specific amino acid side chain losses [8, 9]. ECD has enabled the analysis of post-translational modifications (PTM's) such as phosphorylation and glycosylation, both in terms of identification and localization. Another important difference with CID is the preference of ECD to cleave disulfide and monosulfide bonds in peptides or proteins [10-13]. This allows for a higher sequence coverage compared to slow heating techniques like CID. Furthermore, ECD is well-known for its examples on top-down sequencing of intact proteins and it has become the preferred tandem mass spectrometric technique for structural investigations of gas phase polypeptides in the study of protein folding or non-covalent interactions in protein complexes [1, 8, 14-17]. The gentle nature of this technique has made ECD an efficient tool to study proteins with labile modifications [4] and to characterize secondary and tertiary structures of gas-phase proteins [16].

Despite its remarkable applications, the mechanism of ECD is still not well understood. Usually ECD leads to the formation of *c* and *z*-type ions, and a significantly lower abundance of *a* and *y*-type ions are formed [2,18]. The proposed models to explain the preferential cleavage of the N-C$_\alpha$ bond (*i.e. c* and *z*-type fragments) in ECD are based on configuration of the charge solvation shell or the effect of the positive charge on ammonium and amide radicals formed by electron capture. There is experimental evidence that ECD is directed by charge solvation of the (neutralized) proton [16,19-22]. In agreement with this, it has been shown recently that the formation of *a* and *y*-type ions resulting from ECD applied to protonated species strongly depends on the location of the charge [23]. Finally, conformational heterogeneity of the multiply charged ions has been proved to be a key factor in ECD in determining the sites of backbone cleavage and the abundance of the dissociation products [24].

In most cases, dissociation studies reported in the literature are carried out on protonated species. A practical reason to use a metal as a cationizing agent is that it can be advantageous to generate ions from peptides that lack basic amino acid residues. Moreover, it is known that complementary primary sequence information can be obtained by changing the cationizing agent. A more

fundamental consideration is that biomolecules are biologically active upon complexation with different metal ions. For example, oxytocin (OT) and vasopressin (VS) are biologically active only after complexation with metal ions like Zn^{2+}, Ni^{2+} or Co^{2+} [25, 26]. Although the ionization process of peptides and proteins is usually carried out under denaturing conditions, the actual interactions between a metal ion and a biomolecule can still be studied in the gas-phase complex. Several experimental MS approaches have been reported concerning complexes of metal ions with amino acids, peptides and proteins. Complexes are either formed in solution [25-28] or through gas-phase ion/ion reactions [25-28]. From these studies it was concluded that the presence of a metal ion can change the secondary and/or the tertiary structure of the peptide.

Only a few ECD studies have been carried out on peptide-metal complexes. Iavarone *et al.* found that ECD on synthetic peptides complexed with alkali metal ions (Li^+ and Cs^+) resulted exclusively in *c*- and *z*-type fragments containing the metal [29]. Zubarev *et al.* observed metal-containing *c*- and *z*-type fragments in the ECD spectrum of angiotensinII+Zn^{2+} and in addition metal-lacking *a*- and *y*-type ions [30]. Fung *et al.* reported that glycine-rich linear peptides complexed with different alkaline-earth metal ions generate very similar ECD spectra that predominantly show metal-containing *c* and *z*-type ions. A recent ECD study on triply charged metal-complexed substance P ([substance P+H^++M^{2+}]$^{3+}$ where M^{2+} is a group II metal ion Mg^{2+}, Ca^{2+}, Sr^{2+}, or Ba^{2+}, or $M^{2+}$is a transition metal ion Mn^{2+}, Fe^{2+}, Zn^{2+}, Co^{2+}, Ni^{2+}, or Cu^{2+}) showed both metal-containing and metal-lacking *c* and *z*-type fragments [31]. The formation of these ions can be rationalized both with the hot hydrogen mechanism and the amide superbase mechanism with initial electron capture occurring at the metal. However, the observed fragmentation patterns for Co^{2+}, Ni^{2+}, and Cu^{2+}-containing complexes differed drastically from the other metals. These differences in ECD behavior seemed to correlate with the second ionization energy of the metal. Moreover, the observation of *b* and *y*-type ions for Cu^{2+}-complexed substance P is in agreement with our ECD results on [OT+Cu^{2+}] [13]. Here, it was proposed that the captured electron is involved in reduction of Cu^{2+} to Cu^+. The redistribution of the recombination energy explains the observed low-energy CID-type fragmentation.

The observed dissimilarities in ECD spectra of oxytocin complexed with different metal cations suggest that ECD reflects the coordination of the metal ion in a complex [13]. Molecular modeling has shown that complexation of OT with a divalent metal ion leads to structural changes compared to protonated analogues [32]. In other words, the ECD behavior can be directed ("tuned") by using a divalent metal cation for energy deposition due to the change in peptide conformation [31]. To study this aspect in more detail three similar nonapeptides were chosen, namely OT (CysTyrIleGlnAsnCysProLeuGly), VS (CysTyrPheGlnAsnCysProArgGly) and Thr4-Gly7-oxytocin (TGOT, CysTyrIleThrAsnCysGlyLeuGly). These three nonapeptides share an important common structural feature namely the disulfide bridge between the cysteines at positions 1 and 6, also referred to as the tocin ring. This intramolecular linkage defines and stabilizes the secondary and tertiary structure of the peptide. All three nonapeptides are amidated at the C-terminus. The ECD behavior of protonated peptides and complexes with transition metal cations (Zn^{2+}, Ni^{2+} or Cu^{2+}) will be discussed. Both the effect of complexation compared to the protonated species will be evaluated, as well as the ECD behavior of each metal ion in different peptides.

6.2   Experimental

6.2.1 Sample preparation

All three nonapeptides, oxytocin (OT), Thr4Gly7oxytocin (TGOT) and Arg8Vasopressin (VS) were purchased from Sigma Aldrich and were used without further purification. All these peptides are amidated at C-terminus and contain a disulfide bridge between Cys-1 and Cys-6. Fresh sample solutions of 49:49:2 water:methanol:acetic acid at a concentration of 20 μM were prepared. Complexation of these peptides with Ni^{2+}, Zn^{2+} and Cu^{2+} was carried out by adding the metal acetate salt 25 times in excess in the absence of acetic acid. All ECD settings were optimized for maximum fragmentation of quadruply protonated melittin (Sigma, from honey bee venom).

6.2.2 Mass spectrometry and electron capture dissociation

All ECD experiments were performed using a heavily modified Bruker APEX 7.0eT FTICR mass spectrometer equipped with a 7 T superconducting magnet and an infinity[TM] ICR cell. The experimental parameters were controlled using in-house developed software and hardware [33, 34]. Data analysis was performed both manually and automatically using in-house developed processing tools [35]. Peptide ions were generated using an electrospray ion source at a flow rate of approximately 500 nl/min (NewObjective PicoTip at 2.1 kV). Subsequently the ions were accumulated for 300-500 ms in an octopole ion trap followed by ejection of the ion packet to the ICR via two quadrupole ion guides. There, the ions were trapped using a 200 ms gas pulse (Ar) at 10^{-6} mbar. The full isotopic cluster of a doubly charged precursor ion ([peptide+metal]$^{2+}$) was isolated using a stored waveform inverse Fourier transformed (SWIFT) excitation pulse [36] to be further subjected to irradiation with low energy electrons. In some cases, an additional SWIFT isolation was applied to avoid noise signals at the lower mass range. The low energy electron beam was produced with an indirectly heated barium-tungsten dispenser cathode (TB-198, HeatWave Labs, Inc.) mounted inside the magnet at approximately 30 cm behind the ICR cell. The cathode was heated with a current of 1.3 A and a potential of 5.8 V, yielding a power of 7.5 W. To increase electron extraction efficiency, a copper grid was placed at 5 mm in front of the cathode. During irradiation period (200 ms) the grid was pulsed from –100 V to +100 V and the cathode surface potential from +25 V to –0.18 V.

6.3   Results and discussion

6.3.1 Nomenclature

For OT the peptide region that is closed by the disulfide bond is called the tocin ring and the remaining part is referred to as the tail. The tocin ring is a rather rigid structure, whereas the tail is flexible. In this paper, the terms "tocin ring" and

"tail" will also be used for describing regions of the other two nonapeptides due to the structural similarities with oxytocin. For the calculation of the exact mass of the metal-containing complexes (peptide with Zn^{2+}, Ni^{2+} or Cu^{2+}) two hydrogen atoms were subtracted from the neutral nonapeptide. All ECD fragments from metal-containing complexes retained the metal cation, which is not explicitly annotated. The fragments observed in ECD spectra of all three peptides (OT, TGOT and VS) originate both from the tocin ring and from the tail region. For calculation of the exact masses of the fragments for each cysteine one hydrogen atom was subtracted because of the disulfide bridge between Cys1 and Cys6. Backbone fragments from the tocin ring require an additional cleavage of the disulfide bridge. This bridge can be cleaved at three different positions, namely at the middle or at one of the cysteine side chains. The "regular" fragments correspond to the cleavage of the S-S bond. When the S-C bond is cleaved in combination with the backbone bond the corresponding fragment will be referred as "+S or –S". Thus, these backbone fragments contain two or zero sulphur atoms. The assignment of the peptide backbone fragments is based on Roepstorff-Fohlman-Biemann nomenclature [37-39]. Backbone C_{α}-C, C-N, and N-C_{α} bond cleavages produce *a*/*x*, *b*/*y* and *c*/*z* fragments, respectively. In principle, in ECD homolytic cleavage of all bonds is assumed, yielding two radical species [18]. Here, we have chosen not to indicate the dots for the radicals, *i.e.* in our nomenclature the homolytic cleavage of the N-C_{α} bond results in *c* and *z* fragments. The loss of hydrogen radical from the precursor ion is indicated as "[M-H]". Similarly, the loss neutral HS- and CH_2S radical species from the precursor ion or from a product ion is designated as "-HS" and "-CH_2S", respectively. The presence of a hydrogen-atom transfer in a product ion is explicitly indicated using a prime (*e.g. c*' after hydrogen-atom transfer to the N-terminal fragment). Hydrogen rearrangements are abundant in radical species and also lead to fragments that lack a hydrogen atom (*e.g.* '*c* or '*z*) [7]. Also for *a*/*x* and *b*/*y* fragments the prime is used to indicate a hydrogen transfer. The intensity of each product ion was determined from all corresponding peak intensities in the isotope cluster. In the case of a Ni^{2+}- or Cu^{2+}-complexed peptide at least three isotopes were observed in one cluster, whereas in the case of Zn^{2+} at least four peaks were taken into account.

6.3.2 ECD spectra of protonated and metal-complexed nonapeptides

Tandem FTICR mass spectra of [OT+2H$^+$] and [VS+2H$^+$] were obtained after SWIFT-isolation followed by ECD. For TGOT, no doubly protonated precursor ion was observed, probably due to the absence of basic amino acids. Additionally, all three nonapeptides were complexed with Zn^{2+}, Ni^{2+} or Cu^{2+} ions. For [VS+Zn^{2+}] the precursor ion was of too low intensity for MS/MS, thus eight ECD spectra of metal-complexed species were obtained. As an example, the ECD spectra of the Cu^{2+}– and Ni^{2+}–complexes of OT and TGOT are shown in Figures 6.1a and 6.1b. A detailed discussion on the different types of fragments will be given in the next paragraph.

In Figures 6.1a and 6.1b, the typical isotope profiles of the transition metals are reflected in most clusters. In all cases the assigned fragment ions contain the metal ion. Most assignments were done with a mass accuracy well below 5 ppm. Mass accuracies between 5 and 10 ppm were usually a result of significant intensity differences (more than 100-fold) between the fragments used for calibration and the ion of interest [40]. For all ten ECD spectra, the total number of assigned fragments is given in Table 6.1. This number varied between 10 and 36. Also, the assigned fragments are given as a percentage of the total product ion intensity (PII). This percentage varied from 52% for [TGOT+Cu^{2+}] to 91% for [OT+Ni^{2+}]. All observed backbone cleavages in the ten ECD spectra are summarized in Figure 6.2.
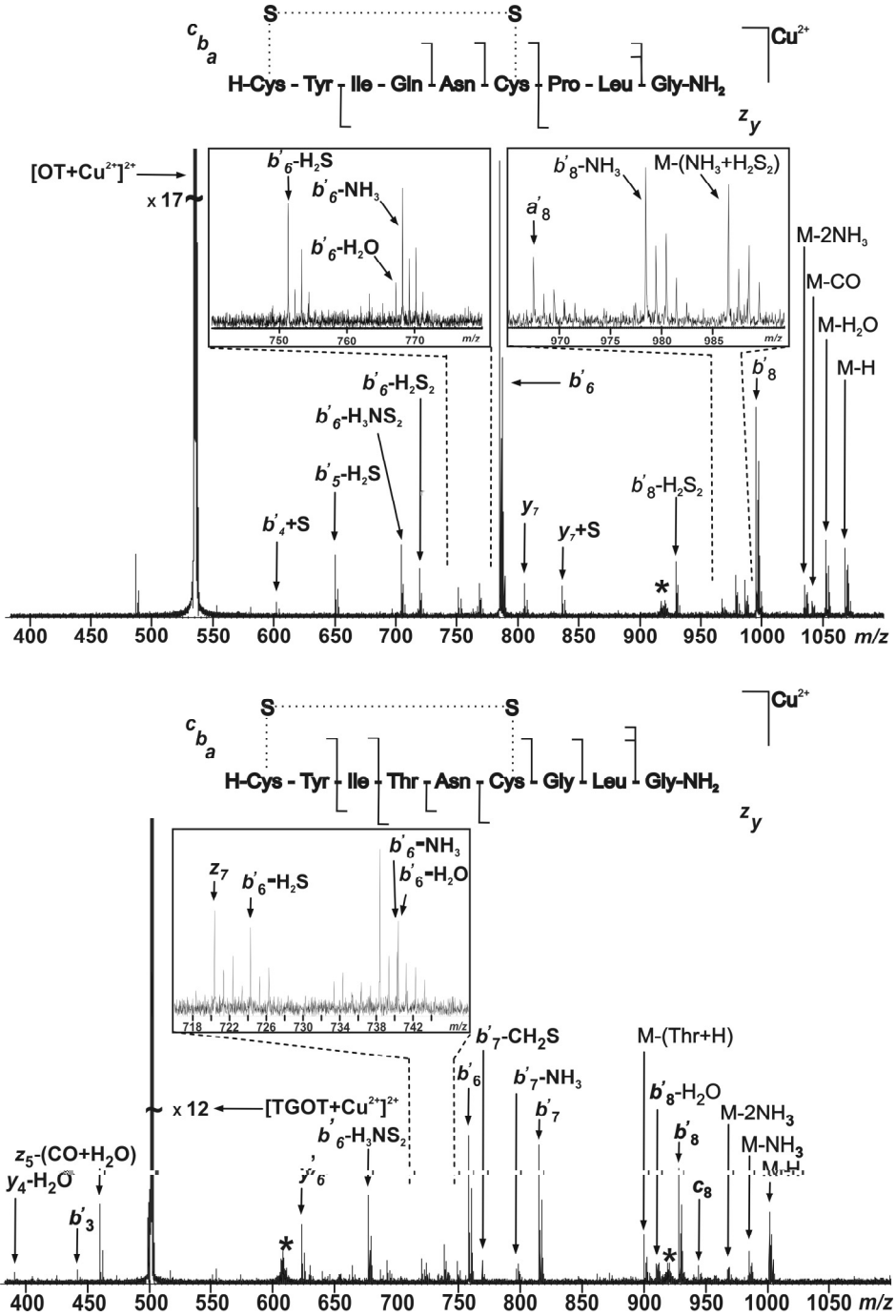
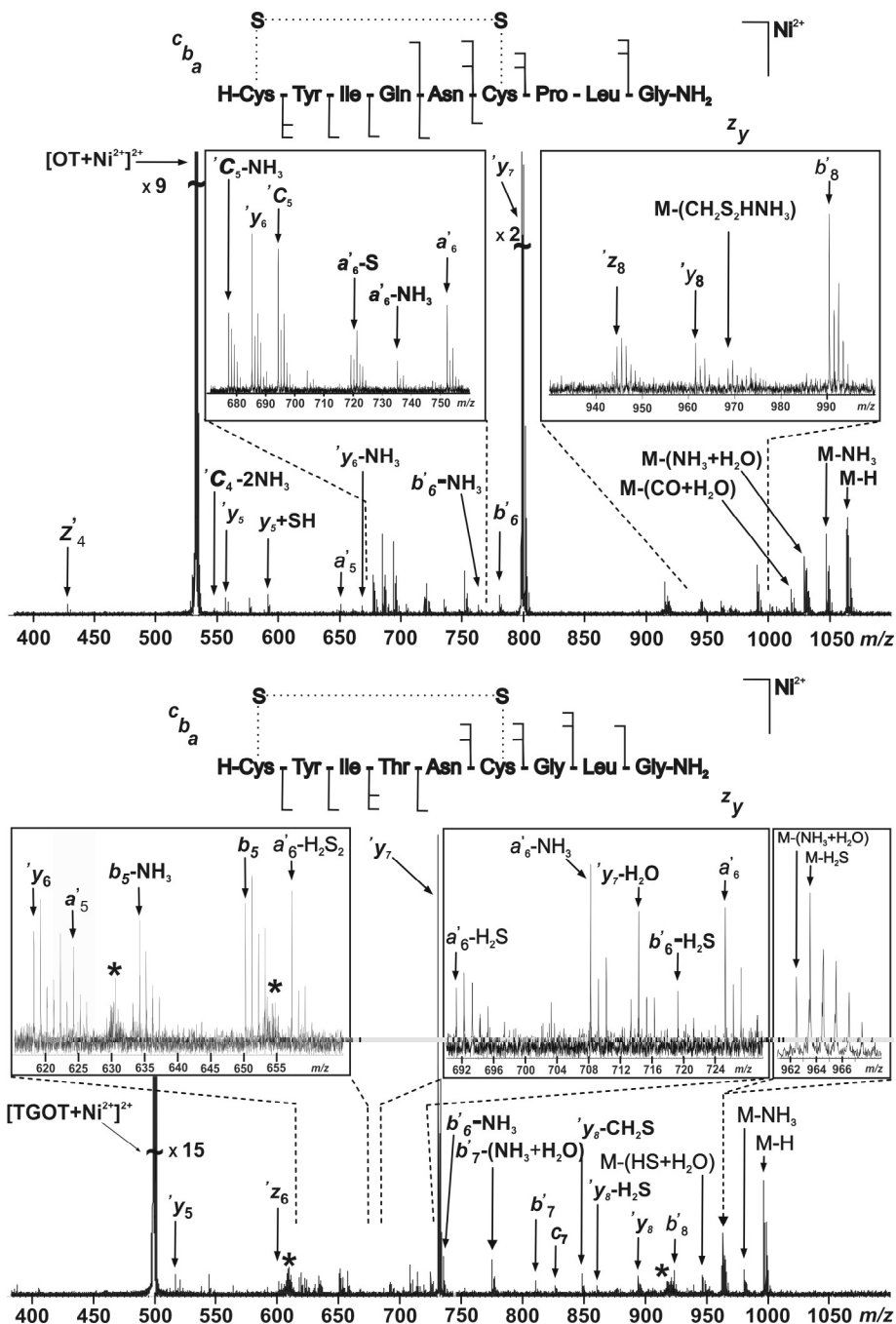**Figure 6.1**a. ECD spectra of [OT+Cu^{2+}] and [TGOT+Cu^{2+}].

137

Figure 6.1b. ECD spectra of [OT+Ni^{2+}] and [TGOT+Ni^{2+}].

Figure 6.2 Summary of all backbone cleavages observed in ten different ECD spectra.

The sequence coverage obtained from the ECD spectra of [OT+2H$^+$] and [VS+2H$^+$] is remarkably high. As is known from other ECD studies, abundant cleavage of the disulfide bridge is observed. Despite this high content of ECD information from protonated species, the use of a transition metal as a cationizing agent is still advantageous. In the case of TGOT the usefulness of metal-complexation is evident due to the absence of the doubly protonated species. For OT and VS the practical advantage is less obvious, because the number of fragments *decreases* upon complexation. However, in terms of primary peptide sequence information it is clear from Figure 6.2 that metal-complexation results in complementary cleavages. For example, Zn^{2+}- or Ni^{2+}-complexation of OT results in a cleavage at Cys1-Tyr2 compared to the protonated analogue, and Cu^{2+}–complexation of VS results in Cys6-Pro7 cleavage. In the next section it will be shown that in addition the *types* of fragments change dramatically upon complexation.

6.3.3 Different types of fragments in the ECD spectra

The fragment ions from OT, TGOT, and VS either result from neutral losses from the precursor or from peptide backbone cleavages, or a combination thereof. The neutral losses often involve cleavage of the disulfide bridge, which can occur at S-S or at C-S. Because ECD is well known for the cleavage of mono- and disulfide bridges in peptides and proteins, these ions are considered as typical ECD fragments. The backbone cleavages occur either at the tail or in the ring of the nonapeptide. Here, the typical ECD backbone fragments result from *c/z*- and to a lesser extend *a/y* pathways [2,18]. However, also *b*-ions are observed in the spectra, which result from "ECD-atypical" *b/y*-fragmentation. Another indication for the occurrence of *b/y*-fragmentation is the relatively high abundance of *y*-ions in some of the spectra. All fragments can be summarized in four different types of product ions. As an example, the fragment ions observed in the ECD spectrum of [TGOT+Zn^{2+}] are shown in Figure 6.3.
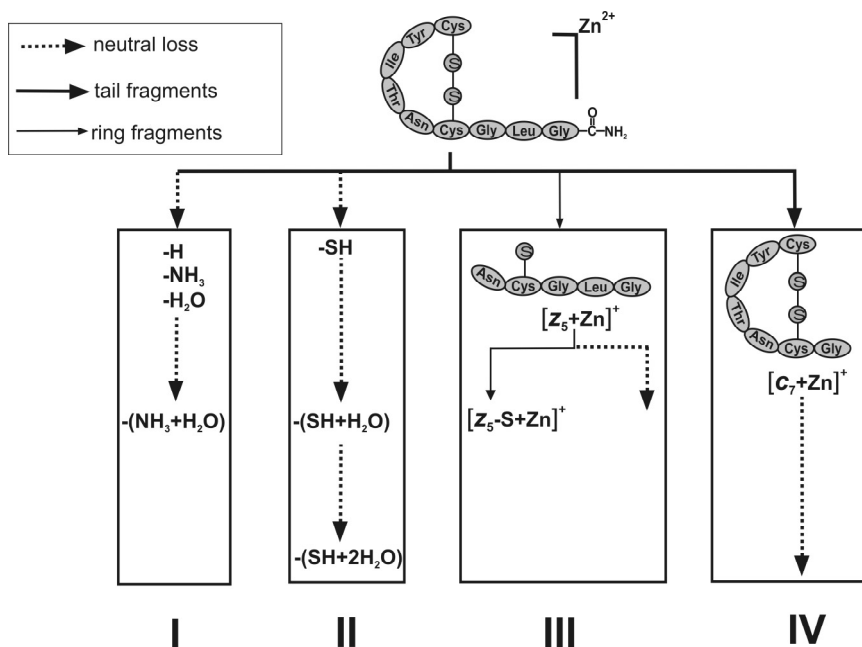
Figure 6.3 Different types of fragment ions observed in the ECD spectrum of [TGOT+Zn^{2+}].

Each fragment of [TGOT+Zn^{2+}] contains the metal ion. Type I ions result from a single or multiple neutral loss such as NH$_3$, H$_2$O, or CO and ECD-specific loss of an H radical. Type II ions are neutral losses that require cleavage of the disulfide bridge (*e.g.* H$_2$S, or radical species HS and CH$_2$S). Type III ions result from "ECD-regular" *c/z*- or *a/y*-fragmentation, or from "ECD-atypical" *b/y*-fragmentation of the tocin ring. Note that also this type of fragments requires the cleavage of the disulfide bridge. Finally, type IV ions result from backbone cleavages of the tail.

The intensities of the different types of fragments are plotted in Figure 6.4. The total height of the bar indicates the percentage of fragment ions that is assigned (see Table 6.1). Thus, the considered fragments of [OT+Ni^{2+}] describe 91% of all ions whereas in [TGOT+Cu^{2+}] only 52% is covered. It is clear from Figure 6.4 that when looking at one nonapeptide the type of fragments varies significantly upon using a different metal ion for complexation. For example, [OT+Cu^{2+}] predominantly shows tail fragments in the ECD spectrum, whereas ECD of [OT+Ni^{2+}] results in mainly ring fragmentation.
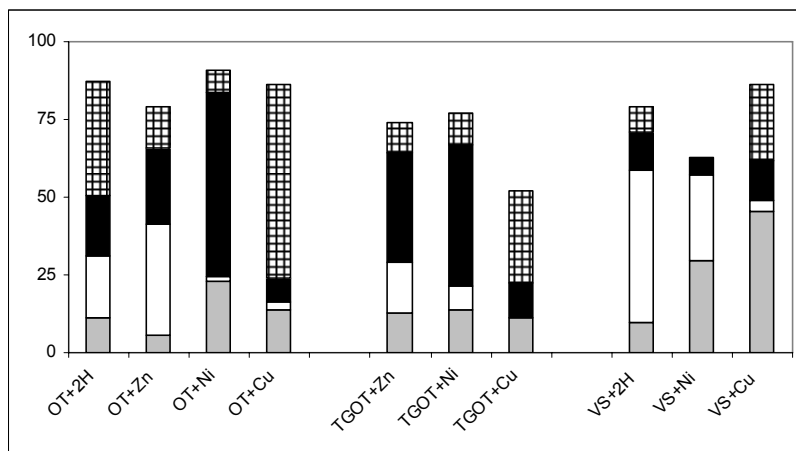
Figure 6.4 Relative intensities of different types of fragment ions in ECD spectra of ten different species. On the y-axis the percentage of assigned fragments is indicated (%PII, see Table 1). The colors in the bars represent the four different types of fragments as shown in Figure 3 (grey = neutral loss (I), white = neutral loss including cleavage of disulfide bridge (II), black = ring fragmentation (III), grid = tail fragmentation (IV)).

These observations are in agreement with our previous ECD study on oxytocin [13]. To a lesser extend TGOT shows similar behavior upon Ni^{2+}– or Cu^{2+}– complexation. ECD of $[VS+2H]^{2+}$ results mainly in loss of neutral sulfur-containing species, whereas after complexation with Cu^{2+} the disulfide bridge of VS remains intact upon ECD. In Figure 6.5, the three different nonapeptides are compared. It is obvious that subtle amino acid changes can result in significantly different ECD spectra [41-43]. However, here are examples that show common ECD features. In Zn^{2+}–complexed OT and TGOT mostly c/z-ions are observed (in both ring- and tail fragments) and in Cu^{2+}–complexed OT, TGOT, and VS the tail fragments mainly consist of b-ions. On the other hand, the ring fragments of both the Ni^{2+}– and Cu^{2+}– complexes are different for each species.

In a previous SORI-CID study on OT it was found that coordination of Zn^{2+} or Cu^{2+} in the corresponding complexes differed significantly [44]. Also, we hypothesized that

the differences in backbone cleavage sites of OT complexes upon ECD point at structural differences [13]. In this work the ECD behavior of three similar nonapeptides has been evaluated. Obviously, the small differences in amino acid sequences result in different ECD spectra. However, also common features were observed which suggest structural similarities between the various species.
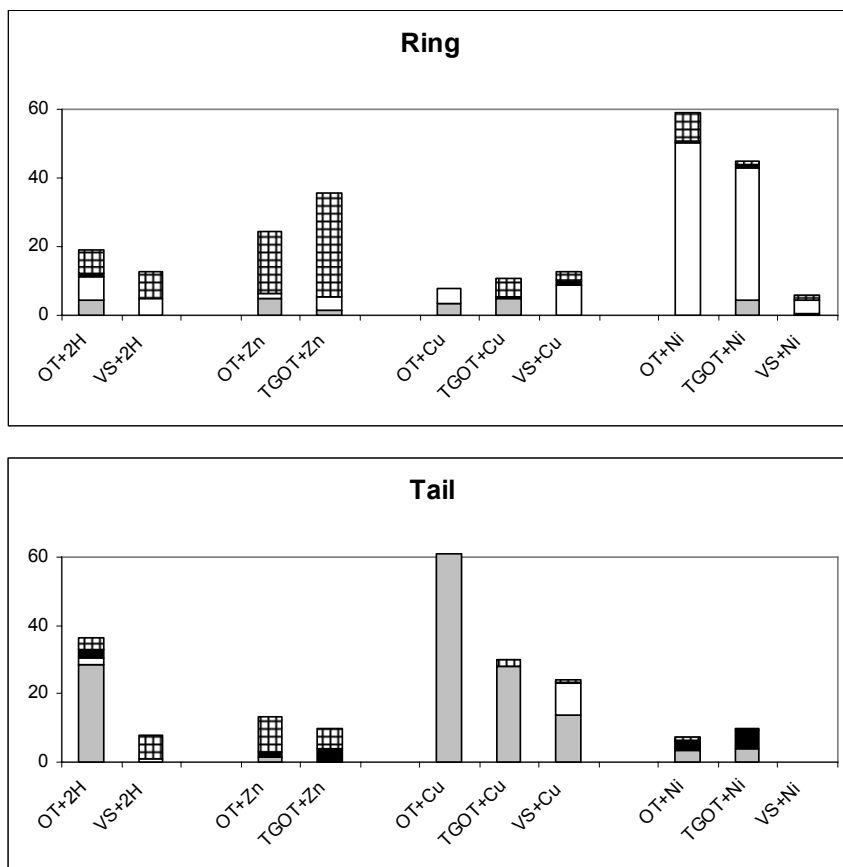

Figure 6.5 The relative composition of the product ion intensity (PII) of ring- and tail fragment ions (grid = total of *c*- and *z*-ions, black = *a*-ions, white = *y*-ions, grey = *b*-ions). On the y-axis the percentage of assigned fragments is indicated (%PII, see Table 1). For VS+Cu^{2+}, also an x_7-ion was observed.

6.4 Conclusions

ECD spectra of doubly protonated nonapeptides OT and VS contain multiple fragments that involve the cleavage of the disulfide bridge. As a result, the sequence coverage is higher than obtained from CID experiments. The use of a transition metal ion (in this work Zn^{2+}, Ni^{2+} and Cu^{2+}) as a cationizing agent showed complementary cleavages in the backbone of OT and VS. For TGOT, no doubly protonated precursor could be obtained whereas the metal-peptide complexes resulted in rich ECD spectra. It was found that for all three nonapeptides the different types of metal ions resulted in different types of fragments. In all three cases, fragmentation of the tail after Cu^{2+}–complexation increased. For OT and TGOT, Ni^{2+}–complexation predominantly resulted in ring fragments. When comparing the three different peptides complexed with the same metal cation both differences and similarities were seen. The ring fragments of the Ni^{2+}– and Cu^{2+}–complexes are different for each species. Examples of common ECD features are the occurrence of mostly *c*/*z*-ions after Zn^{2+}–complexation and mainly *b*-ions using Cu^{2+} as the cationizing agent. Such common features suggest structural similarities between the various species.

Acknowledgements

References

(1) Zubarev, R. A.; Kelleher, N. L.; McLafferty, F. W. J. Am. Chem. Soc. **1998**, 120, 3265.

(2) Zubarev, R. A.; Horn, D. M.; Fredricksson, E. K.; Kelleher, N. L.; Kruger, N. A.; Lewis, M. A.; Carpenter, B. K.; McLafferty, F. W. Anal. Chem. **2000**, 72, 563-573.

(3) Horn, D. M.; Zubarev, R. A.; McLafferty, F. W. Proc. Natl. Acad. Sci. U.S.A. **2000**, 97, 10313.

(4) Kelleher, N. L.; Zubarev, R. A.; Bush, K.; Furie, B.; Furie, B. C.; McLafferty, F. W.; Walsh, C. T. Anal. Chem. **1999**, 71, 4250-4253.

(5) Coon, J. J.; Ueberheide, B.; Syka, J. E. P.; Dryhurst, D. D.; Ausio, J.; Shabanowitz, J.; Hunt, D. F. Proc. Natl. Acad. Sci. U.S.A. **2005**, 102, 9463-9468.

(6) Coon, J. J.; Shabanowitz, J.; Hunt, D. F.; Syka, J. E. P. J. Am. Soc. Mass Spectrom. **2005**, 16, 880-882.

(7) Savitski, M. M.; Kjeldsen, F.; Nielsen, M. L.; Zubarev, R. A. Angew. Chem. **2006**, 45, 5301-5303.

(8) Kjeldsen, F.; Haselmann, K. F.; Budnik, B. A.; Jensen, F.; Zubarev, R. A. Chem. Phys. Lett. **2002**, 356, 201-206.

(9) Cooper, H. J.; Hudgins, R. R.; Hakansson, K.; Marshall, A. G. J. Am. Soc. Mass Spectrom. **2002**, 13, 241-249.

(10) Zubarev, R. A.; Kruger, N. A.; Fridriksson, E. K.; Lewis, M. A.; Horn, D. M.; Carpenter, B. K.; McLafferty, F. W. J. Am. Chem. Soc. **1999**, 121, 2857-2862.

(11) Mirgorodskaya, O. A.; Haselmann, K. F.; Kjeldsen, F.; Zubarev, R. A. J. Mass Spectrom. **2003**, 9, 139-148.

(12) Kleinnijenhuis, A. J.; Duursma, M. C.; Breukink, E.; Heeren, R. M. A.; Heck, A. J. R. Anal. Chem. **2003**, 75, 3219-3225.

(13) Kleinnijenhuis, A. J.; Mihalca, R.; Heeren, R. M. A.; Heck, A. J. R. Int. J. Mass Spectrom. **2006**, 253, 217-224.

(14) Cooper, H. J.; Hakansson, K.; Marshall, A. G. Mass Spectrom. Rev. **2005**, 24, 201-222.

(15) Meng, F.; Forbes, A. J.; Miller, L. M.; Kelleher, N. L. Mass Spectrom. Rev. **2005**, 24, 57-77.

(16) Oh, H.; Breuker, K.; Sze, S. K.; Ge, Y.; Carpenter, B. K.; McLafferty, F. W. Proc. Natl. Acad. Sci. U.S.A. **2003**, 99, 15863-15868.

(17) Geels, R. B. J.; van der Vies, S. M.; Heck, A. J. R.; Heeren, R. M. A. Anal. Chem. **2006**, 78, 7191-7196.

(18) Zubarev, R. A. Mass Spectrom. Rev. **2003**, 22, 57-77.

(19) Breuker, K.; Oh, H.; Horn, D. M.; Cerda, B. A.; McLafferty, F. W. J. Am. Chem. Soc. **2002**, 124, 6407-6420.

(20) Fung, Y. M. E.; Duan, L.; Chan, T.-W. D. Eur. J. Mass Spectrom. **2004**, 10, 449-457.

(21) Adams, C. M.; Kjeldsen, F.; Zubarev, R. A.; Budnik, B. A.; Haselmann, K. F. J. Am. Soc. Mass Spectrom. **2004**, 15, 1087-1098.

(22) Haselmann, K. F.; Budnik, B. A.; Kjeldsen, F.; Polfer, N. C.; Zubarev, R. A. Eur. J. Mass Spectrom. **2002**, 8, 461-469.

(23)   Tsybin, Y. O.; Haselmann, K. F.; Emmet, M. R.; Hendrickson, C. L.; Marshall, A. G. J. Am. Soc. Mass Spectrom. **2006**, 17, 1704-1711.
(24)   Mihalca, R.; Kleinnijenhuis, A. J.; McDonnell, L. A.; Heck, A. J. R.; Heeren, R. M. A. J. Am. Soc. Mass Spectrom. **2004**, 15, 1869.
(25)   Cerda, B. A.; Cornett, L.; Wesdemiotis, C. Int. J. Mass Spectrom. **1999**, 193, 205-226.
(26)   Hu, P. F.; Loo, J. A. J. Am. Chem. Soc. **1995**, 117, 11314-11319.
(27)   Taraszka, J. A.; Li, J. W.; Clemmer, D. E. J. Phys. Chem. B **2000**, 104, 4545-4551.
(28)   Newton, K. A.; McLuckey, S. A. J. Am. Chem. Soc. **2003**, 125, 12404-12405.
(29)   Iavarone, A. T.; Paech, K.; Williams, E. R. Anal. Chem. **2004**, 76, 2231-2238.
(30)   Zubarev, R. A.; Haselmann, K. F.; Budnik, B. A.; Kjeldsen, F.; Jensen, F. Eur. J. Mass Spectrom. **2002**, 8, 337-349.
(31)   Liu, H.; Hakansson, K. J. Am. Soc. Mass Spectrom. **2006**, 17, 1731-1741.
(32)   Liu, D.; Seuthe, A. B.; Ehrler, O. T.; Zhang, X.; Wyttenbach, T.; Hsu, J. F.; Bowers, M. T. J. Am. Chem. Soc. **2005**, 127, 2024-2025.
(33)   Römpp, A.; Taban, I. M.; Mihalca, R.; Duursma, M. C.; Mize, T. H.; McDonnell, L. A.; Heeren, R. M. A. Eur. J. Mass Spectrom. **2005**, 11, 443-456.
(34)   Mize, T. H.; Taban, I. M.; Duursma, M. C.; Seynen, M.; Konijnenburg, M.; Vijftigschild, A.; Doornik, C. v.; Rooij, G. v.; Heeren, R. M. A. Int. J. Mass spectrom. **2004**, 235, 243-253.
(35)   van der Burgt, Y. E. M.; Taban, I. M.; Konijnenburg, M.; Biskup, M.; Duursma, M.; Heeren, R. M. A.; van Nieuwpoort, R. V.; Bal, H. E.; Rompp, A. J. Am. Soc. Mass Spectrom. **2006**, submitted.
(36)   Guan, S.; Marshall, A. G. Int. J. Mass Spectrom. Ion Proc. **1996**, 157-158, 5-37.
(37)   Roepstorff, P.; Fohlman, J. Biomed. Mass Spectrom. **1984**, 11, 11.
(38)   Biemann, K. Annu. Rev. Biochem. **1992**, 61, 977-1010.
(39)   Steen, H.; Mann, M. Nature Rev. **2004**, 5, 699-711.
(40)   Amster, I. J. J. Mass Spectrom. **1996**, 31, 1325-1337.
(41)   Cooper, H. J.; Hudgins, R. R.; Håkansson, K.; Marshall, A. G. J. Am. Soc. Mass Spectrom. **2001**, 13, 241-249.
(42)   Fung, Y.; Dual, Y.; Chan, T. EJMS **2004**, 10, 449.
(43)   Cooper, H. J. J. Am. Soc. Mass Spectrom. **2005**, 16, 1932-1940.
(44)   Mihalca, R.; van der Burgt, Y. E. M.; Heck, A. J. R.; Heeren, R. M. A. J. Mass Spectrom. **2006**, in press.

Chapter 7

Future outlook

The structural analysis of biomolecules has always been a challenge for organic and analytical chemists. The results from the work on carbohydrates and proteins at the beginning of the 20th century now seem trivial and are basic knowledge for all scientists. However, taking into account instrumentation and technology from those early days one can still appreciate the complexity and genius of this research. No mass spectrometer was available, or any other device that was capable of analyzing compounds at a molecular level. Still analytical and instrumental challenges remain in the field of mass spectrometry, specifically for electron transfer processes. Electron capture dissociation (ECD)[1] and electron-transfer dissociation (ETD) [2,3] exhibit a great potential to generate extended information about polypeptide structure in the gas-phase. These two fragmentation processes retain labile post-translational modifications (PTM's) while a large variety of backbone cleavages occur in the peptide or protein. In addition, ECD is applicable to larger proteins which contain intramolecular non-covalent bonds using the so-called activated ion – ECD (AI-ECD) [4]. The fact that ECD does not affect non-covalent interactions makes this technique very suitable for the study of large non-covalently bounded protein complexes or protein-ligand systems.

The complementarity of ECD in molecular sequencing has been recently demonstrated by Savitsky *et al*. [5]. The fact that ECD and CID produce complementary fragments supports the non-local ECD mechanism, decoupling thereby the proton location from the position where the $N-C_\alpha$ bond is cleaved. This ECD feature is extremely important for proteomics because it produces valuable information that combined with those obtained from CID or IRMPD facilitates rapid and unambiguous sequence determination of peptides and proteins. Together with the ability to retain PTM`s and to preferentially cleave sulfide bonds, ECD is an

important tool for structural investigation of different classes of peptides and proteins. Part of these polypeptides can be indicative for a particular state of an organism or the evolution of a disease. These biomolecules can be biomarkers and their study reveals information about biochemical and pathogenic processes or about pharmacologic responses to a therapeutic intervention. Because structural studies with mass spectrometry rely in general on molecular sequencing, a trend in proteomics is to combine "top-down" and "bottom-up" mass spectrometric approaches using ECD and IRMPD/CID to discover, identify and characterize biomarkers for different diseases [6,7]. For example, a recent study based on this combined approach resulted in identification of a phosphorylation site in *Drosophilia* stem-loop-binding proteins that play a role in high-affinity RNA binding [8].

A complete understanding of the ECD mechanism and the role of the experimental parameters in ECD is essential in the effort to improve performances of this mass spectrometric technique. Knowing the factors which play a key role in ECD helps us to further development in order to achieve high rate ECD for on-line tandem mass spectrometry coupled with chromatographic separation techniques. From a technical point of view, a challenge in ECD instrumentation development is the improvement of electron injection systems using cold, bright, and large emitting area, source of low-energy electrons. Other developments are expected on making ECD accessible for the mass spectrometry community as a "plug-and-play" technique compatible with different commercial mass spectrometers such as ion trap MS.

ECD will play a future role in the structural analysis of synthetic polymers. The difficulty in studying polymers using MS resides in the fact that oligomers with different sequences, but identical masses, are present in the same sample. This is translated into a large structural diversity for a certain molecular ion. In the last years some articles were published with ECD on different types of polymers ranging from PEG`s to hyper-branched polyesteramides. These studies reveal ECD behaviours that have not been previously observed and show that ECD of branched polymers yields more complex spectra than CID. Some product ions require multiple cleavages to be generated. Hence, in order to explain this

complexity, further investigation is needed to elucidate the free radical chemistry involved in ECD.

As has been shown in chapter 2, ECD has major advantages compared with other mass spectrometric techniques that make it very attractive for structural studies. Unfortunately, ECD is still a technique that is currently implemented on FTICR mass spectrometers. Stimulated by the analytical potential of the reactions between multiply charged molecular cations and low energy electrons, in 2004 Hunt and co-workers introduced ETD [2,3]. A major advantage of ETD is that it can be used on widely accessible quadrupole ion trap instruments that are financially more attractive than FTICR mass spectrometers. In ETD, the anions (e.g. anthracene anion radicals) are used to carry low-energy electrons that react with multiply charged polypeptide cations. After electron transfer, the dissociation of the charged reduced molecular ion is believed to follow the same fragmentation mechanisms as in ECD. Therefore, the dissociation products generated in ETD are mainly *c* and *z* type fragment ions. Similar to ECD, the reaction times to produce backbone fragments are short (5- to 100-ms) and typically result in extensive backbone cleavage. Another remarkable feature of ETD is that it seems independent of the peptide sequence and the presence of labile PTM's. The first reported ETD spectra performed on phosphorylated peptides resulted in almost complete sequence coverage with retention of the PTM on the backbone fragments. Moreover, ETD was used on a chromatographic time scale for a mixture containing 10 protonated synthetic peptides at the 1- to 100-fmol level by nanoHPLC-µESI-MS/MS. Ion/ion reactions between multiply protonated peptides and singly charged anions in a quadrupole linear ion trap (QLT) yielded products associated with both proton and electron transfer. It was observed that some anions function as strong bases and react exclusively with the protonated peptide through proton abstraction. Interestingly, other anions display a dual behaviour: both proton and electron transfer. Another observation was that the observed product ions ratio depends on the anion structure. Moreover, it has been noticed that some fragments produced in ETD remain non-covalently bound, similar to ECD. Collisional activation of the charged reduced species releases the already formed *c* and *z* fragments ions. The obtained fragments can undergo further ion/ion

reactions resulting in either formation of secondary fragments or charge neutralization. Therefore, new techniques are investigated to prevent these unwanted reactions in ETD. A remarkable example of ETD is the possibility to differentiate isomeric species. For instance, aspartic and isoaspartic acidic residues can be differentiated with ETD using the same *c*+57 and *z*-57 peaks that were observed with ECD [9,10]. Observation of these pairs of backbone fragments assesses the presence and the position of the isoaspartic acid residues. With this unique feature ETD is a very attractive addition to the arsenal of MS techniques for proteomics investigation. However, up-to-date ETD studies have been reported in the literature only on protonated species. The strategies described in this thesis have the potential to be applied in ETD and deliver enhanced structural insights.

A good part of our understanding about the high order (secondary, tertiary and quaternary) structure of peptides and proteins in gas-phase comes from ion mobility spectrometry. The results of some of these studies have been contradictory and resulted in a growing interest in alternative methods to explore the gas-phase structure of (bio)molecular species. The last few years show an increase in the application of infrared spectroscopy to yield conformational information on amino acids and di- and tripeptides in the gas-phase. Application of infrared spectroscopy for gas-phase studies, however, requires production of sufficiently high concentrations of gas-phase protein ions and intense source of irradiation that operates with wavelengths suitable for studying protein structure. Soft ionization techniques like MALDI and ESI can transfer intact biomolecules from liquid to gas-phase in multiple charge states. Coupling these ion sources to MS instrumentation with ion trapping facilities (e.g.: FTICR-MS) creates the possibility to expose the ion cloud to intense, tunable wavelength, sources of infrared irradiation. Free electron lasers have recently been shown to be very suitable for this purpose. In the gas-phase wavelength resolved IRMPD is used to induce ion fragmentation and changes in the mass spectra of the irradiated species. Infrared irradiation of cytochrome *c* ions, for instance, with FELIX laser reveals amide I (C=O stretching modes) and amide II (N-H bending modes) absorption bands, commonly observed for proteins in solution. Moreover, the same spectrum shows a third band at a lower wavenumber (1483 cm^{-1}) that is not

observed in solution. This is more prominent for higher charge states and was interpreted as an evidence for unfolding of cytochrome *c* in the gas-phase. The band positions suggest mostly an α-helical structure of this protein with a similar conformational distribution compared to solution [11].

Many peptides and proteins in their biologically active form are complexed with different metal cations. There is evidence that metal ion binding to peptides and proteins induces structural changes. Metal cations can be solvated by electronegative atoms such as N or O at different sites in biomolecule or by an aromatic ring therefore defining several possible gas-phase structures. Hence, the role of mass spectrometry to establish which structure is favoured can be sometimes quite challenging. Using IR irradiation in the $1400 - 1800$ cm^{-1} spectral range where the amide I and amide II bands are located, can provide detailed structural information about the groups involved in metal ion solvation. Despite the fact that IR spectroscopy can produce valuable structural and dynamical information the open literature is quite poor in IR studies of gas-phase metalated complexes. In many cases these species consists of metal ion and aromatic molecules. These organometallic complexes are used as model systems in order to understand the metal ion-ligand interaction or metal ion solvation in gas-phase. Examples of such studies include IR spectroscopic studies performed at FELIX facility at the FOM Institute on Cr$^+$ coordinated complexes with aromatic ligands (acetophenone, anisole, aniline and dimethyl aniline) [12, 13] or at the FEL facility in Orsay on Fe$^+$ complexes of unsaturated hydrocarbons [14]. These fundamental studies can elucidate the binding site of the metal providing valuable information about the gas-phase structure or the mechanism involved in fragmentation. Recently, Polfer *et al*. performed IR studies on metal tagged amino acids and small peptides in the gas phase and the results were compared with the data obtained from simulations based on density functional theory. For K$^+$ tagged tyrosine and phenylalanine they showed that the charge solvation (CS) is favoured instead of a salt bridge (SB) structure and the preferred binding of K$^+$ determines a tridentate N/O/ring structure. Contrary to this finding, the results obtained from bradykinin fragment 1-5 tagged with K$^+$ suggest that the SB structure is predominant indicating a head-to-tail looped structure [15]. Tridentate charge solvation N/O/ring

structures was also reported for phenylalanine Ag(I) and Zn(II) complexes in the gas phase [16].

In an attempt to determine the preferred binding sites of metals in peptides and to probe structural differences we performed infrared multiple-photon dissociation (IR-MPD) spectroscopy on doubly protonated oxytocin and on oxytocin complexed with Zn^{2+}. Preliminary results indicate a clear band near 1580 cm^{-1} for doubly protonated oxytocin. For Zn^{2+}-oxytocin complex, compared with doubly protonated oxytocin, this band is shifted to 1560 cm^{-1} (see fig. 7.1).
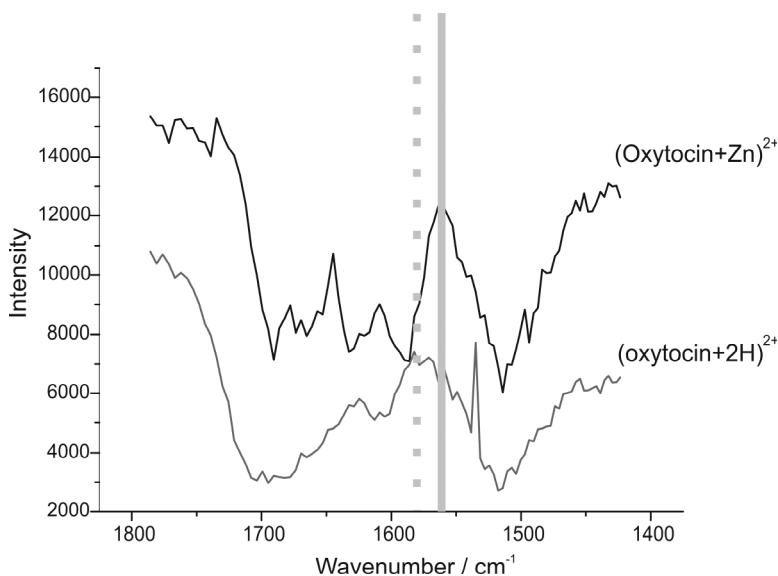
Figure 7.1 Infrared photodissociation spectra for doubly protonated oxytocin and oxytocin complexed with Zn^{2+}.

This observed band shift suggest structural changes in nonapeptide oxytocin induced by the metal ion. This is in agreement with our previously reported results obtained with ECD and SORI-CID. It would be very interesting to observe IR spectra on oxytocin complexed with Cu^{2+} as it is experimental evidence

that the presence of Cu^{2+} leads to dramatic structural changes which are quite unexpected for such a small, seemingly rigid, peptide.

The quality of information obtained from gas-phase IR spectroscopy is unique as it offers the possibility to selectively probe a large number of vibrations. This versatile technique can be extended to larger (bio)molecules and provide structural information complementary to that obtained with other dissociation techniques in gas phase.

References

(1)   Zubarev, R. A.; Horn, D. M.; Fredricksson, E. K.; Kelleher, N. L.; Kruger, N. A.; Lewis, M. A.; Carpenter, B. K.; McLafferty, F. W. Anal. Chem. **2000**, 72, 563-573.

(2)   Syka, J. E. P.; Coon, J. J.; Schroeder, M. J.; Shabanowitz, J.; Hunt, D. F. Proc. Natl. Acad. Sci. U.S.A. **2004**, 9528-9533.

(3)   Coon, J. J.; Shabanowitz, J.; Hunt, D. F.; Syka, J. E. P. J. Am. Soc. Mass Spectrom. **2005**, 16, 880-882.

(4)   Horn, D. M.; Ge, Y.; McLafferty, F. W. Anal. Chem. **2000**, 72, 4778-4784.

(5)   Savitsky, M. M.; Kjeldsen, F.; Nielsen, M. L.; Zubarev, R. A. Angew. Chem. **2006**, 45, 5301-5303.

(6)   Chalmers, M. J.; Hakansson, K.; Johnson, R.; Smith, R.; Shen, J.; Emmet, M. R.; Marshall, A. G. Proteomics **2004**, 4, 970-981.

(7)   Chalmers, M. J.; Mackay, C. L.; Hendrickson, C. L.; Wittke, S.; Walden, M.; Mischak, H.; Fliser, D.; Just, I.; Marshall, A. G. Anal. Chem. **2005**, 77, 7163-7171.

(8)   Borchers, C. H.; Thapar, R.; Petrotchenko, E. V.; Torres, M. P.; Speir, J. P.; Easterling, M. E.; Dominski, Z.; Marzluff, W. F. Proc. Natl. Acad. Sci. U.S.A. **2006**, 103, 3094-3099.

(9)   O`Connor, P. B.; Cournoyer, J. J.; Pitteri, S. J.; Chrisman, P. A.; McLuckey, S. A. J. Am. Soc. Mass Spectrom. **2006**, 17, 15-19.

(10)   Cournoyer, J. J.; Lin, C.; O`Connor, P. B. Anal. Chem. **2006**, 78, 1264-1271.

(11)   Oomens, J.; Polfer, N. C.; Moore, D. T.; van de Meer, L.; Marshall, A. G.; Eyler, J. R.; Meijer, G.; von Helden, G. Phys. Chem. Chem. Phys. **2005**, 7, 1345-1348.

(12)   Oomens, J.; Moore, D. T.; von Helden, G.; Meijer, G.; Dunbar, R. C. J. Am. Chem. Soc. **2004**, 126, 724-725.

(13)   Moore, D. T.; Oomens, J.; Eyler, J. R.; von Helden, G.; Meijer, G.; Dunbar, R. C. J. Am. Chem. Soc. **2005**, 127, 7243-7254.

(14)   Lemaire, J.; Boissel, P.; Heninger, M.; Mauclaire, G.; Bellec, G.; Mestdagh, H.; Simon, A.; Le Caer, S.; Ortega, J. M.; Glotin, F.; Maitre, P. Phys. Rev. Lett. **2002**, 89, 273002.

(15)   Polfer, N. C.; Paizs, B.; Snoek, L. C.; Compagnon, I.; Suhai, S.; Meijer, G.; von Helden, G.; Oomens, J. J. Am. Chem. Soc. **2005**, 127, 8571-8579.

(16)   Polfer, N. C.; Oomens, J.; Moore, D. T.; von Helden, G.; Meijer, G.; Dunbar, R. C. J. Am. Chem. Soc. **2006**, 128, 517-525.

Summary

Mass spectrometry (MS) is an indispensable tool for proteomic research. Nowadays, most life scientists are familiar with structural analysis of gas-phase biomolecules using MS-based methods. Soft ionization techniques like matrix assisted laser desorption ionization (MALDI) and electrospray ionization (ESI) assure a gentle transfer of peptides and proteins from solid or liquid phase into gas phase with minimal fragmentation. An arsenal of mass spectrometric techniques and methods can then be used to identify, quantify and characterize such molecular species at different structural levels. Within the field of mass spectrometry, Fourier transform ion cyclotron resonance mass spectrometry (FTICR-MS) plays a distinguished role as it enables measurements at an extremely high mass resolution and mass accuracy.

Chapter 1 of this thesis describes the fundamentals of FTICR-MS and summarizes the frequently used dissociation techniques in FTICR-MS. The description of the experimental setup is structured according to the experimental sequence. First, the ionization part is discussed followed by the ion optics used to transport the gas-phase ions into the ion cyclotron resonance (ICR) cell. Two types of ICR cells, the infinity and the capacitively coupled open ended cell are used in this thesis to trap and detect the ions. Different methods are presented to manipulate the trapped ions in order to fragment them and to detect the dissociation products. In this work the dissociation techniques based on ion-neutral collisions and photon- or electron irradiation are emphasized. A set of data analysis software and data mining tools which are used to process the mass spectra are shortly pointed in the last part of this chapter.

One fragmentation technique, namely electron capture dissociation (ECD), plays a central role in this thesis. Therefore, **Chapter 2** is fully dedicated to ECD and ECD related techniques. A brief history of ECD is presented here continued with fundamental aspects of ECD in protonated species with the goal to familiarize the reader with the mechanistic and energetic aspects of this technique. ECD has some remarkable features that are of great advantage in proteomics: short irradiation time, high sequence coverage, facile cleavage of mono- and disulfide bonds and preservation of labile groups. Therefore, the impact of ECD in the field of proteomics is nowadays well acknowledged: post-translational modifications can be identified and localized with ECD; mono- and disulfide bridged peptides and proteins are extensively sequenced with ECD; investigation of protein folding and suitability for top-down proteomics of intact proteins and protein complexes. Moreover, ECD can also be applied to (bio)molecular species complexed with charge carriers other than protons. Previous ECD studies on polypeptides containing metal cations revealed interesting dissociation behaviours. In order to improve ECD fragmentation efficiency various groups worked on method- and instrumental development. This has resulted in ECD spectra that are obtained with irradiation times less than 1 millisecond. An ECD like technique called electron transfer dissociation (ETD) was recently developed and implemented on quadrupolar ion traps attracting. This fragmentation technique is extremely suitable and promising for future proteomics.

Chapter 3 reports on a fundamental study of ECD, namely the role of molecular conformation in this ion-electron reaction. We showed that at 85 K, ECD of the linear peptide substance P results in just two backbone fragments whereas at room temperature, under identical conditions (except temperature) eight backbone fragments are formed. Same ECD behaviour is observed for the cyclic peptide gramicidin S: one backbone fragment at 85 K compared with five backbone fragments at room temperature. In both cases, all observed backbone cleavages are typical N-C_α scissions which have a high rate constant and involve radical intermediates. The observation that less number of backbone fragments are

produced in ECD at low temperatures is rationalized by the fact that the ion cloud is populated with a smaller number of ion conformations compared with elevated temperatures. This statement is supported by the reduced or inactive hydrogen loss at low temperatures, a fragmentation channel which has previously shown to be affected by conformation. It is concluded that ECD fragments represent a snapshot of conformational (intramolecular solvation shell) heterogeneity. As a result, a high sequence coverage in ECD can be obtained by increasing the conformational heterogeneity of the precursor ion population.

A way to increase the conformational heterogeneity of the ion cloud is heating of the ions using photon irradiation. Based on a novel approach we developed an experimental set-up that allows simultaneous or sequential infrared multiphoton dissociation (IRMPD) and electron irradiation to be performed on-axis in the ICR cell. **Chapter 4** describes the instrumental design and the implementation of this approach in our FTICR-MS system. The infrared beam is directed through the ion optics into the ICR cell using a pneumatically actuated probe (mirror), which is mechanically auto-aligned. The dispenser cathode is placed at the rear of the magnet. The advantage of this set-up is a better overlap between the electron beam, laser beam and the ion cloud. We hypothesize the electron beam induces focusing of the ion cloud, resulting in a better overlap of the ion cloud with the infrared beam. The concept was validated using independent and simultaneous irradiation scenarios on two standard peptides: substance P and melittin. An increased number of primary backbone fragments and thus a higher sequence coverage of these two peptides was obtained in simultaneous IRMPD and ECD compared to IRMPD or ECD experiments only. Such higher coverage increases the confidence level in peptide and protein assignments.

High sequence coverage is difficult to obtain when slow heating methods are applied to peptides or proteins containing monosulfide- or disulfide intramolecular linkages. In **Chapter 5** we show that complexation of oxytocin with transition metal dications results in very rich SORI-CID mass spectra including backbone fragments that require the cleavage of the disulfide bond up to 50% of

the total product ion intensity. This behaviour was not observed for SORI-CID of the doubly protonated analogues. Our disulfide bond containing nonapeptides (Oxytocin, Thr4Gly7Oxytocin and Vasopressin) complexed with a metal dication (Ni^{2+}, Zn^{2+} or Cu^{2+}) dissociate under SORI-CID conditions forming four types of dissociation products: 1) small neutral losses, 2/3) backbone fragments with and without scission of the disulfide bond and 4) internal amino acid losses without rupture of the disulfide bridge. The most abundant disulfide bond cleavage (37% - 56%) was observed in SORI-CID spectra of Zn^{2+} and Cu^{2+}-complexed peptides while for peptides containing Ni^{2+} this type of cleavage is significantly lower. We suggest that the observed disulfide bond cleavage for peptide-metal complexes is likely to reflect conformational changes induced by the presence of the metal ion. Moreover, we show here that the region of the binding site of the metal can be estimated based on complementary fragments from peptide-metal complexes.

The complexes of transition metal cations with three nonapeptides (Oxytocin, Thr4Gly7Oxytocin and Vasopressin) were also studied using ECD, as described in **Chapter 6**. We found that ECD fragmentation behaviour of these three peptide complexes depends on the type of metal cation. ECD spectra of doubly protonated oxytocin and vasopressin contain many fragments that involve cleavage of the disulfide bond bridge. ECD of the corresponding metal-peptide complexes results also in fragments that involve the scission of the disulfide bridge. In addition, the backbone cleavage sites are complementary to those observed at doubly protonated analogues. Differences in ECD spectra are expected from these three peptides because they differ in their amino acid composition by two amino acids. We show in this chapter that, for the same metal, ECD behaviour of these peptide-metal ion complexes displays not just differences but also similarities. For all three peptides, complexation with Cu^{2+} leads to an increase of the tail fragments. In contrast with this behaviour, complexation of Oxytocin and Thr4GlyOxytocin with Ni^{2+} results mainly in ring fragments. Also we noticed common behaviours such as formation of mainly *c/z* fragments for Zn^{2+} complexes while *b/y* fragments dominates ECD spectra when Cu^{2+} is used as cationizing

agent. We suggest that these common features are indicative for structural similarities between different species.

Chapter 7 gives a perspective for structural studies of gas-phase ions employing fragmentation techniques based on ion-electron and ion-photon interactions. Some challenges in ECD are presented not just from a technical point of view but also in the applications of for example biomarker research and structural analysis of synthetic polymers. Electron transfer dissociation (ETD) and its attractiveness for the proteomics community are briefly discussed. It is presented that infrared spectroscopy using tunable infrared wavelengths offers unique possibilities for structural investigation of biomolecules in the gas phase.

Summary

Samenvatting

Massaspectrometrie (MS) is noodzakelijk voor het uitvoeren van *proteomics* onderzoek. Tegenwoordig zijn de meeste onderzoekers in de *life sciences* bekend met de massaspectrometrische structuuranalyse van biomoleculen in de gasfase. Zachte ionisatietechnieken zoals matrix-geassisteerde laser desorptie ionisatie (MALDI) en electrospray ionisatie (ESI) zorgen ervoor dat peptiden en eiwitten uit een vaste of vloeibare fase zonder noemenswaardige fragmentatie in de gasfase kunnen worden gebracht. Vele verschillende MS technieken worden gebruikt voor het identificeren, kwantificeren en karakteriseren van zulke moleculen op verschillende structuurniveaus. Fourier transformatie ion cyclotron resonantie (FTICR) speelt een belangrijke rol binnen het veld van MS, omdat het metingen mogelijk maakt met een zeer hoge massaresolutie en massanauwkeurigheid.

In **Hoofdstuk 1** van dit proefschrift wordt de theoretische achtergrond van FTICR-MS beschreven en een overzicht gegeven van de meest gebruikte dissociatietechnieken. Verschillende aspecten van een FTICR-MS experiment worden beschreven in volgorde van de experimentele sequentie. Allereerst komt het ionisatieproces aan bod, gevolgd door een beschrijving van de ionenoptica die gebruikt wordt voor het transport van ionen naar de ion cyclotron resonantie (ICR) cel. Daarna worden de twee typen ICR cellen die in dit proefschrift worden gebruikt voor het vangen en detecteren van ionen genoemd, namelijk de *infinity* en de capacitief-gekoppelde *open* cel. Verschillende methoden voor het manipuleren en fragmenteren van gevangen ionen worden beschreven. De nadruk in dit werk ligt bij dissociatietechnieken die gebaseerd zijn op botsingen tussen ionen en neutrale deeltjes, en processen van electronen- of fotonenbestraling. Tenslotte wordt kort

aandacht gegeven aan software voor data analyse en *processing* (uitwerking) van de massaspectra.

Bij het in dit proefschrift beschreven onderzoek speelt electronenvangst dissociatie (electron capture dissociation, ECD) een cruciale rol als massaspectrometrische fragmentatietechniek. **Hoofdstuk 2** is daarom volledig gewijd aan ECD en ECD-gerelateerde technieken. Een korte beschrijving van de geschiedenis van ECD wordt gevolgd door energetische en mechanistische aspecten uit eerder fundamenteel onderzoek aan geprotoneerde moleculen. ECD heeft een aantal opvallende voordelen voor *proteomics*, namelijk een korte fragmentatietijd, veel sequentie informatie, verbreking van mono- en disulfide bruggen en behoud van labiele ketens. Hierdoor is ECD niet meer weg te denken in het veld: post-translationele modificaties kunnen worden geïdentificeerd en gelokaliseerd, en zwavelbrug-houdende peptiden en eiwitten worden uitvoerig *gesequenced* met ECD. Tevens speelt ECD een belangrijke rol bij de bestudering van eiwitvouwing en eiwitcomplexen. ECD wordt ook gebruikt bij (bio)moleculaire verbindingen die gecomplexeerd zijn met ladingsdragers anders dan protonen. Eerder ECD onderzoek aan polypeptiden gecomplexeerd met een metaal cation liet interessant fragmentatiegedrag zien. Voor het verbeteren van ECD fragmentatie efficiëntie hebben verschillende groepen aan methode- en instrumentontwikkeling gewerkt. ECD spectra kunnen nu verkregen worden met stralingstijden korter dan 1 milliseconde. Recentelijk heeft electron overdracht dissociatie (*electron transfer dissociation*, ETD) zijn intrede gedaan op een quadrupool ion trap instrument. Deze ECD-gerelateerde techniek is veelbelovend voor *proteomics*.

In **Hoofdstuk 3** wordt een fundamenteel ECD onderzoek beschreven. De rol van de molecuulconformatie tijdens electronenoverdracht wordt bestudeerd door ECD fragmentatie van het lineaire peptide substance P bij 85 K te vergelijken met experimenten bij kamertemperatuur. Hierbij werden respectievelijk twee en acht peptide *backbone* fragmenten waargenomen. Voor het cyclische peptide gramicidin S werd slechts één fragment bij lage temperatuur waargenomen, in

vergelijking met vijf bij hogere temperatuur. Alle fragmenten zijn typische *backbone* brekingen van N-C$_\alpha$–bindingen, die relatief snel verlopen via radicaal intermediairen Deze verschillen worden verklaard door aan te nemen dat bij lagere temperatuur de ionenwolk is opgebouwd uit minder verschillende conformaties. Deze aanname wordt ondersteund door het feit dat bij lagere temperatuur minder of geen waterstofverlies wordt waargenomen, een fragmentatiekanaal waarvan bekend is dat het afhankelijk is van de conformatie. Geconcludeerd wordt dat ECD fragmenten een *snapshot* weergeven van conformationele heterogeniteit. Als gevolg hiervan neemt ECD sequentie informatie toe wanneer deze heterogeniteit van de *precursor* conformatie toeneemt.

Een manier om de conformationele heterogeniteit toe te laten nemen is door de ionenwolk te verwarmen met behulp van infrarood bestraling. Gebaseerd op een vernieuwende aanpak ontwikkelden wij een experimentele opzet waarin zowel simultaan als sequentiëel infrarood multifoton dissociatie (IRMPD) en ECD kunnen worden toegepast in de ICR cel. In **Hoofdstuk 4** wordt het instrumenteel ontwerp en de implementatie hiervan beschreven. De infraroodbundel komt via een pneumatisch gestuurde spiegel (die zichzelf mechanisch uitlijnt) de ionenoptiek en vervolgens de ICR cel binnen. De cathode bevindt zich aan de achterzijde van de magneet, zodat electronen en fotonen in één lijn (co-axiaal) bewegen met de ionenwolk. Een betere overlap is mogelijk het gevolg van een focusserend effect van de electronenbundel. Dit concept werd gevalideerd in een studie van twee peptiden, namelijk substance P en melittine. Simultane IRMPD en ECD resulteerde in meer *backbone* brekingen dan in het geval van enkelvoudige fragmentatie scenario's, waardoor in het simultane experiment meer sequentie informatie werd verkregen. Dit laatste aspect verhoogt de scoringskans in *database searches* voor eiwitidentificaties.

Een manier om de conformationele heterogeniteit toe te laten nemen is door de ionenwolk te verwarmen met behulp van infrarood bestraling. Gebaseerd op een vernieuwende aanpak ontwikkelden wij een experimentele opzet waarin zowel simultaan als sequentiëel infrarood multifoton dissociatie (IRMPD) en ECD

kunnen worden toegepast in de ICR cel. In **Hoofdstuk 4** wordt het instrumenteel ontwerp en de implementatie hiervan beschreven. De infraroodbundel komt via een pneumatisch gestuurde spiegel (die zichzelf mechanisch uitlijnt) de ionenoptiek en vervolgens de ICR cel binnen. De cathode bevindt zich aan de achterzijde van de magneet, zodat electronen en fotonen in één lijn (co-axiaal) bewegen met de ionenwolk. Een betere overlap is mogelijk het gevolg van een focusserend effect van de electronenbundel. Dit concept werd gevalideerd in een studie van twee peptiden, namelijk substance P en melittine. Simultane IRMPD en ECD resulteerde in meer *backbone* brekingen dan in het geval van enkelvoudige fragmentatie scenario's, waardoor in het simultane experiment meer sequentie informatie werd verkregen. Dit laatste aspect verhoogt de scoringskans in *database searches* voor eiwitidentificaties.

Vaak is het moeilijk sequentie informatie te verkrijgen van zwavelbrug-houdende peptiden of eiwitten gebruikmakend van conventionele fragmentatiemethoden. In **Hoofdstuk 5** laten wij zien dat complexering van oxytocine met tweevoudig geladen transitie metaal cationen resulteert in zeer rijke SORI-CID massaspectra. Tot wel 50% van de totale productionen intensiteit is hierbij afkomstig van fragmenten die ontstaan door breking van de intramoleculaire zwavelbrug. Eenzelfde resultaat werd verkregen voor vergelijkbare nonapeptiden Thr4-Gly7-oxytocine and vasopressine. De SORI-CID spectra van de verschillende complexen worden in vier catogorieën besproken: 1) verlies van neutrale moleculen, 2/3) *backbone* fragmenten met en zonder breking van de zwavelbrug en 4) verlies van interne aminozuren. In de SORI-CID spectra van Zn^{2+}- en Cu^{2+}-gecomplexeerde peptiden zijn aanzienlijk meer fragmenten afkomstig van breking van de zwavelbrug dan in het geval van de Ni^{2+}-complexen. Wij denken dat de verschillen in het breken van de disulfide binding conformationele veranderingen van het peptide weergeven, die geïnduceerd zijn door het metaal cation. Daarnaast laten we zien dat de resultaten gebruikt kunnen worden voor het lokaliseren van het metaal cation in het peptide complex door gebruik te maken van corresponderende fragmentparen.

De complexen van deze drie nonapeptiden met verschillende transitie metaal cationen zijn bestudeerd met ECD, zoals beschreven in **Hoofdstuk 6**. Het fragmentatiegedrag van deze complexen is afhankelijk van het soort metaal. De ECD spectra van dubbel-geprotoneerd oxytocine en vasopressine bevatten voornamelijk fragmenten die gevormd worden na breking van de zwavelbrug. Tevens wordt deze zwavelbrug verbroken tijdens ECD van de metaal-gecomplexeerde peptiden, echter daarbij worden complementaire *backbone* fragmenten verkregen. Op grond van de verschillende aminozuurvolgorden van deze drie nonapeptiden worden verschillende ECD spectra verwacht. Wij laten zien dat er ook overeenkomsten zijn, bijvoorbeeld Cu^{2+}-complexering verhoogt de bijdrage aan *tail* (staart) fragmenten. Ni^{2+}-complexering daarentegen resulteert in met name ring fragmenten. In het algemeen leveren Zn^{2+}-complexen *c/z* fragmenten op, terwijl Cu^{2+}-complexen met name *b/y* fragmenten in de ECD spectra laten zien. Deze overeenkomsten in ECD gedrag zijn indicatief voor structuurovereenkomsten in de verschillende verbindingen.

In **Hoofdstuk 7** wordt kort een toekomstvisie uiteengezet voor structuuranalyse aan ionen in de gasfase. Voor deze studies zijn fragmentatietechnieken gebaseerd op ion-electron en ion-foton interacties zeer geschikt. Uitdagingen in het ECD veld worden beschreven, zowel op technologisch gebied als in de toepassingen. Ook wordt gekeken naar de mogelijkheden van electron overdracht dissociatie (ETD). Tenslotte laten wij zien dat infrarood spectroscopie met een flexibel instelbare golflengte unieke mogelijkheden biedt voor de studie aan biomoleculen in de gasfase.

Samenvatting

Acknowledgements

In the last four and half years I have had the pleasure to work at AMOLF in Amsterdam, an excellent research institute with a dynamic and international environment. Looking back over this period, I have the feeling it was a productive and intensive stage of my life. However, to come to this end would not have been possible without the help of many people both from the scientific community and outside of the academic environment. I want to thank all those who have been generous to me and helped me by any means during these years.

First of all I want to thank my two promoters Albert Heck and Ron Heeren who gave me the opportunity to do my Ph.D. research at AMOLF. I'm grateful to both of you for your careful and professional guidance, patience, understanding and constant encouragement, even during the difficult moments of my doctoral studies. I learned from you how to approach a problem, to ask relevant questions, how to make a plan and finally how to present useful results. Especially you Ron I have to thank for your help in recording my first hot/cold ECD spectra when the instrument, late in the evening, refused to collaborate with me. Also thanks for your help in writing this thesis. I learned from you not just science but also other things which are very helpful for my personal development.

Two members from our group I want to thank in particular, namely Liam McDonnell and Yuri van der Burgt for their sustained efforts in teaching me how to interpret the experimental results and for their endless patience in guiding this rebel student to write articles. Yuri, you played a crucial role in these crowded last months of my Ph.D. by helping me to successfully finish this thesis. The summary in Dutch of my thesis would not be possible without your generous help. For that and for many other things I want to thank you once again.

Polfer and Jos Oomens thank you for your help with my first FELIX experiments in Rijnhuizen.

Intermezzo

It would be unfair to not mention here some people who made my life in Amsterdam more thrilling than I thought. With amazing talent they took care of five of my bicycles (the last one very recently) so I don't have to repair them anymore. For this and for the fact that they caused me a huge bump in the third year of my Ph.D., I thank you and I reserved you a place in my …..!

My thoughts now turn to my friends and colleagues from Romania who encouraged me all these years and whose visits to Amsterdam made me very happy.

I wish to express my gratitude to my parents, sister and brothers in law for their love and for everything they did for me since I moved with my family to Holland.

Le mulțumesc din inimă părinților mei pentru întregul sprijin pe care mi l-au oferit pe parcursul acestor ani şi pentru tot ce au făcut pentru mine pentru a duce la bun sfârşit acest capitol al vieții mele. Mihaela, Bogdan, Cătălin, Iulia şi Ilinca, Dan şi Ina vă mulțumesc pentru că ați fost alături de mine, pentru încurajările voastre permanente şi puținele dar extrem de plăcutele momente petrecute impreună.

Minunatei mele soții Daciana şi băiețelului nostru Raul le mulțumesc că au fost alături de mine in tot acest timp. Fără ajutorul vostru nimic din ceea ce am realizat in aceşti ani n-ar fi fost cu putință.

Vouă tuturor vă dedic aceasta teză împreună cu toată dragostea mea.

Romulus Mihalca, 7 February 2007

Acknowledgements

List of publications

Mihalca R., Kleinnijenhuis A. J., McDonnell L. A., Heck A. J. R., Heeren, R. M. A. Electron capture dissociation at low temperatures reveals selective dissociations, *J. Am. Soc. Mass Spectrom.*, **2005**, 15, 1869.

Römpp A., Taban I. M., Mihalca R., Duursma M. C., Mize T. H., McDonnell L. A., Heeren R. M. A. Examples of Fourier transform ion cyclotron resonance mass spectrometry development: from ion physics to remote access biochemical mass spectrometry, *Europ. J. Mass spectrum.*, **2005**, 11, 443.

Mihalca R., Duursma M. C., van der Burgt Y. E. M., McDonnell L. A., Heck A. J. R., Heeren R. M. A., Combined infrared multiphoton dissociation and electron capture dissociation using co-linear and overlapping beams in Fourier transform ion cyclotron resonance mass spectrometry, *Rapid Comm. Mass Spectrom.*, **2006**, 20, 1838.

Kleinnijenhuis A. J., Mihalca R., Heeren R. M. A., Heck A. J. R., *Atypical behaviour in the electron capture induced dissociation of biologically relevant transition metal ion complexes of the peptide hormone oxytocin*, Int. J. Mass Spectrom., **2006**, 253(3), 217.

Mihalca R., van der Burgt Y. E. M., Heck A. J. R., Heeren R. M. A., Disulfide bond cleavages observed in SORI-CID of three nonapeptides complexed with divalent transition metal cations, accepted by *J. Mass Spectrom.* **2007**.

Mihalca R., van der Burgt Y. E. M., Heck A. J. R., Heeren R. M. A., ECD behaviour of disulfide bond containing peptides is determined by the type of divalent metal cation (in preparation).